Neotropical Ichthyology

Original article

https://doi.org/10.1590/1982-0224-2025-0003

urn:lsid:zoobank.org:pub:E3C456C3-250E-46A2-936F-C39358D1A6EE

Systematic assessment of the *Hypomasticus steindachneri* (Characiformes: Anostomidae) species complex, with the description of a new species

Correspondence:
Ian Solon B. Ito
ian.solon.ito@gmail.com

Ian Solon B. Ito[1,2], Lenice Souza-Shibatta[2], Osvaldo T. Oyakawa[3], Júlio C. Garavello[4], Heraldo A. Britski[3] and José L. O. Birindelli[2]

This study provides a taxonomic revision of *Hypomasticus steindachneri*, based on an extensive analysis of specimens from various basins along the Brazilian coastal region. Specimens were analyzed using molecular and morphological methodologies for the purpose of species delimitation. *Hypomasticus steindachneri* is redescribed with an integration of new evidence and data from the holotype, and a new species is described from the Southeast Atlantic Forest. The new species is diagnosed from its congeners by the following combination of features: 12 scale rows around the caudal peduncle, a subterminal mouth with cleft aligned longitudinally with the ventral margin of the second infraorbital bone and three diffuse dark midlateral blotches, extending horizontally by 4–5 scales and vertically by 2–3 rows of scales. Osteological examination revealed notable findings, including the first record of pronounced hypertrophy in the first pair of ribs within the genus, which may be related to mating behaviors. Additionally, a bar formed by the processes of the orbitosphenoid and parasphenoid bones was identified. The clear delimitation of new, undescribed species in the phylogenetic analysis highlights the need for a comprehensive taxonomic review of the genus *Hypomasticus*, utilizing new sets of molecular and morphological evidence.

Keywords: Atlantic Forest, Coastal drainages, Integrative taxonomy, Osteology, Species delimitation.

Submitted January 10, 2025
Accepted August 29, 2025
Epub November 14, 2025

Associate Editor Juan Mirande
Section Editor Bruno Melo
Editor-in-chief Carla Pavanelli

1 Programa de Pós-graduação em Ciências Biológicas, Universidade Estadual de Londrina, Rodovia Celso Garcia Cid, PR-445, km 380, Caixa Postal 10.001, 86057-970 Londrina, PR, Brazil. (ISBI) ian.solon.ito@gmail.com (corresponding author).

2 Departamento de Biologia Animal e Vegetal, Universidade Estadual de Londrina (UEL), Rodovia Celso Garcia Cid, PR-445, km 380, Caixa Postal 10.001, 86057-970 Londrina, PR, Brazil. (JLOB) josebirindelli@uel.br, (LSS) lenicesouza@hotmail.com.

3 Museu de Zoologia da Universidade de São Paulo (MZUSP), Laboratório de Ictiologia, Avenida Nazaré 481, 04263-000 São Paulo, SP, Brazil. (OTO) oyakawa@usp.br, (HAB) heraldo@usp.br.

4 Universidade Federal de São Carlos (UFSCAR), Centro de Ciências Biológicas e da Saúde (CCBS), Departamento de Ecologia e Biologia Evolutiva (DEBE), Rodovia Washington Luis, s/n, 13565-905 São Carlos, SP, Brazil. (JCG) jgaravello@ufscar.br.

Online version ISSN 1982-0224
Print version ISSN 1679-6225

Neotrop. Ichthyol.
vol. 23, no. 3, Maringá 2025

Uma revisão taxonômica de *Hypomasticus steindachneri* é realizada com base em uma análise abrangente de espécimes de diferentes bacias ao longo da região costeira do Brasil. Os espécimes foram analisados através de métodos moleculares e morfológicos para delimitação de espécies. *Hypomasticus steindachneri* é redescrito, combinando um novo conjunto de evidências com os dados do holótipo, e uma nova espécie é descrita para a Mata Atlântica Sudeste. A nova espécie é diagnosticada entre seus congêneres por apresentar a combinação de 12 fileiras de escamas ao redor do pedúnculo caudal, boca em posição subterminal, com a abertura alinhada longitudinalmente com a margem ventral do segundo infraorbital e três manchas difusas na região mediolateral, estendendo-se horizontalmente por 4–5 escamas e verticalmente por 2–3 fileiras de escamas. A análise osteológica revelou características marcantes, como o primeiro registro no gênero de hipertrofia no primeiro par de costelas, possivelmente relacionado ao acasalamento e a presença de uma barra formada pelos processos dos ossos orbitosfenóide e parasfenóide. A clara delimitação de novas espécies não descritas na análise filogenética destaca a necessidade de uma revisão taxonômica do gênero *Hypomasticus* utilizando novos conjuntos de evidências moleculares e morfológicas.

Palavras-chave: Delimitação de espécies, Drenagens costeiras, Mata Atlântica, Osteologia, Taxonomia integrativa.

INTRODUCTION

The family Anostomidae, comprising neotropical fishes commonly known as piaus, aracus, piaparas and headstanders, is among the most species-rich lineages within Characiformes (Toledo-Piza *et al*., 2024), with a substantial number of new species frequently recognized and described (Britski *et al*., 2023; Garavello *et al*., 2021). This diverse group exhibits extensive variation in body shape, size and color pattern (Géry, 1977) and has a broad distribution, with species found across multiple basins from southern Central America to central Argentina (Garavello, Britski, 2003). The family comprises 17 recognized genera (Sidlauskas *et al*., 2025) including *Hypomasticus* Borodin, 1929, a distinct and understudied group.

Hypomasticus was described by Borodin (1929) as a subgenus of *Leporinus* Agassiz, 1829 to group species with a downturned mouth. Although it was later considered a synonym of *Leporinus* and deemed invalid (Garavello, 1979; Taphorn, 1992; Garavello, Britski, 2003), it was subsequently resurrected through phylogenetic analysis and elevated to genus status (Sidlauskas, Vari, 2008). Recent molecular studies support the monophyly of the genus; however, they also reveal taxonomic inconsistencies (Ramirez *et al*., 2016; Birindelli *et al*., 2020) and have led to the inclusion of numerous terminal-mouthed species previously assigned to *Leporinus* within the genus (Sidlauskas *et al*., 2025), leaving the current species composition of the group still uncertain.

Hypomasticus steindachneri (Eigenmann, 1907) is a large, migratory anostomid (Pompeu, Martinez, 2007) that inhabits Brazil's coastal drainages, where it is commonly

known as Piau-Três-Pintas. It was described in 1875 by the Austrian zoologist Franz Steindachner, based on a single large specimen collected in the Rio Araçuaí, a tributary of rio Jequitinhonha (Fig. 1). Steindachner originally named the species *Leporinus affinis*, unaware that Günther had already used the name in 1864 for a banded species. The species was later renamed *Leporinus steindachneri* by Eingenmann in 1907. In a recent study describing *Hypomasticus santanai* (Birindelli *et al*., 2020), *Leporinus steindachneri* was reassigned to the genus *Hypomasticus* based on phylogenetic analysis using mitochondrial DNA.

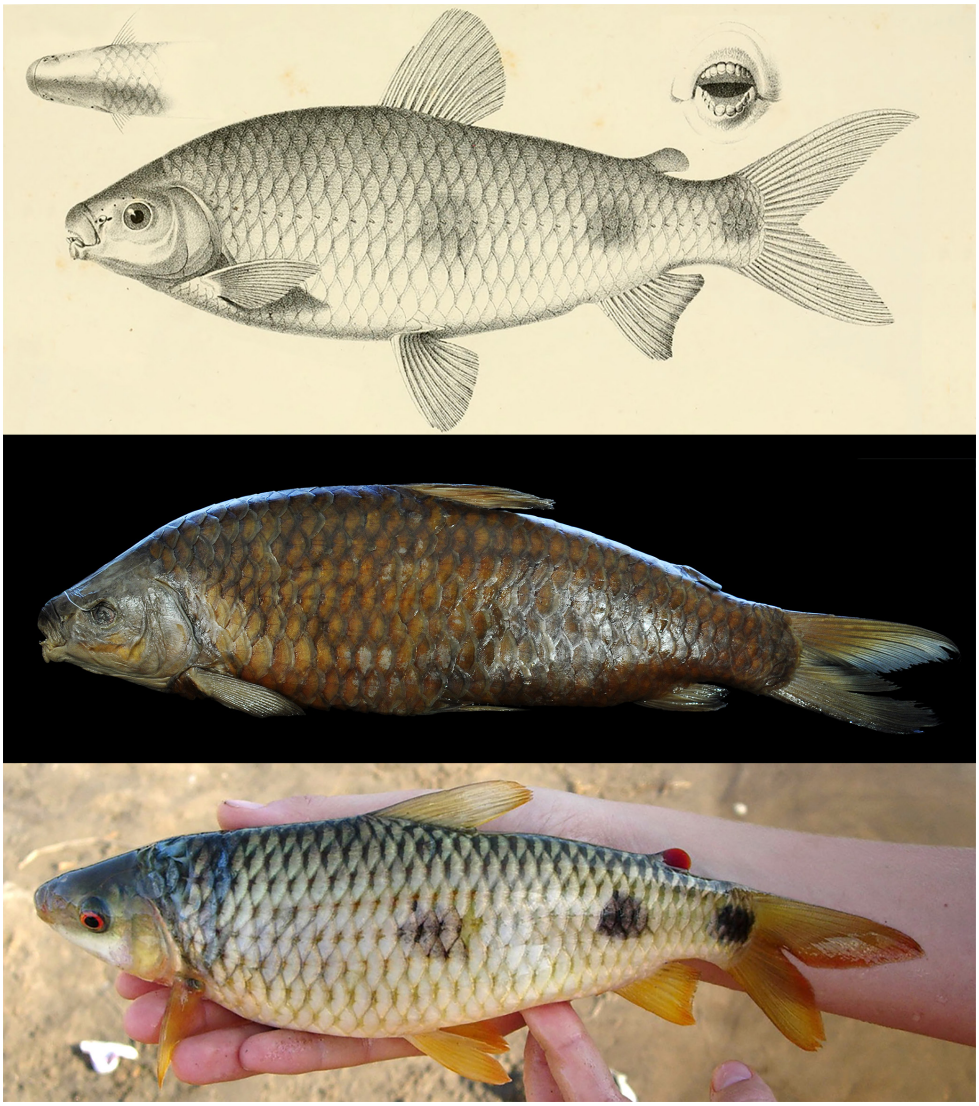

FIGURE 1 | Illustration from the 1875 description (top) and photograph (middle) of the *Hypomasticus steindachneri* holotype deposited in the Natural History Museum in Vienna, NMW 68405. A live specimen (bottom) collected in the Itacambiruçu River, a tributary of the Jequitinhonha River (Photo by Francisco Andrade Neto).

Hypomasticus steindachneri is widely distributed in southeast coastal Brazil, with occurrences spanning from the rio Pardo basin in the states of Bahia and Minas Gerais to the Ribeira de Iguape basin in São Paulo and Paraná states (Camelier, Zanata, 2015; Silva *et al*., 2020). Birindelli *et al*. (2020) recovered the species as closely related to *H. santanai* Birindelli & Melo, 2020, and *H. copelandii* (Steindachner, 1875), the latter a similar-looking species also widespread across coastal drainages in Southeast Brazil. A recent study investigating populations of the congener *Hypomasticus copelandii* from different coastal basins revealed remarkable molecular diversity within the species and identified two well-defined sub-clades (Mendes *et al*., 2022). Such species complexes are common within Anostomidae (Burns *et al*., 2017; Ramirez *et al*., 2017; Nascimento *et al*., 2023) demonstrating that molecular data are an important tool in the taxonomic investigation of the group, particularly for species that display very similar morphological features. Most species of the genus *Hypomasticus* were described in brief descriptions about a century ago. Some, like *H. copelandii* and *H. megalepis* (Günther, 1863), have type-series that include specimens from different drainages or even different species (Géry *et al*., 1988; Britski, Birindelli, 2013; JLOB and HAB, pers. obs.), while others, such as *H. steindachneri*, were described based on a single specimen but have since been reported from a much wider range. This lack of consistent information leads to uncertainty regarding the distribution and validity of these species.

We investigated the populations of *Hypomasticus steindachneri* from different basins along Brazil's coastal region, employing a taxonomic approach that integrates molecular and morphological data. We compared our findings with the species holotype, and we present a redescription of *H. steindachneri* as well as the description and diagnosis of a new species identified through our analyses.

MATERIAL AND METHODS

Material examined. Studied specimens belong to Academy of Natural Sciences of Drexel University, Philadelphia (ANSP), Laboratório de Biologia e Genética de Peixes, Universidade Estadual Paulista "Júlio de Mesquita Filho", Botucatu (LBP), Laboratório de Ictiologia Sistemática, Universidade Federal de São Carlos (LISDEBE), Museu de Ciências Naturais da PUC Minas Gerais (MCNIP, JEQUI, JEQUIJQ, JEQUILGC, LGC), Museu Nacional, Rio de Janeiro (MNRJ), Museu de Zoologia da Universidade Estadual de Londrina (MZUEL), Museu de Zoologia da Universidade de São Paulo (MZUSP), Naturhistorisches Museum, Wien (NMW), and Núcleo de Pesquisas em Limnologia, Ictiologia e Aqüicultura, Universidade Estadual de Maringá, Maringá (NUP), and Museu de Zoologia da Universidade Estadual de Campinas (ZUEC).

A significant gap exists in the sampling of *H. steindachneri* populations from the Doce and Mucuri river basins. For the Doce River, it was not possible to obtain tissue samples for molecular analysis, and no genetic sequences are currently available in public databases. Nonetheless, a considerable number of preserved specimens were located in ichthyological collections and included in the morphometric analysis. In contrast, although some molecular data are available for specimens from the Mucuri River, the number of individuals represented in ichthyological collections is remarkably low. This limited representation may reflect the reduced frequency of sampling efforts in

the Mucuri River, which is smaller than the other basins included in this study. Due to their limited availability, specimens from the Mucuri basin were not included in the morphometric analysis. Nevertheless, biogeographic studies suggest a close relationship between the ichthyofauna of the Doce and Mucuri river basins, with numerous species shared between them (Carvalho, 2007; Camelier, Zanata, 2015). Therefore, it is plausible that specimens from these two basins belong to the same species.

Specimens collected in the Jequitinhonha river basin were initially identified as *Hypomasticus steindachneri*, whereas specimens collected in other drainages, including the Pardo, Mucuri, Doce, Ribeira de Iguape and Rio de Janeiro coastal drainages were initially identified as *H.* cf. *steindachneri*. Based on our results, specimens from the latter two drainages, which are the furthest south, were recognized as a new species and formally described in this study.

The holotype of the new species was designated from material analyzed at MZUSP. The type-series was chosen from undamaged specimens that retained essential meristic information, such as scale and fin-ray counts. Only specimens from a single river basin were included to avoid creating a mixed type-series. A geographic distribution map for each species was created using QGIS 3.12.1 software, following the procedures outlined by Calegari *et al.* (2016).

Morphological analysis. Meristic counts and morphometric measures followed Birindelli, Britski (2013), and included the following counts: scales on the lateral line, scale rows around the caudal peduncle, scale rows between the lateral line and dorsal fin origin, scale rows between the lateral line and pelvic fin origin and pre-dorsal scales, unbranched dorsal-fin rays, branched dorsal-fin rays, branched pectoral-fin rays, branched pelvic-fin rays, unbranched anal-fin rays, branched anal-fin rays, dorsal branched caudal-fin rays, ventral branched caudal-fin rays, premaxillary teeth, dentary teeth, and the following measurements: standard length, snout tip to dorsal-fin origin, snout tip to adipose-fin origin, snout tip to pelvic-fin origin, snout tip to anal-fin origin, dorsal-fin origin to caudal-fin origin, dorsal-fin origin to adipose-fin origin, caudal peduncle length, caudal peduncle depth, body depth at dorsal-fin origin, body width at dorsal-fin origin, head length, preopercle length, snout length, eye diameter, snout depth at anterior eye margin, head depth at tip of supraoccipital, head width at opercle and interorbital distance.

Two specimens, one of *H. steindachneri* and one of the new species, were cleared and counterstained (c&s) for cartilage and bone using the method outlined by Taylor, Van Dyke (1985) and two specimens of *H. steindachneri* were prepared as dry skeletons following the method described by Bemis *et al*. (2004). Five specimens from each basin were radiographed with a KUBTEC XPERT 40 System. Dissections followed the Ridewood method, as described in Bemis *et al*. (2004). Vertebrae of the Weberian apparatus were counted as four elements and the fused PU1+U1 of the caudal region as a single element. The osteological nomenclature followed Weitzman (1962) with modifications proposed by Sidlauskas, Vari (2008), and following the updates available on the Teleost Anatomy Ontology (TAO).

Images were taken using a Nikon DSLR, following the procedures of Sabaj Pérez (2009) and the stained specimens were photographed with a DFC295 digital camera attached to a Leica M205A stereomicroscope. The images were subsequently edited

in image editing software to standardize background lighting/contrast. Counts and measurements were taken on the left side of the specimens using a digital caliper with a precision of 0.01 mm. The measurements were compared through minimum, maximum, mean, and standard deviation. A Principal Component Analysis (PCA) was performed with logarithmic measures in PAST v. 4.10 software (Hammer *et al*., 2001). To correct the influence of body size on morphometric variation (*i.e*., allometry), each variable was regressed against standard length (SL), and the residuals from these regressions were used for subsequent multivariate analyses. PCA was applied to the residuals using the correlation matrix, which standardizes the variables prior to analysis. The first two principal components were used to visualize morphometric differentiation through scatterplots.

Molecular analysis. The DNA was isolated from muscle tissue using the Wizard Kit (Promega) and GoTaq Master Mix Kit (Promega) was used to amplify the region of interest, following the manufacturer's recommendations. A ±640 bp segment of the mitochondrial gene Cytochrome Oxidase I (COI), (the DNA Barcode of Hebert *et al*., 2003), was amplified and sequenced using Fish F1 and Fish R1 primers (Ward *et al*., 2005). The sequences were edited in the MEGA v. 11 program (Tamura *et al*., 2021) and aligned using the MUSCLE v. 5.1 algorithm (Edgar, 2021) implemented in MEGA. The Tamura-3 model (Tamura K., 1992) with gamma distribution (T92+G) was calculated as the most appropriate model in MEGA and used to calculate a genetic distance matrix between and within species. Sequences of the species available in the GenBank and BoldSystem were also used (Tab. 1). Phylogenetic relationships were investigated through an analysis of Bayesian Inference in BEAST v. 2.7.1 using strict uniform clock and Birth Death Model, on a run of 10 million generations, with parameters sampled every 1,000 steps and a burn-in of 10%.

Species delimitation was based on the analysis of morphological evidence (meristic, morphometric and coloration) combined with molecular data, including three delimitation analyses using mitochondrial DNA and the genetic distance analysis. Three models were used for the delimitation analyses: Poisson Tree Processes - PTP (Zhang *et al*., 2013), Generalized Mixed Yule-Coalescent - GMYC (Pons *et al*., 2006) and Assemble Species by Automatic Partitioning - ASAP (Puillandre *et al*., 2021). The PTP model infers putative species boundaries on a given non-ultrametric phylogenetic tree, for this, a Maximum Likelihood tree was calculated on MEGA using the (T92+G) model and uploaded to the website (https://species.h-its.org/ptp/). ASAP recovers species partitions from single locus sequence alignments. For this analysis, aligned sequences were submitted to the online server, with the K80 distance used as the model and other parameters used in default (https://bioinfo.mnhn.fr/abi/public/asap/). GMYC infers putative species boundaries on a given ultrametric phylogenetic tree. For this analysis, the ultrametric tree generated by BEAST was used in R v. 4.4.1 (Posit Team, 2024) with the package Species Limits by Threshold Statistics - SPLITS (Ezard *et al*., 2009). Outgroup taxa for DNA-based analyses included all species of the *Hypomasticus mormyrops* clade, as defined by Birindelli *et al*. (2020), *i.e*., *H. copelandii*, *H. mormyrops* (Steindachner, 1875), *H. santanai*, *H. steindachneri*, and *H. thayeri* (Borodin, 1929).

TABLE 1 | Voucher specimens of *Hypomasticus* species, accession numbers and locality information of taxa used in the molecular analysis.

Taxon	Voucher	Locality	Basin	Acession	References
H. cf. *steindachneri*	LBP 7502-35577	Rio Juquiá	Ribeira de Iguape	PX391179	Present study
H. cf. *steindachneri*	LBP 7502-35578	Rio Juquiá	Ribeira de Iguape	PX391180	Present study
H. cf. *steindachneri*	LBP 7444-35781	Lagoa Jurumirim	Ribeira de Iguape	FBCR032-09	Bold System
H. cf. *steindachneri*	LBP 26376-91938	Rio Poço Verde	Una do Prelado	PX391181	Present study
H. cf. *steindachneri*	LBP 2380-16073	Lagoa Feia	Rio de Janeiro	HM065002	Pereira *et al.* (2011)
H. cf. *steindachneri*	LBP 18618-49708	Rio Macabú	Rio de Janeiro	MT427927.1	Birindelli *et al.* (2020)
H. cf. *steindachneri*	LBP 10727-49707	Rio Macabú	Rio de Janeiro	MT427926.1	Birindelli *et al.* (2020)
H. cf. *steindachneri*	MCNIP 1465	Rio Mucuri	Mucuri	MUCU038-13	Bold System
H. cf. *steindachneri*	MCNIP 1396-1	Rio Mucuri	Mucuri	MUCU171-14	Bold System
H. cf. *steindachneri*	MCNIP 1396-2	Rio Mucuri	Mucuri	MUCU161-14	Bold System
H. cf. *steindachneri*	MCNIP 1396-3	Rio Mucuri	Mucuri	MUCU162-14	Bold System
H. cf. *steindachneri*	MCNIP 1466	Rio Mucuri	Mucuri	MUCU190-13	Bold System
H. cf. *steindachneri*	MZUEL 16474	Rio Pardo	Pardo	PX391179	Present study
H. cf. *steindachneri*	MZUEL 17996	Rio Pardo	Pardo	PX391180	Present study
H. steindachneri	JEQUI 4034	Rio Itacambiruçu	Jequitinhonha	JEQUI045-12	Pugedo *et al.* (2016)
H. steindachneri	JEQUIJQ 48	Rio Jequitinhonha	Jequitinhonha	JEQUI091-12	Pugedo *et al.* (2016)
H. steindachneri	JEQUIJQ 47	Rio Jequitinhonha	Jequitinhonha	JEQUI090-12	Pugedo *et al.* (2016)
H. steindachneri	JEQUI 6009	Rio Jequitinhonha	Jequitinhonha	JEQUI132-12	Pugedo *et al.* (2016)
H. steindachneri	JEQUI 6023	Rio Itacambiruçu	Jequitinhonha	JEQUI134-12	Pugedo *et al.* (2016)
H. steindachneri	JEQUILGC 2984	Rio Araçuai	Jequitinhonha	JEQUI224-13	Pugedo *et al.* (2016)
H. steindachneri	JEQUILGC 2983	Rio Araçuai	Jequitinhonha	JEQUI223-13	Pugedo *et al.* (2016)
H. steindachneri	MCNIP 379	Rio Jequitinhonha	Jequitinhonha	KF568994.1	Ramirez *et al.* (2016)
H. thayeri	LGC 5784	Rio Santo Antônio do Cruzeiro	Doce	MK770210	Mendes *et al.* (unpub.)
H. copelandii	LGC 7107	Rio Paraíba do Sul	Paraíba do Sul	MK770216	Mendes *et al.* (2022)
H. copelandii	LGC 7108	Rio Paraíba do Sul	Paraíba do Sul	MK770217	Mendes *et al.* (2022)
H. copelandii	LGC 7109	Rio Paraíba do Sul	Paraíba do Sul	MK770218	Mendes *et al.* (2022)
H. copelandii	LGC 5393	Rio Corrente Grande	Doce	MK770205	Mendes *et al.* (2022)
H. copelandii	LGC 5394	Rio Corrente Grande	Doce	MK770206	Mendes *et al.* (2022)
H. copelandii	MCNIP 459	Rio Manhuaçu	Doce	KF568978.1	Ramirez *et al.* (2016)
H. mormyrops	MZUEL 8022	Rio Bananal	Paraíba do Sul	KX020572	Ramirez *et al.* (2016)
H. mormyrops	LBP 8103-37539	Rio Pomba	Paraíba do Sul	MT427916	Birindelli *et al.* (2020)
H. mormyrops	LBP 8103-37540	Rio Pomba	Paraíba do Sul	MT427917	Birindelli *et al.* (2020)
H. mormyrops	ZUEC 8198 - LGC 4965	Rio Mutum	Doce	RDOCE282-14	BOLD System
H. mormyrops	ZUEC 8198 - LGC 4966	Rio Mutum	Doce	RDOCE283-14	BOLD System
H. mormyrops	ZUEC 8198 - LGC 4967	Rio Mutum	Doce	RDOCE293-14	BOLD System
H. santanai	LBP 28094-96860	Rio Gongogi	Contas	MT427922	Birindelli *et al.* (2020)
H. santanai	LBP 28094-96862	Rio Gongogi	Contas	MT427924	Birindelli *et al.* (2020)
H. santanai	LBP 28094-96863	Rio Gongogi	Contas	MT427925	Birindelli *et al.* (2020)
H. santanai	LBP 28094-96861	Rio Gongogi	Contas	MT427923	Birindelli *et al.* (2020)

RESULTS

Morphological differentiation

Morphometry. Although some overlap was observed in the scatterplot, the principal component analysis (PCA), revealed meaningful morphological variation among specimens from the five sampled populations. The first three principal components (PCs) together accounted for 56.8% of the total morphological variance after allometric correction (Tab. 2), with PC1 explaining 32.9%, PC2 15.1%, and PC3 8.7%. PC1 primarily represented variation in head morphology, with high positive loadings for head width at the opercle (0.32), interorbital distance (0.31), head depth at the tip of the supraoccipital (0.29), and preopercle length (0.29). This axis also captured differences in overall body configuration, particularly the distances from the snout tip to the origins of the dorsal and pelvic fins (0.32 and 0.31, respectively), in contrast with a negative loading for the distance between the dorsal-fin origin and the caudal-fin origin (-0.21). PC2 was positively associated with variation in head and in snout length (0.29 and 0.38, respectively), the distance from the dorsal-fin origin to the adipose-fin origin (0.37), and negatively associated with the distance from the snout tip to the anal-fin origin (-0.33) and body depth at the dorsal-fin origin (-0.31).

TABLE 2 | Variable loadings, eigenvalues, and variance in percentages in the two first axes of a PCA of *H. steindachneri* and *H.* cf. *steindachneri* populations; discriminant characters in bold.

	PC 1	PC 2
Eigenvalue	5.928	2.712
% variance	32.937	15.069
Snout tip to dorsal-fin origin	**0.32688**	0.03479
Snout tip to adipose-fin origin	0.1436	0.20841
Snout tip to pelvic-fin origin	**0.30981**	-0.22224
Snout tip to anal-fin origin	0.26154	**-0.33435**
Dorsal-fin origin to caudal-fin origin	-0.21008	0.26634
Dorsal-fin origin to adipose-fin origin	-0.17341	**0.3769**
Caudal peduncle length	-0.13581	0.20942
Caudal peduncle depth	0.12707	-0.263
Body depth at dorsal-fin origin	0.065593	**-0.31671**
Body width at dorsal-fin origin	0.11333	-0.073941
Head length	**0.27078**	**0.2994**
Preopercle length	**0.29943**	0.24021
Snout length	0.17237	**0.38642**
Eye diameter	0.19135	-0.044524
Snout depth at anterior eye margin	0.24789	0.19482
Head depth at tip of supraoccipital	**0.29568**	0.0089302
Head width at opercle	**0.32373**	0.15197
Interorbital distance	**0.31498**	0.051129

The scatterplot (Fig. 2) showed partial separation among specimens from different river basins. Specimens from the Jequitinhonha basin (type-locality) formed a distinct cluster, with minimal overlap with other groups and high PC1 scores, indicating broader heads, wider interorbital distances, and shorter bodies. Specimens from the Ribeira de Iguape basin also clustered separately, overlapping slightly with other populations but positioned negatively along PC1 and positively along PC2, suggesting narrower heads, longer snouts, and more elongated bodies. Specimens from the Doce, Rio de Janeiro, and Pardo basins overlapped considerably among themselves, though they also partially separated. Individuals from the Doce and Rio de Janeiro basins were mostly located on the negative side of PC1, whereas those from the Pardo basin were more centrally positioned in the plot. The substantial overlap among populations indicates that, although they differ in mean morphology, morphological variation within species is of similar magnitude to variation among the species means.

Meristic. Most of the counts did not differ significantly between populations from different drainages (*e.g.*, all share 12 scales around the peduncle, four premaxillary teeth, four dentary teeth, two unbranched and ten branched dorsal fin rays). However, some specimens from the Pardo basin exhibited counts that are rare, not only within populations of *H. steindachneri*, but also among most of the anostomids. These included nine branched pelvic-fin rays in nine of 19 specimens (*vs.* eight), nine branched anal-fin

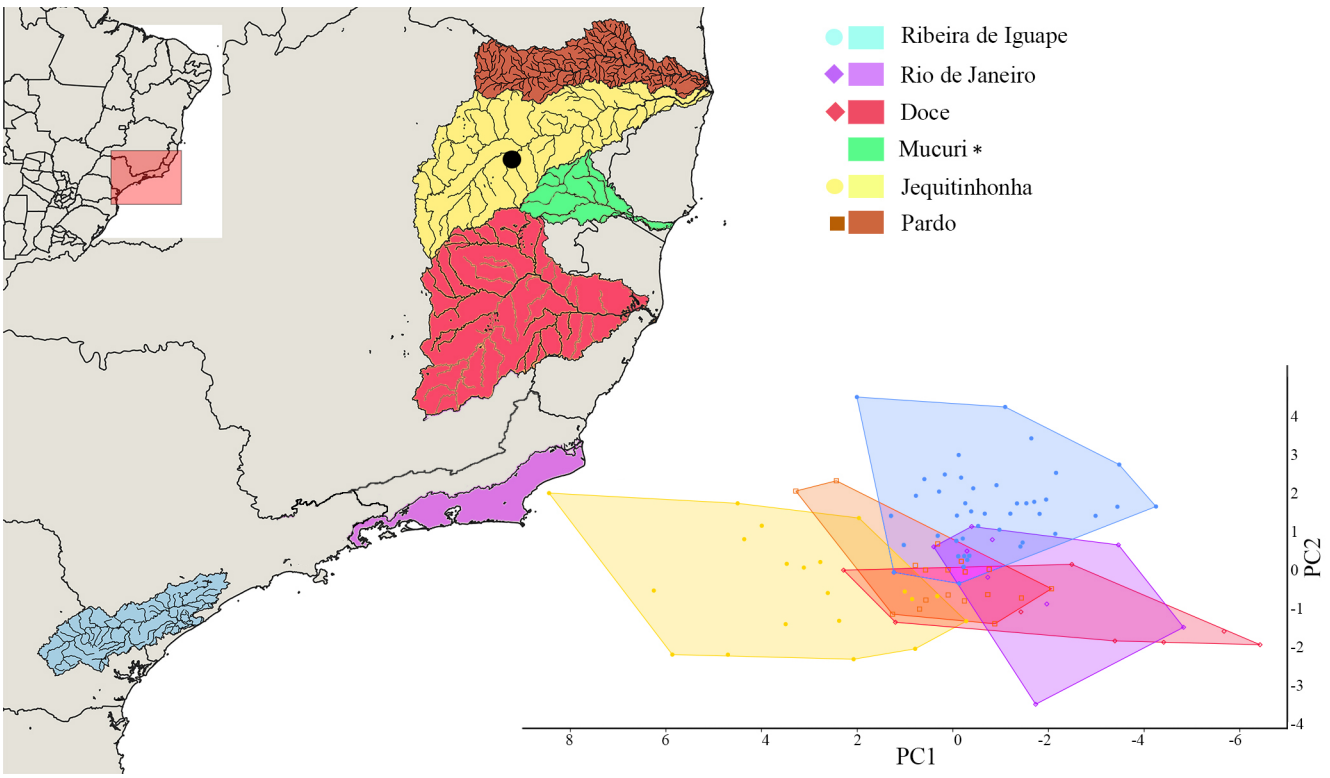

FIGURE 2 | Map highlighting the coastal basins where *Hypomasticus steindachneri* is found and the projection of individual scores of the first and second principal components of the samples of *H. steindachneri* from the different basins. Asterisk indicates specimens not included in the analysis. Black circle indicates type-locality.

rays in one of 19 specimens (*vs*. eight) and eight dorsal branched caudal-fin rays in one of 19 specimens (*vs*. nine). The variation in pelvic-fin rays is particularly noteworthy, as it was observed in almost half of the analyzed specimens. In some individuals, this variation was present only on one side of the body, while the other side displayed the typical condition of eight rays. It is important to note that most of the specimens from the Pardo River were collected from or around the Machado Mineiro Fish Hatchery Station, and these atypical variations may be related to captive breeding.

The number of scales on the lateral line did differ appreciably among the populations. The northernmost populations (Pardo, Jequitinhonha, Doce, Mucuri) exhibited a consistent range of 35 to 37 scales, with a mode of 36 scales (n = 51). In contrast, the southernmost populations (Rio de Janeiro and Ribeira de Iguape) had a range of 36 to 38 scales, with a mode of 37 scales (n = 53). Both groups possess an exclusive condition (35 and 38 scales), that allow some distinction between the specimens, despite having a considerable overlap (36 and 37 scales).

Coloration. All specimens exhibit the characteristic pattern of three large dark blotches on the midlateral portion of the body: the first below the dorsal fin, the second above the anal fin, and the third at the end of the caudal peduncle. This distinctive pattern is shared with most of its congeners (*e.g*., *H. copelandii*, *H. mormyrops*, *H. thayeri* and *H. santanai*) but also with several other anostomids, such as most species of *Megaleporinus* Ramirez, Birindelli & Galetti, 2017 and many *Leporinus* (*e.g*., *L. friderici* (Bloch, 1794), *L. piau* Fowler, 1941, *L. lacustris* Amaral Campos, 1945, *L. trimaculatus* Garavello & Santos, 1992). The populations of *H. steindachneri* vary somewhat in the intensity and size of these blotches.

Specimens from the Jequitinhonha, Doce, Mucuri and Pardo basins display very conspicuous dark blotches extending across two or three scales horizontally and one or two scale rows vertically. On the other hand, specimens from Rio de Janeiro and Ribeira de Iguape River basins exhibited lighter, very diffuse blotches, extending through four or five scales horizontally and two or three scale rows vertically. As observed in the meristic data, the northernmost and southernmost populations of *H. steindachneri* each display an exclusive pattern.

Mouth position. Despite the descriptive name *Hypomasticus* (from Greek "hypo" meaning less than, under, or beneath, and "masticus" from "mastáx", meaning "that with which one chews"), the genus currently includes many species that do not exhibit inferior or subterminal mouths. This trait appears to be more homoplastic within the family than previously hypothesized (Sidlauskas, Vari, 2008; Sidlauskas *et al*., 2025). Both the holotype of *H. steindachneri* and other individuals collected in the Jequitinhonha basin have the mouth in a terminal position, with the mouth cleft longitudinally aligned with the ventral margin of the eye orbit (Figs. 3D, E, F). This condition is also observed in the populations of the Pardo, Mucuri and Doce basins, but not in the specimens from Rio de Janeiro and Ribeira de Iguape basins. In the southernmost populations, the mouth cleft aligns longitudinally with the ventral margin of the second infraorbital bone in specimens larger than 90 mm SL, a position more appropriately classified as subterminal (Figs. 3A, B, C). This characteristic resembles the condition in the congeners *H. santanai* and *H. thayeri*, though not *H. mormyrops*, which possesses a fully inferior mouth position.

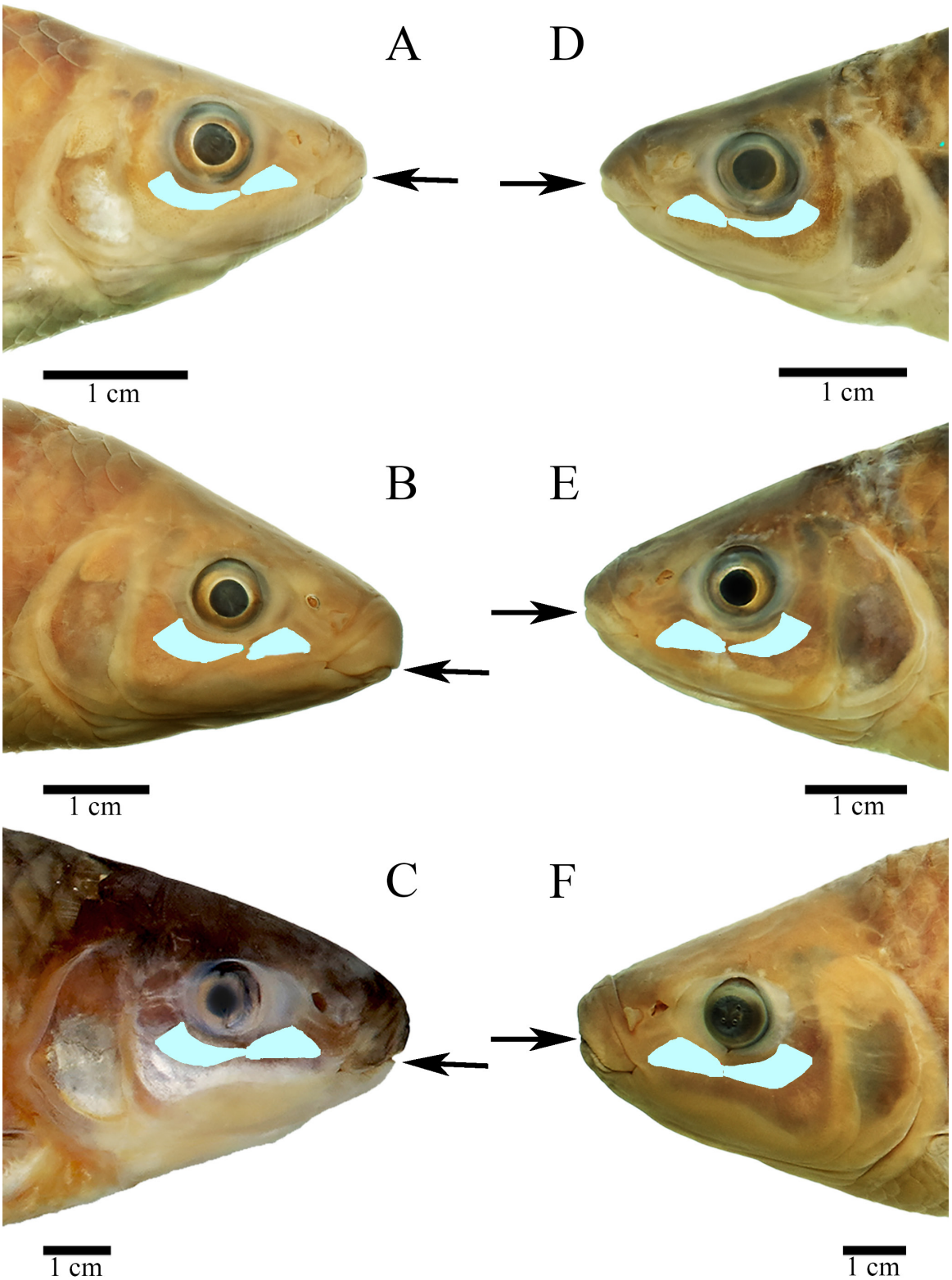

FIGURE 3 | Comparison of mouth position through the alignment of the mouth opening with the margin of the orbit and the infraorbital bones (highlighted in gray). On the left, Ribeira de Iguape specimens (*Hypomasticus* cf. *steindachneri*): **A.** MZUSP 38608, 100.3 mm SL, **B.** LISDEBE 3, 135.7 mm SL, **C.** MZUSP 125891, 273.4 mm SL. On the right, Jequitinhonha (type-locality) and Pardo specimens: **D.** MZUEL 16474, 102.1 mm SL, **E.** MZUEL 16474, 140.6 mm SL, **F.** LISDEBE 7905, 241.2 mm SL.

Molecular differentiation

Genetic distance. A total of 39 COI sequences were used in the molecular analysis (Tabs. 1, 3), including all *Hypomasticus* species inhabiting the Brazilian coastal drainages. The results corroborate the morphological distinctions discovered among specimens of *Hypomasticus steindachneri* (and *H.* cf. *steindachneri*) herein. Namely, both analyses clearly divide the specimens into two groups: a northern group, comprising fish from the Contas, Pardo, Jequitinhonha, Mucuri and Doce basins, and a southern group, comprising the Rio de Janeiro and Ribeira de Iguape basins. Within *H. steindachneri*, this pattern is evident in the relatively low mean genetic distances between specimens from the type-locality (Jequitinhonha) and specimens from the Pardo and Mucuri rivers (0.07% and 1.8%, respectively). In contrast, higher distances were observed between the type-locality specimens and those from Rio de Janeiro and Ribeira de Iguape (6.9% and 7%, respectively). The mean distance between the latter two was also relatively low (1%). A similar pattern of high genetic distances between specimens from northern and southern drainages was observed in populations of *H. copelandii* (3.6% between Doce and Paraíba do Sul specimens) and *H. mormyrops* (5.4% between Doce and Paraíba do Sul specimens). On the other hand, all intraspecific distances were significantly low, ranging from 0 to 0.3%.

Species delimitation analyses. The GMYC and ASAP analyses recovered the same nine Molecular Operational Taxonomic Units (MOTUs). These delimitations suggest that the specimens identified as *H. steindachneri* are three distinct MOTUs: one composed of the specimens from the Rio de Janeiro and Ribeira de Iguape basins, another from the Mucuri basin and the last from the Jequitinhonha and Pardo basins (Fig. 4). The PTP delimitation recovered 14 MOTUs and presented an alternative scenario for *H. steindachneri*, splitting the southernmost group into two MOTUs: one for the Rio de Janeiro specimens and one for those from Ribeira de Iguape. It also divided the Mucuri specimens into four MOTUs but agreed with the other delimitations in grouping the Jequitinhonha and Pardo specimens into a single MOTU.

TABLE 3 | T92+G mean genetic distance among the nominal species of *Hypomasticus* and the populations of *H. steindachneri* (below the diagonal) and values of standard error (above the diagonal) using the COI gene dataset. Numbers in bold represent intragroup distances. Values expressed as percentage.

	1	2	3	4	5	6	7	8	9	10	11
1. *H. santanai* (Contas)	**0.0**	1.0	1.1	1.2	1.2	1.4	1.0	1.0	1.0	1.3	1.3
2. *H. mormyrops* (Doce)	5.5	**0.2**	0.9	1.0	0.9	1.2	0.8	0.7	0.8	1.2	1.1
3. *H. mormyrops* (Paraiba do Sul)	6.7	5.4	**0.0**	0.8	1.0	1.1	0.8	0.8	1.0	1.2	1.2
4. *H. copelandii* (Doce)	6.6	5.4	3.6	**0.0**	0.7	0.8	1.0	1.0	1.1	0.9	0.9
5. *H. copelandii* (Paraiba do Sul)	7.4	5.5	4.7	3.6	**0.1**	0.8	1.1	1.0	1.1	0.9	0.9
6. *H. thayeri* (Doce)	8.1	7.2	6.3	3.7	3.4	**n/c**	1.3	1.2	1.2	0.6	0.6
7. *H. cf. steindachneri* (Pardo)	5.9	4.5	5.1	3.8	7.2	8.6	**0.3**	0.3	0.6	1.2	1.2
8. *H. steindachneri* (Jequitinhonha)	5.2	3.3	4.6	3.9	6.5	7.9	0.7	**0.2**	0.5	1.2	1.2
9. *H. cf. steindachneri* (Mucuri)	5.4	4.2	6.0	4.0	6.7	8.2	2.8	1.8	**0.2**	1.1	1.3
10. *H. cf. steindachneri* (Rio de Janeiro)	7.7	6.9	6.7	4.1	3.7	2.3	7.5	6.9	7.0	**0.2**	0.3
11. *H. cf. steindachneri* (Ribeira de Iguape)	8.0	7.0	6.0	4.2	3.0	2.1	8.0	7.0	8.0	1.0	**0.1**

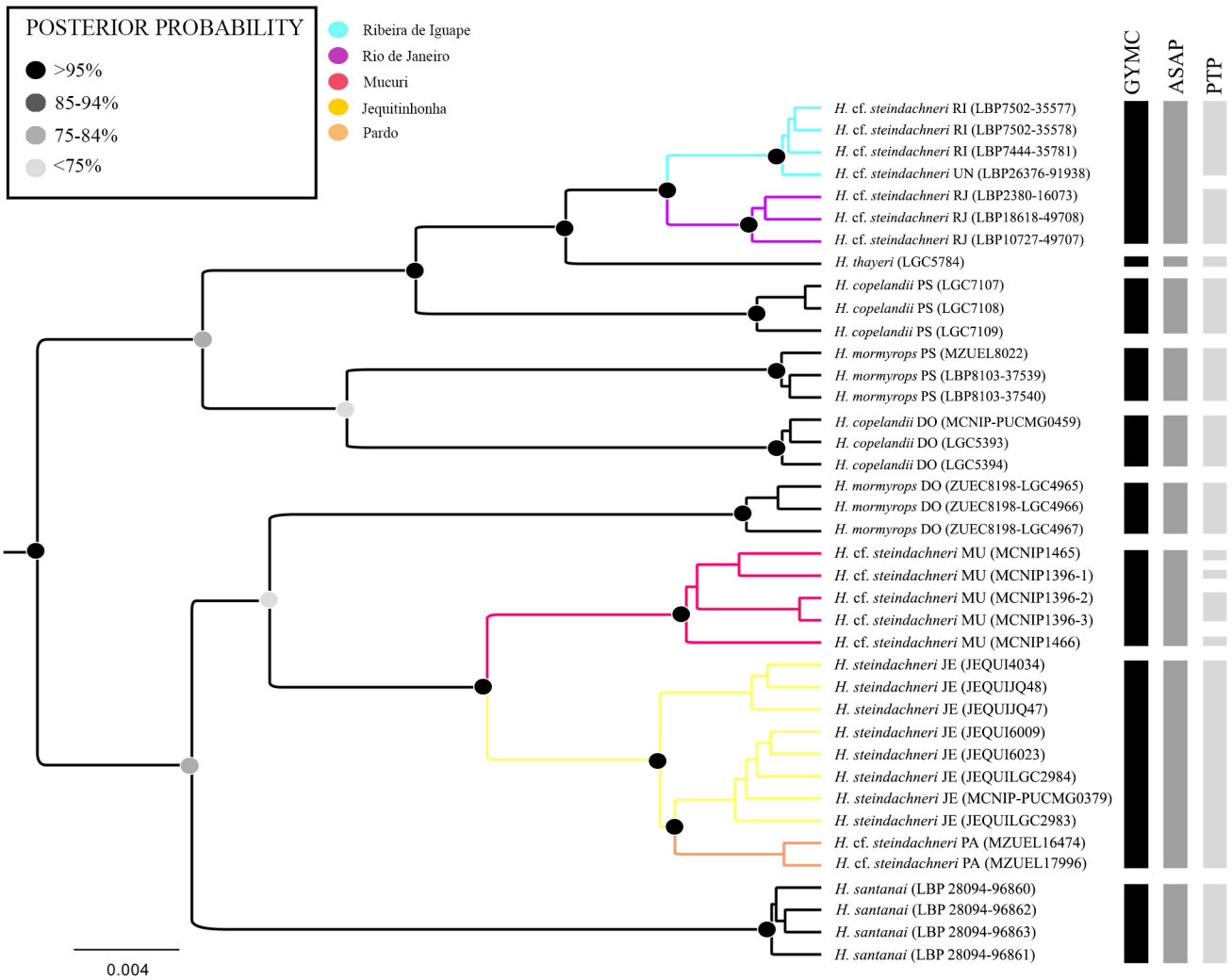

FIGURE 4 | Bayesian inference ultrametric phylogenetic tree showing the relationships among *Hypomasticus* species based on DNA barcode. Vertical bars indicate the results of the species delimitation analysis. DO: Doce, JE: Jequitinhonha, MU: Mucuri, RJ: Rio de Janeiro, PA: Pardo and RI: Ribeira de Iguape.

All the delimitations provided the same result for the remaining species analyzed. They recovered nine MOTUs, separating both the *H. copelandii* and *H. mormyrops* specimens in one MOTU of the Doce River and one MOTU of the Paraíba do Sul River. The *H. santanai* specimens were recovered as a single MOTU in all analyses.

Taxonomic assessment. Meristic and molecular analysis both revealed a consistent separation of specimens from the northernmost basins, all included in the Northeastern Atlantic Forest ecoregion, from those in the southernmost basins, which are part of the Fluminense and Ribeira de Iguape ecoregions (Abell *et al.*, 2008). This division is further strengthened by the phylogenetic tree generated by Bayesian inference. Specimens from the southernmost basins were found to be sister group to *H. thayeri* and nested within a clade composed of specimens of *H. copelandii* and *H. mormyrops* from the Paraíba do Sul basin. In contrast, the specimens from the northernmost basins

were recovered as the sister group to specimens of *H. mormyrops* from the Doce basin, together forming the sister clade to *H. santanai.* This topology not only suggests that *H. steindachneri* is currently composed of more than one species, but also that these species are more closely related to other congeners than to each other.

Specimens from the Rio de Janeiro and Ribeira de Iguape diverged by only 1% at the COI locus and were proposed as representing a single species (or MOTU) by two of the delimitation analyses. Additionally, these populations shared several morphological traits not found in other populations, including a greater number of scales on the lateral line, larger and more diffuse dark midlateral blotches and a subterminal mouth. Although there is a minor genetic distance, the combination of the molecular and morphological evidence strongly suggests that the Ribeira de Iguape and Rio de Janeiro specimens represent populations of the same species, which can be confidently described and visually distinguished from *H. steindachneri*.

The northeastern clade, which includes specimens from the Jequitinhonha River basin (type-locality), was grouped with specimens from the Pardo River basin, with less than 1% molecular distance between them, and identified as a single species in all delimitation analyses. In contrast, specimens from the Mucuri River basin exhibited a notable molecular distance (1.8% with Jequitinhonha and 2.8% with Pardo specimens) and were distinctly separated in all the molecular delimitation analyses. Specimens from the northeastern clade shared a distinctive set of morphological traits (disregarding the anomalous counts observed among the Pardo specimens of likely hatchery origin), including fewer scales on the lateral line, smaller conspicuous midlateral blotches, and a terminal mouth. Although the molecular data indicate that the Mucuri specimens may belong to a different species, the few Mucuri specimens available did not differ in meristics or coloration from the Doce, Pardo and Jequitinhonha specimens. Their phylogenetic proximity and the shared coloration and meristic traits suggest that all specimens from the northeastern Atlantic Forest may belong to a single species with deep population-level structuring.

The primary factors influencing our decision to include all these populations in a single species is the limited availability of specimens from the Mucuri River and the absence of molecular data from the Doce River basin. A larger number of specimens from the Mucuri population would allow a more robust morphometric analysis, particularly in assessing whether these individuals are indeed morphologically similar to those from the Doce basin. Likewise, molecular data from Doce specimens would provide critical insights into their genetic distinctiveness. This population appears to have a more restricted distribution within the basin (see Ecological notes), and although it shares similar meristic counts and coloration patterns with the Mucuri specimens, it may exhibit significant genetic divergence. The inclusion of these specimens in future analyses could therefore impact species delimitation. In view of these limitations and based on the available evidence, we have chosen to include the populations from the Jequitinhonha, Pardo, Mucuri, and Doce rivers within our concept of *Hypomasticus steindachneri.*

Hypomasticus steindachneri (Eigenmann, 1907)

(Figs. 5–15; Tab. 4)

Leporinus affinis Steindachner, 1875b:228, Pl.3 (original description; type-locality: rio Araçuaí, tributary of rio Jequitinhonha, Minas Gerais, Brazil; holotype: NMW 68405). Preoccupied by *Leporinus affinis* Günther, 1864. Replaced by *Leporinus steindachneri* Eigenmann, 1907.

Leporinus megalepis Günther, 1864:307 (part).

Leporinus steindachneri Eigenmann, in Eigenmann, Ogle, 1907:9 (type-locality: rio Araçuaí, tributary of Rio Jequitinhonha, Minas Gerais, Brazil; holotype: NMW 68405. Replacement for *Leporinus affinis* Steindachner, 1875). —Garavello, Britski in Reis *et al*., 2003:78 (in part, catalog). —Latini, Petrere Jr., 2004:74 (mention, Doce River basin, Brazil). —Pompeu, Martinez, 2007 (register of migratory behavior, Mucuri River basin). —Andrade Neto, 2009:25 (checklist). —Sarmento-Soares *et al*., 2010:52–55 (checklist, Itanhém River basin, Brazil). —Meireles, 2012 (ontogeny). —Camelier, Zanata, 2015 (distribution). —Pugedo *et al*., 2016:344 (comparative molecular material: Jequitinhonha River basin, Brazil). —Ramirez *et al*., 2016:1206, 1210, 1211 (phylogenetic relationships based on molecular data: Jequitinhonha River basin, Brazil). —Ramirez *et al*., 2017:310, 320 (phylogenetic relationships based on molecular data: Jequitinhonha River basin, Brazil). —Assega, Birindelli, 2019:142 (comparative material, Pardo basin, Brazil). —Silva *et al*., 2020:4 (catalog: Pardo River basin).

Hypomasticus steindachneri. —Birindelli *et al*., 2020:416, 417, 421–423 and supplemental material (comparative material and phylogenetic relationships based on molecular data: Jequitinhonha, Pardo and Mucuri basins, Brazil). —Salgado *et al*., 2021:65–73 (cytogenetic analysis: Doce River basin, Brazil). —Sidlauskas *et al*., 2021:629, 633 (phylogenetic relationships based on molecular data: Jequitinhonha River basin, Brazil). —Mendes *et al*., 2022:5, 10 (phylogenetic relationships based on molecular data: Jequitinhonha River basin, Brazil). —Toledo-Piza *et al*., 2024:48 (in part, catalog). —Sidlauskas *et al*., 2025:26–27, figs. 5, 7 and supplemental material (phylogenetic relationships based on molecular data: Jequitinhonha River basin, Brazil).

Hypomasticus cf. *steindachneri*. —Birindelli *et al*., 2020:423 (in part, comparative material, Doce, Jucuruçu, Mucuri and São Mateus basins, Brazil).

FIGURE 5 | *Hypomasticus steindachneri*, MZUEL 16474, 142.9 mm SL, preserved (**A**) and live specimen (**B**).

Diagnosis. *Hypomasticus steindachneri* can be distinguished from *Hypomasticus arcus* (Eigenmann, 1912), *H. despaxi* (Puyo, 1943), *H. granti* (Eigenmann, 1912), *H. lebaili* (Géry & Planquette, 1983), *H. lineomaculatus* Birindelli, Peixoto, Wosiacki & Britski, 2013, *H. melanostictus* (Norman, 1926), *H. megalepis*, *H. santosi* (Britski & Birindelli, 2013) and *H. torrenticola* Birindelli, Teixeira & Britski, 2016 by possessing 12 scale rows around the caudal peduncle (*vs*. 16), can be distinguished from *H. australis* (described below), *H. mormyrops*, *H. santanai* and *H. thayeri* by possessing a terminal mouth (*vs*. an inferior mouth in *H. mormyrops* or a subterminal mouth in *H. australis*, *H. santanai* and *H. thayeri*), can be distinguished from *H. gomesi* (Garavello & Santos, 1981), *H. nijsseni* (Garavello, 1990) and *H. tepui* (Birindelli, Britski & Provenzano, 2019) by possessing three midlateral blotches (*vs*. additional smaller blotches formed by dermal pigment, five of which form an interrupted "X" in *H. gomesi* and *H. nijsseni* or four dark longitudinal stripes in *H. tepui*), can be distinguished from *H. copelandii* by possessing 35–37 perforated scales in the lateral line (*vs*. 38–41 in *H. copelandii*). Additionally, it further differs from *H. australis* by possessing the mouth cleft longitudinally aligned with the ventral margin of the eye orbit (*vs*. mouth cleft longitudinally aligned with the ventral margin of second infraorbital bone) and three conspicuous midlateral blotches, extending through 2–3 scales horizontally and 1–2 scale rows vertically (*vs*. three diffuse midlateral blotches, extending through 4–5 scales horizontally and 2–3 scale rows vertically).

Description. Morphometric data of examined specimens in Tab. 4. Large-sized species of *Hypomasticus*, largest examined specimen 357.8 mm SL. Body tall, elongated and laterally compressed. Dorsal profile almost straight from snout to tip of supraoccipital and gently convex from tip of supraoccipital to dorsal-fin origin, straight to slightly convex in dorsal-fin base, somewhat straight or slightly convex from posterior insertion of dorsal fin to adipose fin origin, broadly convex in adipose-fin base and gently concave from posterior insertion of adipose-fin to origin of upper lobe of caudal fin. Ventral profile straight to slightly convex from lower jaw to end of branchiostegal rays and broadly convex from end of branchiostegal rays to posterior insertion of anal-fin rays, gently concave from this point to origin of lower lobe of caudal-fin. Greatest body depth at dorsal-fin origin. Mouth terminal, its cleft longitudinally aligned with ventral margin of eye orbit, upper lip thicker than lower, both covered with small papillae, snout truncate. Teeth incisiform, unicuspid and with blunt cutting edge.

Vertebrae 36 (6), with ribs present on vertebrae 5 to 18 (6). Supraneurals 7 (5) or 8 (1). First dorsal-fin pterygiophore inserted posterior to neural spine of vertebra 11 (6). First anal-fin pterygiophore inserted posterior to haemal spine of vertebra 25 (6). Premaxillary bone with 4 (47) teeth arranged side by side and gently decreasing in size from symphyseal tooth. Dentary bone with 4 (47) teeth arranged side by side, and gently decreasing in size from symphyseal tooth.

Scales large and cycloid, with 10–14 radii (3). Lateral line complete with 35 (4), 36* (27) or 37 (16) perforated scales. Transverse series with 3 (2) or 4* (45) scales from dorsal-fin origin to lateral line and 3.5* (42) or 4 (5) scales from lateral line to pelvic-fin base. 10* (4), 11 (23) or 12 (14) predorsal scales. 12* (46) horizontal scale rows around caudal peduncle.

Dorsal fin ii,10* (47), origin slightly anterior of vertical through pelvic-fin origin, distal margin rounded. Pectoral fin i,14 (19), 15* (25), or 16 (4), base located posterior to

TABLE 4 | Morphometric data of *Hypomasticus steindachneri* (50 specimens). SD = Standard deviation. Asterisks represent unavailable data of the holotype.

	Holotype	Mean	Min-Max	SD
Standard length (mm)	323	185.6	79.37–357.8	–
Percentages in standard length				
Snout tip to dorsal-fin origin	46	48.6	45.4–51	1.2
Snout tip to adipose-fin origin	*	84.1	82.3–86.8	1.1
Snout tip to pelvic-fin origin	50.4	52.4	48.3–56.8	1.8
Snout tip to anal-fin origin	*	80.3	77.5–84.7	1.6
Dorsal-fin origin to caudal-fin origin	*	51.3	47.6–56.9	1.7
Dorsal-fn origin to adipose-fin origin	38.9	37.6	34.7–43.4	1.6
Caudal peduncle length	11.2	10.3	7.2–12.5	1
Caudal peduncle depth	11.2	10.9	10.2–11.9	0.3
Body depth at dorsal-fin origin	32.1	28.9	26.9–32.5	1.4
Body width at dorsal-fin origin	*	15.3	12.3–18.2	1.6
Head length	21.5	23.4	20.4–26.4	1.3
Percentages in head length				
Preopercle length	73.1	76.4	71.5–83.2	2.7
Snout length	40.3	39.8	33.4–52.8	2.9
Eye diameter	15.3	18.8	14.8–22.6	1.7
Snout depth at anterior eye margin	*	53.9	47.9–59.7	2.8
Head depth at tip of supraoccipital	93	82.6	73.4–91.5	4.2
Head width at opercle	*	57.6	49.1–63.6	3.8
Interorbital distance	46.9	41.5	35.9–47.4	2.6

gill opening, its tip extending more than half distance between origins of pectoral and pelvic fin, distal margin rounded. Pelvic fin i,8* (32) or 9 (15), distal margin rounded. Anal fin iii,8* (46) or iii,9 (1), distal margin straight or slightly rounded. Caudal-fin rays i,8,8,i (1) or i,9,8,i* (46), caudal fin forked, upper lobe slightly more elongated than lower lobe.

Osteology. Seven supraneurals along dorsal midline, each closely associated with anterodorsal margin of neural spine of fourth to tenth vertebrae (Fig. 6A), supraneurals with rod-shape ventral portion with cartilaginous tip that expands dorsally into laminar plate, first supraneural with rounded dorsal tip and positioned between neural complex and neural spine of fourth vertebral centrum. Infraorbital series composed of six plate-like infraorbitals and associated antorbital, supraorbital and nasal (Fig. 6B). First infraorbital more or less triangular, with dorsal lamina well-developed and length almost twice height. Posteroventral portion overlapped by second infraorbital. Sensory canal extending diagonally, bearing 4 pores; first opening below anterior portion of antorbital, second directed to ventral portion of maxilla and third and fourth located on ventralmost portion of first infraorbital.

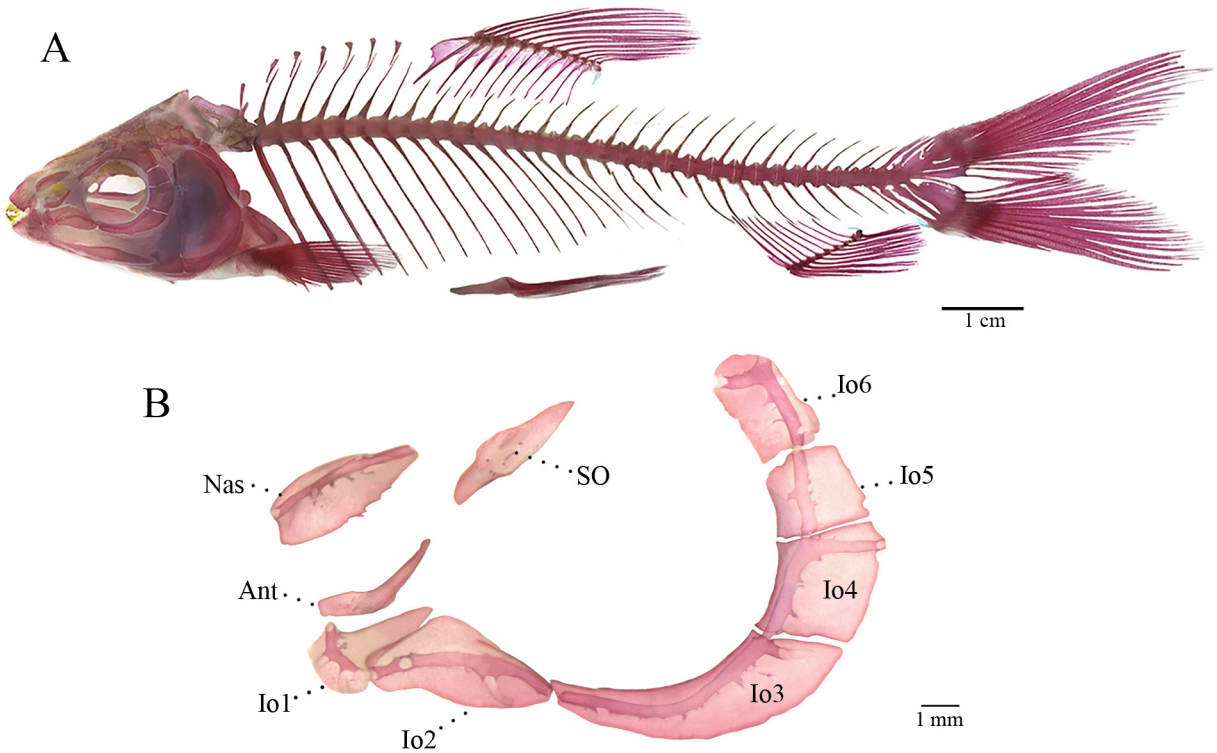

FIGURE 6 | *Hypomasticus steindachneri*, MZUEL 16474, 99.78 mm SL, lateral view of the body skeleton (**A**) and infraorbital bones and associated elements (**B**). Nas: nasal, Ant: antorbital, Io1-6: infraorbital and SO: supraorbital.

Second infraorbital elongated and triangular with dorsal margin convex and wavy ventral margin. Sensory canal slightly curved dorsally and extending horizontally, bearing four pores. First opening connecting to canal system of first infraorbital, second located on anteromedial section, third directed to posteroventral margin and forth connecting to canal system of third infraorbital. Area of contact between second and third infraorbitals narrow. Third infraorbital falciform and elongate, with maximum height contained three times in length. Ventral lamina much larger than dorsal one. Sensory canal extending horizontally, gently ascending after middle portion, bearing four pores. First opening connecting to canal system of second infraorbital, second located at anteroventral region, third directed to posterior bony margin and forth connecting to canal system of fourth infraorbital. Fourth infraorbital almost quadrangular, slightly higher than longer. Sensory canal tripartite, main canal running near anterior margin of bone towards fifth infraorbital and branch long and directed posteriorly towards opercle. Three pores, one on each tip of sensory canal. Fifth infraorbital quadrangular with irregular margins. Sensory canal running vertically towards sixth infraorbital. Two pores, one on each tip of sensory canal. Sixth infraorbital rectangular, with rounded dorsal margin, with maximum length contained two times in height. Sensory canal tripartite, main canal running vertically near posterior margin of bone. Four pores, one on each tip of sensory canal and one on posteroventral margin. Antorbital not bearing

canal, curved (boomerang shaped), with anterior portion slightly broader and posterior ascending process thinner and directed to supraorbital. Supraorbital not bearing canal, rhomboid and with irregular margins. Nasal ovoid and plate-like, with anterior portion broader than posterior and irregular ventral margin. Sensory canal gently ascending near dorsal margin. Five pores, two on anterior portion and three on posterior, with third and fourth proximate, almost united. Jaws composed by premaxilla, maxilla, dentary, anguloarticular and retroarticular (Fig. 7). Teeth incisiform, broad, with concave scoop-like lingual fossa boarded by ridges along lateral margins. Symphyseal teeth with convex cutting edge. Remaining teeth blunt with more irregular cutting edges, second and third teeth of premaxilla almost bicuspid. Teeth decreasing gradually in size laterally.

Premaxillary bone somewhat triangular, with irregular anterior and posterior margins, straight ventral margin and conical dorsal margin, dorsal process slightly bending posteriorly, anterodorsal margin with small protuberance and posteroventral margin distinctly rounded. Maxillary bone arranged vertically, with dorsal tip close to middle portion of premaxilla, bone dumbbell-shaped, with ventral portion wider than dorsal, and dorsal tip thin and curved medially. Lower jaw trapezoidal. Dentary bone large and thick, articulating tightly with anguloarticular. Anguloarticular ascending dorsally with posterodorsal margin of dentary. Retroarticular small, located at depression on anteroventral margin of dentary. Suspensorium L-shaped (Fig. 8), with longitudinal axis longer wider than vertical axis. Subopercle elongated and horn shaped, overlapped by opercle and interopercle. Opercle large and thin, somewhat semicircular, with straight anterior margin, irregular posterodorsal margin and and

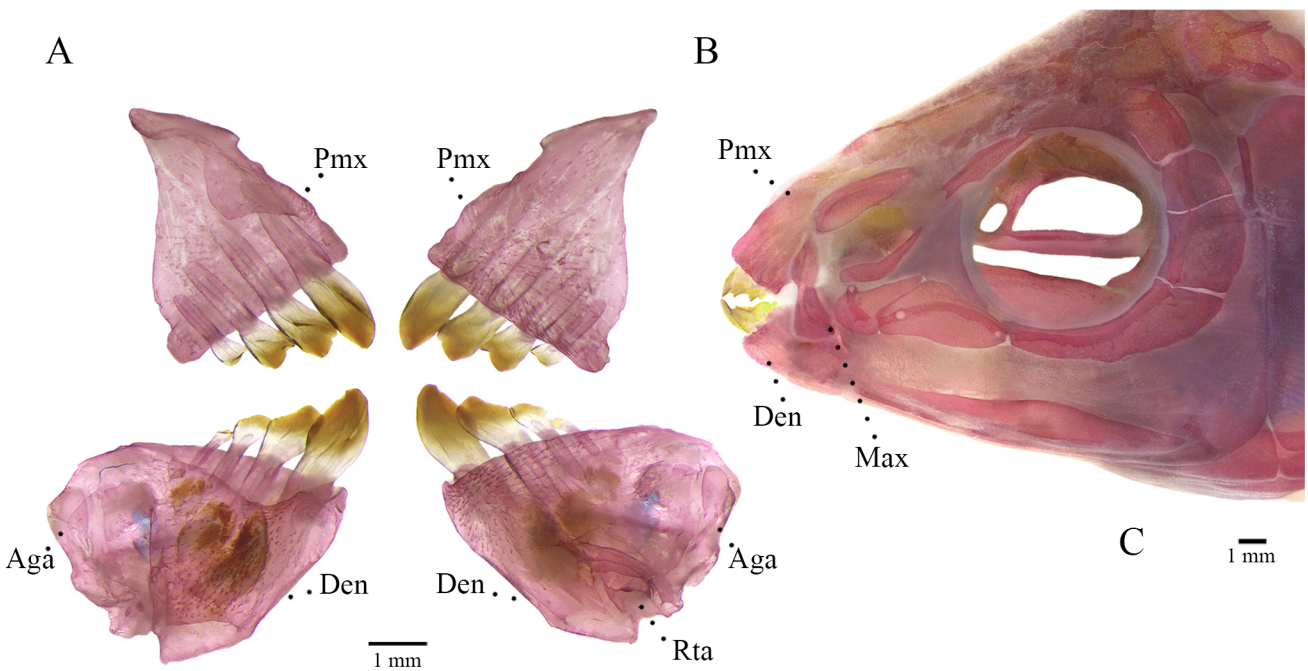

FIGURE 7 | Medial (**A**) and lateral (**B**) view of the jaws and lateral view of the head (**C**) of *Hypomasticus steindachneri*, MZUEL 16474, 99.78 mm SL. Pmx: premaxilla, Max: maxilla, Den: dentary, Aga: anguloarticular and Rta: retroarticular.

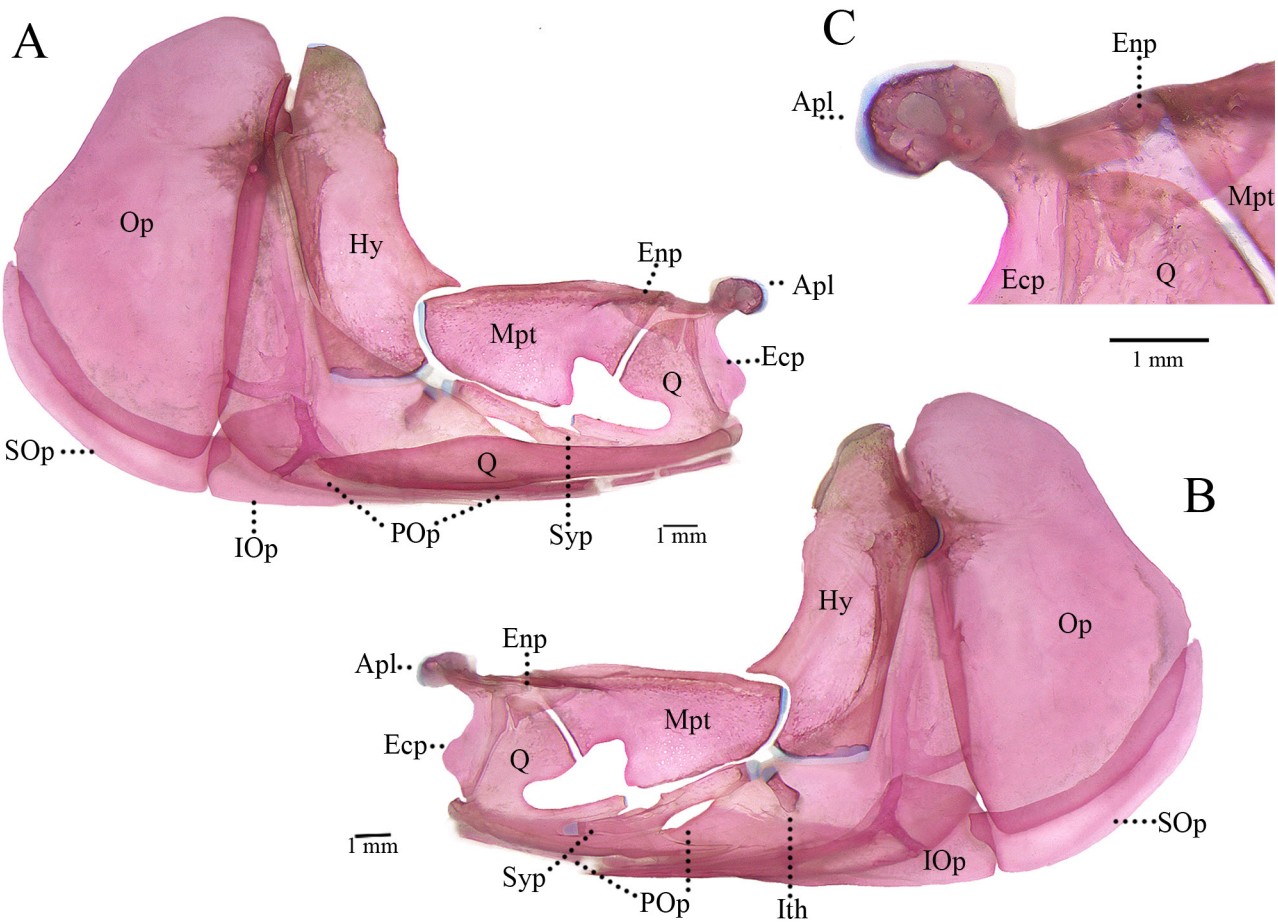

FIGURE 8 | Lateral (**A**) and medial (**B**) view of suspensorium with detail of autopalatine in lateral view (**C**) of *Hypomasticus steindachneri*, MZUEL 16474, 99.78 mm SL. Ecp: ectopterygoid, Enp: entopterygoid, Hy: hyomandibular, IOp: interopercle, Mpt: metapterygoid, Op: opercle, Apl: autopalatine, POp: preopercle, Q: quadrate, SOp: subopercle, Syp: symplectic and Ith: interhyal.

concave posterodorsal margin, overlapped by preopercle and overlapping subopercle. Interopercle teardrop shaped, with sharp anterior and broad posterior portions, overlapped by preopercle and overlapping subopercle. Preopercle L-shaped, large and posteroventrally convex, rounded, overlapped by quadrate and overlapping opercle, interopercle and hyomandibular. Hyomandibular relatively large, higher than long, posterodorsally connected with opercle through opercular condyle and with two dorsal condyles articulated to sphenotic and pterotic, overlapped by preopercle. Sympletic rod-like shaped with posterior portion slightly broader than anterior, located on medial face of suspensorium, extending between quadrate, metapterygoid and hyomandibular.

Interhyal small, with dorsal portion connected with preopercle via cartilage and ventral portion connected with posterior ceratohyal also via cartilage. Metapterygoid trapezoidal, dorsal portion broad and slightly convex and ventral portion with irregular margin due to quadrate-metapterygoid fenestra, overlapped by entopterygoid.

Quadrate large and irregular, with three distinct processes and a lateral shelf, dorsal process triangular with rounded convex margin, contacting entopterygoid, posterodorsal

process narrow and delimiting ventral margin of quadrate-metapterygoid fenestra, posterior process triangular with slender margin, anteroventral portion of quadrate with condyle for articulation with anguloarticular, lateral shelf large, horizontal, and with slender edges, extended from condyle to preopercle, anterior margin of quadrate forms long, straight contact with ectopterygoid. Metapterygoid-quadrate fenestra large and bean-shaped. Entopterygoid relatively small and associated with cartilage on dorsum of quadrate, overlapping anteriormost portion of metapterygoid. Ectopterygoid vertically elongated, with distinctly convex anteroventral margin and somewhat straight posterior portion. Autopalatine elongated, with distinct process extending anteroventrolaterally from main body of bone, enveloped by a semicircular layer of cartilage. Hyoid arch bearing four branchiostegal rays on each side, ceratohyals, hypohyals, interhyal and urohyal (Fig. 9). Branchisostegal rays slender and spatula-shaped, two articulated to anterior ceratohyal and two articulated to posterior ceratohyal.

Anterior ceratohyal larger than posterior, both somewhat rectangular with irregular margins. Dorsal hypohyal small, with cartilaginous dorsal margin. Ventral hypohyal compact, forming anterior margin of hyoid arch. Interhyal small and cylindrical, with cartilaginous tips. Urohyal sagitally positioned and dorsally connected with hypohyals through connective tissue, presenting a distinct V-shape, with dorsal branch longer and

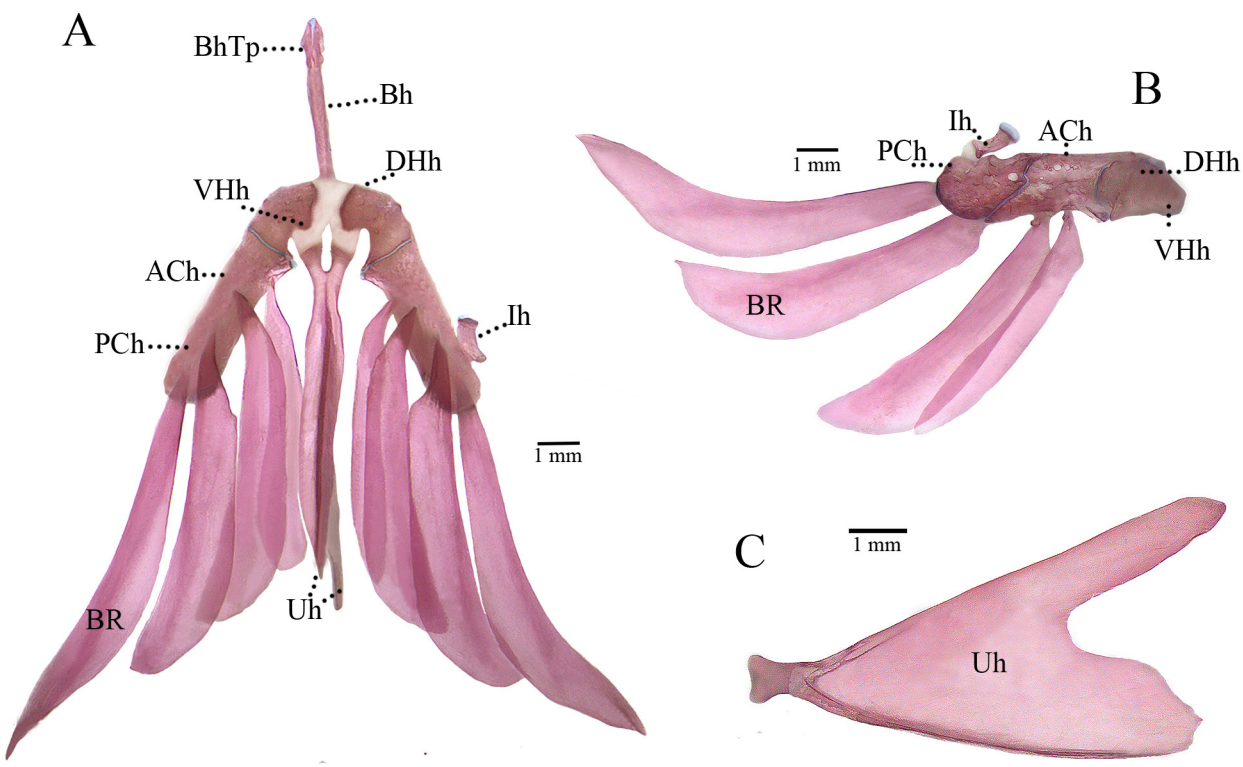

FIGURE 9. Dorsal (**A**) and ventral (**B**) view of hyoid arch with detail of the urohyal in lateral view (**C**) of *Hypomasticus steindachneri*, MZUEL 16474, 99.78 mm SL. BR: branchiostegal rays, Uh: urohyal, DHh: dorsal hypohyal, VHh: ventral hypohyal, ACh: anterior ceratohyal, PCh: posterior ceratohyal, Ih: interhyal, Bh: basihyal and Bhtp: basihyal toothplate.

ventral branch broader, both with irregular convex margins. Basihyal elongated and compressed, with ventral portion concave, basihyal toothplate covering half of bone, with cartilaginous dorsal tip. Three basibranchials (Fig. 10B), all vertically interconnected through ossified channel and laterally connected with hypobranchials, first basibranchial dorsally connected with basihyal. Three pairs of hypobranchials bordered posteriorly, laterally and medially by cartilage, first two rectangular in shape and third somewhat triangular, all ventrally connected with ceratobranchials, first pair of hypobranchials with dorsal acute process. Five pairs of ceratobranchials, with first four elongate and covered with rakers along both anterior and posterior medial margins. Fifth ceratobranchial with rakers restricted to anterior medial margin and semicircular bony expansion on posterior margin, bearing four rows of conical teeth with falciform tip. Four pairs of epibranchials with rakers along ventral margin, fourth Y-shaped epibranchial, with accessory cartilaginous element. Four pairs of small pharyngobranchials, pharyngeal tooth plate bearing three rows of small conical teeth with falciform tip. Neurocranium laterally compressed and relatively narrow (Figs. 10A, 11).

Mesethmoid triangular in dorsal view, located at anterodorsal portion of neurocranium and forming anteriormost border of fontanel, bearing prominent anteroventral process where contralateral premaxilla articulates. Lateral ethmoid articulating with mesethmoid, vomer, orbitosphenoid and frontal, with well-developed lateral process directed posteroventrally and composing anterior margin of orbit. Frontal forming largest portion of dorsal roof of neurocranium, rectangular and elongate, with contralateral bones separated by cranium fontanel along most of length and united by epiphyseal bar anteriorly to suture with parietals (Fig. 11A). Vomer located at anteroventral portion of neurocranium, articulating posteroventrally with lateral ethmoid, pentagonal in ventral view, with a pair of foramina, and prominent rounded dorsal process and paired anterior process that articulates with autopalatine. Parietals somewhat rectangular and wide (width twice length), located on posteriodorsal surface of neurocranium anterior to supraoccipital, contralateral parietals separated by larger portion of cranium fontanel. Supraoccipital located on posterior border of cranium fontanel and anteriorly to neural complex of Weberian apparatus, forming prominent triangular crest at posterodorsal portion of neurocranium. Orbitosphenoid, pterosphenoid, and prootic dorsal to parasphenoid, forming ventral wall of braincase (Fig. 11B). Orbitosphenoid with a very distinct process on posteroventral margin, forming a column that connects orbitosphenoid with parasphenoid and separates contralateral optic chambers. Pterosphenoid roughly hexagonal, forming substantial portion of ventral floor of braincase. Prootic large and roughly hexagonal, forming part of floor of braincase, with well-developed ventromedial process that articulates with parasphenoid and basioccipital. Parasphenoid long and thin, with posterior margin broader than anterior. Parasphenoid forming anteroventral margin of neurocranium, with dorsolateral projection forming border of carotid foramen and paired posteroventral flat projections extending ventrally to basioccipital. Sphenotic located at posterodorsal orbital margin, somewhat triangular, with distinct laminar process ventrolaterally directed and ventral portion with recessed fossa where dorsal condyle of hyomandibular inserts. Pterotic located on posterolateral border of neurocranium, with distinct, well-developed ventrolateral spine-like process, ventral portion of pterotic with recessed fossa where dorsal condyle of hyomandibular inserts. Epiotic forming three-armed bridge on posterior border of neurocranium, with

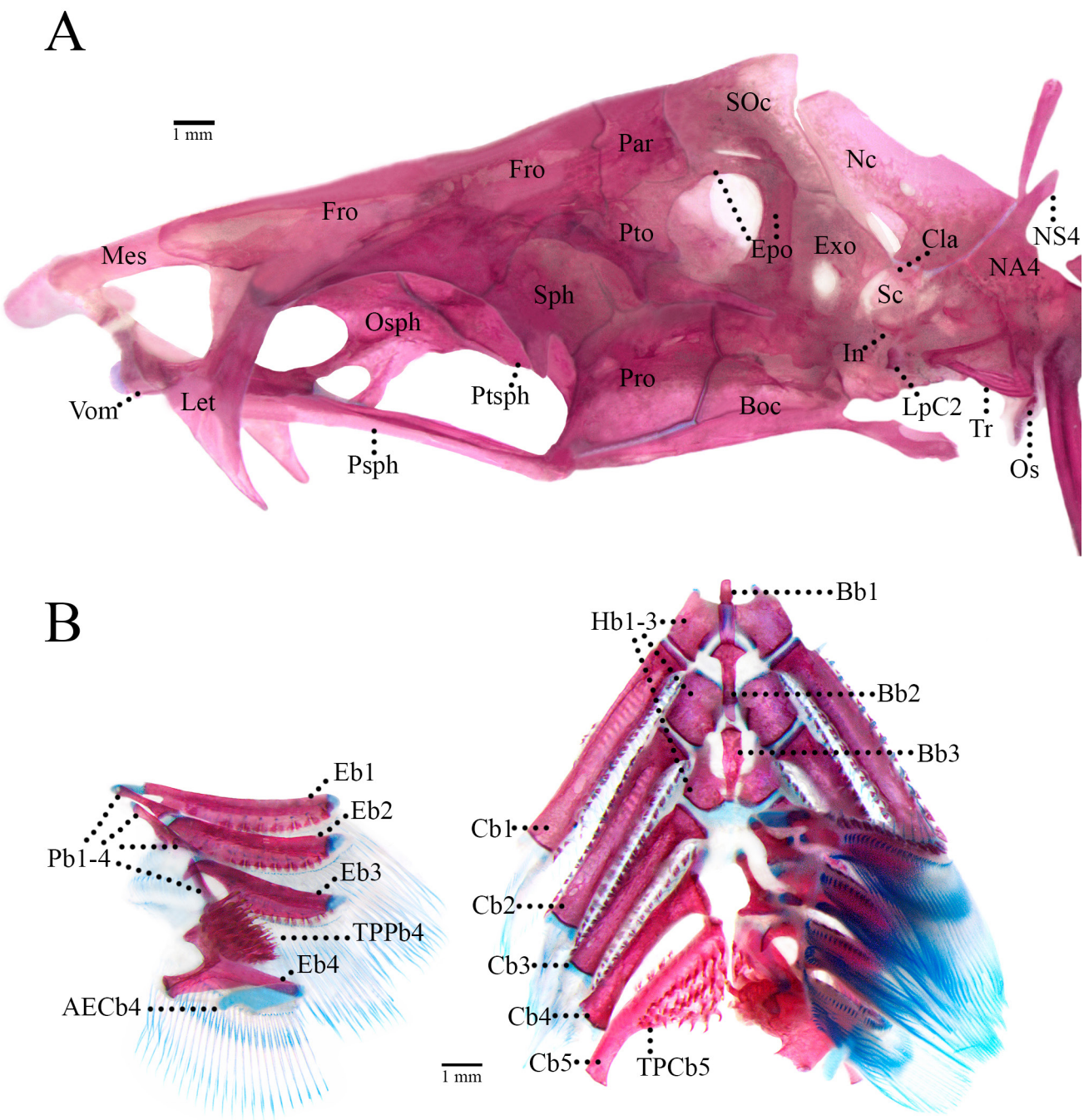

FIGURE 10 | Neurocranium in lateral view (**A**) and branchial apparatus (**B**) of *Hypomasticus steindachneri*, MZUEL 16474, 99.78 mm SL. Mes: mesethmoid, Vom: vomer, Let: lateral ethmoid, Fro: frontal, Osph: orbitosphenoid, Ptsph, pterosphenoid, Psph: parasphenoid, Sph: sphenotic, Pto: pterotic, Pro: prootic, Par: parietal, Epo: epiotic, SOc: supraoccipital, Boc: basioccipital, Exo: exoccipital, Nc: neural complex, Cla: claustrum, Sc: scaphium, In: intercalarium, LpC2: lateral process of centrum 2, Tr: tripus, NA4: neural arch of centrum 4, NS4: neural spine of centrum 4, Os: os suspensorium, Bb1-3: basibranchial, Hb1-3: hypobranchial, Cb1-5: ceratobranchial, TPCb5: tooth plate of fifth ceratobranchial, Pb1-4: pharyngobranchial, Ep1-4: epibranchial, AECb4: accessory element of ceratobranchial 4 and TPPb4: tooth plate of fourth pharyngobranchial.

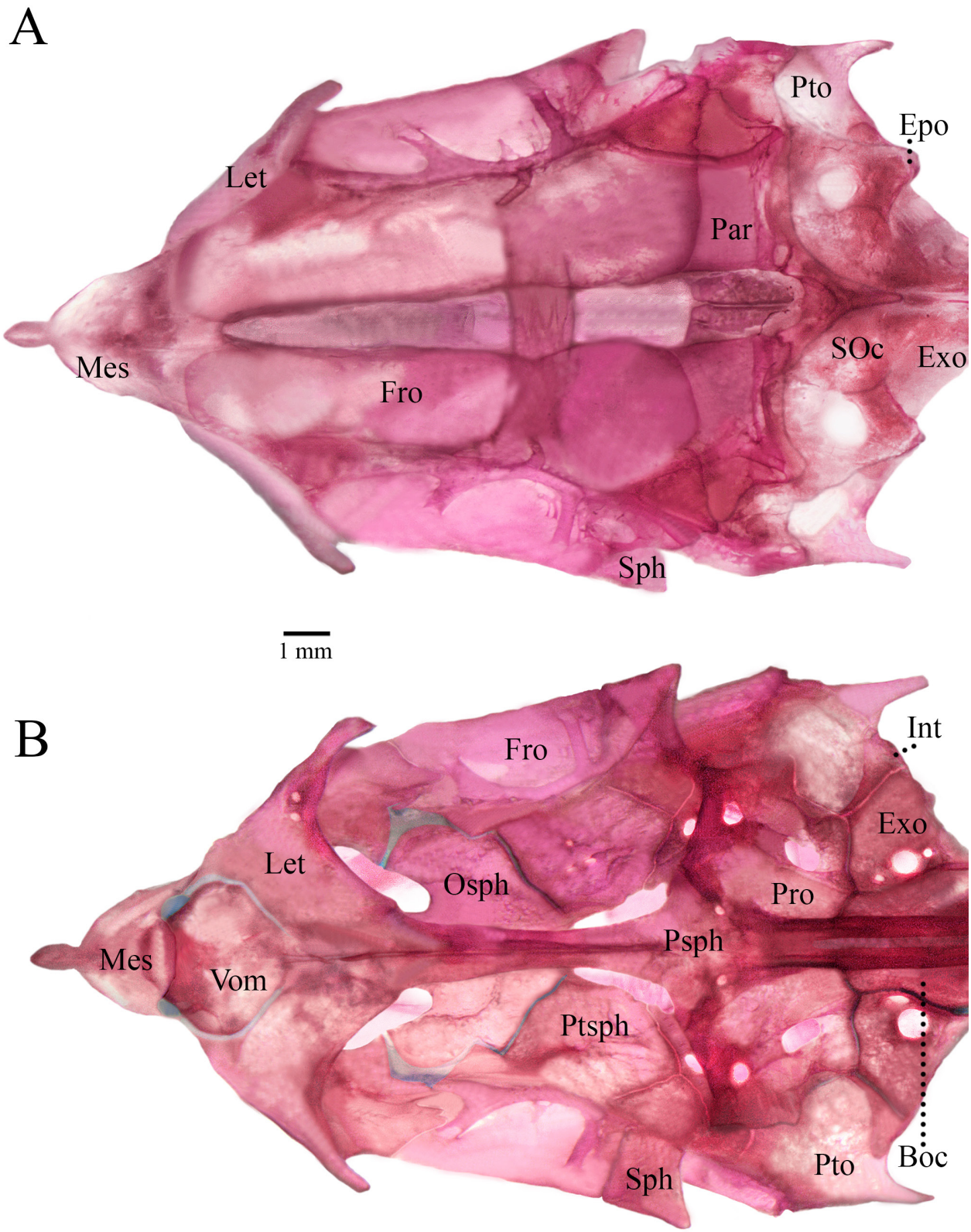

FIGURE 11 | Neurocranium in dorsal (**A**) and ventral view (**B**) of *Hypomasticus steindachneri*, MZUEL 16474, 99.78 mm SL. Mes: mesethmoid, Let: lateral ethmoid, Fro: frontal, Sph: sphenotic, Par: parietal, SOc: supraoccipital, Pto: pterotic, Epo: epiotic, Exo: exoccipital, Vom: vomer, Osph: orbitosphenoid, Ptsph, pterosphenoid, Psph: parasphenoid, Pro: prootic, Boc: basioccipital and Int: intercalar.

well-developed spine-like process that subdivides postemporal fossa. Exoccipital located at posteroventral face of neurocranium and connected to vertebral column, with ventral margin forming dorsal margin of foramen magnum. Intercalar small and L-shaped, located between pterotic and exoccipital. Basioccipital rectangular and robust, located ventral to exoccipitals on posteroventral extreme of neurocranium, forming ventral process of lagenar capsule, Baudelot´s ligament located on ventromedial surface of basioccipital.

Weberian apparatus composed by centra and associated elements of four anteriormost vertebrae. Neural complex laminar and somewhat triangular, with rounded dorsal margin that abuts ventral margin of supraoccipital crest and anteroventral margin with small invagination creating fossa between neural complex and exoccipital. *Claustrum* small and curved, located above *scaphium* and between exoccipital and neural complex. *Scaphium* small and round. *Intercalarium* small and L-shaped, articulating with *scaphium* and *tripus*. *Tripus* distinctly triangular, with long hook-shaped posterior process passing ventral to *os suspensorium*. *Os suspensorium* vertically positioned below fourth rib, composed of lateral and medial processes. Fourth centrum bearing broad neural arch and posterodorsally directed neural spine, with first supraneural ventral tip resting in small pocket on dorsal surface of the neural spine.

Pectoral girdle connected to neurocranium via extrascapular, posttemporal and pterotic (Fig. 12). Extrascapular small and rhomboid with irregular margins, bearing quadripartite sensory canal that articulates medially and posteroventrally with postemporal. Postemporal narrow and bearing sensory canal connected with parietal canal, with two spine-like process, one larger and slightly curved dorsal process associated with epiotic and one smaller and slightly curved medial process associated with pterotic. Supracleithrum large, vertically elongated and laminar, with posterior margin convex, bearing quadripartite sensory canal that continues posteriorly to form lateral line. Cleithrum largest bone of pectoral girdle, triangular with narrow dorsal process and posteroventral triangular lamina. Coracoid large and somewhat triangular, with large central foramen, large dorsal lamina articulating with medial portion of cleithrum, ventral lamina with numerous fenestrae and articulating with anteroventral portion of cleithrum, dorsomedial process articulating with mesocoracoid and scapula forming Y-shaped suture, posteroventral portion of coracoid with acute process. Mesocoracoid columnar, articulating dorsally with cleithrum and forming strut on posterior face of pectoral girdle. Scapula columnar, curved and dumbbell-shaped, located on ventromedial portion of girdle and articulating dorsally with medial surface of cleithrum.

Three postcleithra posteriorly distributed on girdle. First postcleithrum small and ovoid, located between ventral portion of supracleithrum and dorsal portion of cleithrum. Second postcleithrum large and laminar, with rounded ventral margin, located on posteroventral portion of cleithrum. Third postcleithrum articulates dorsally with second postcleithrum, elongate and narrow, extending vertically through base of pectoral-fin rays. Four proximal radials, dorsalmost proximal radial expanded to form separate articular facets articulating with three distal radials, remaining radials elongate and rod-like, with cartilaginous tips, each articulating with one distal radial. Pectoral fin with one unbranched ray and sixteen branched rays, rays with cartilaginous distal tips. Dorsal fin with ten branched rays, two unbranched rays and a very small unbranched

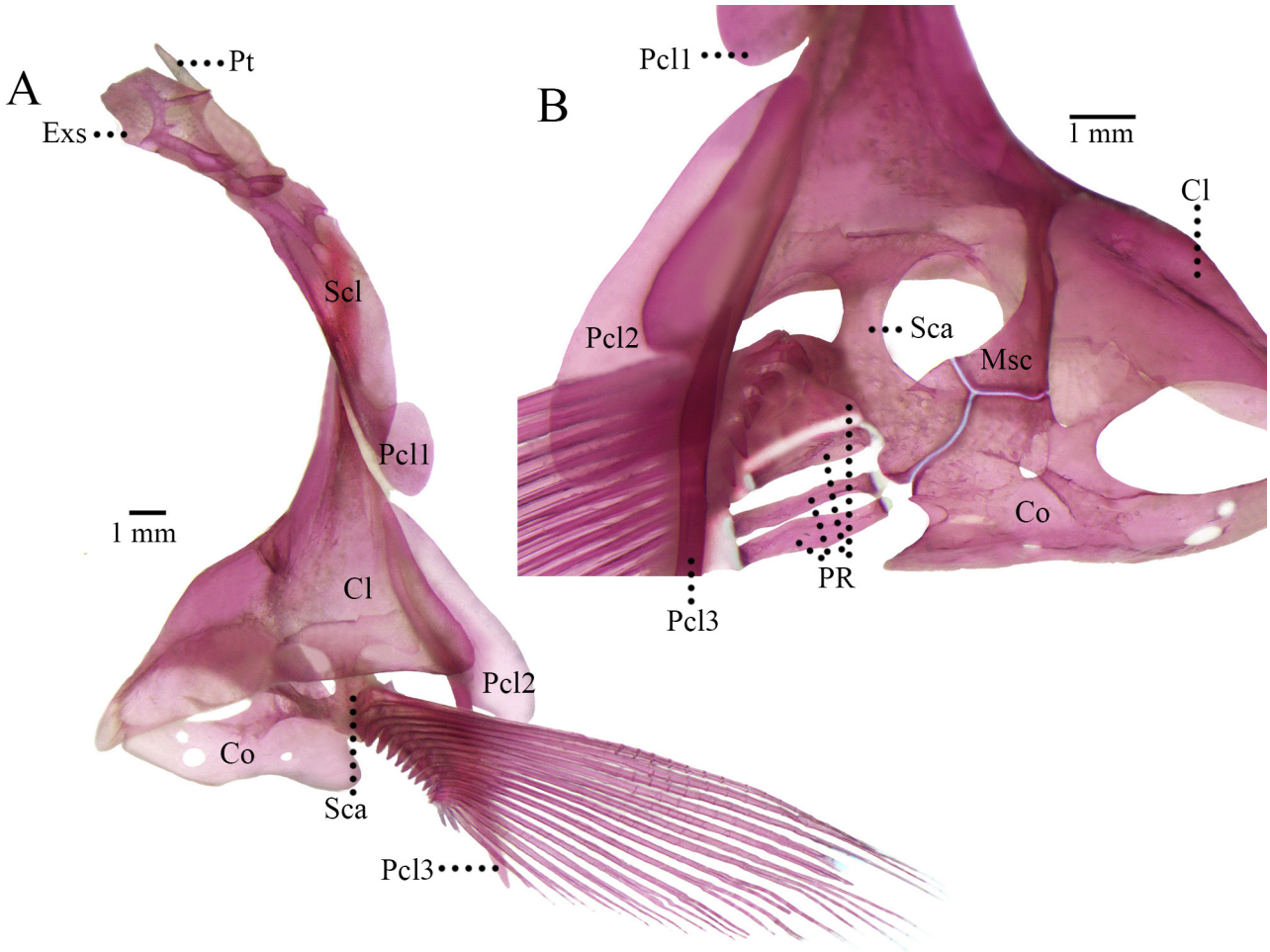

FIGURE 12 | Pectoral girdle in lateral (**A**) and medial view (**B**) of *Hypomasticus steindachneri*, MZUEL 16474, 99.78 mm SL. Pt: posttemporal, Exs: extrascapular, Scl: supracleithrum, Cl: cleithrum, Co: coracoid, Sca: scapula, Msc: mesocoracoid, Pcl 1-3: postcleithra and PR: proximal radials.

ray on the anteriormost portion (Fig. 13A). First unbranched ray significantly smaller than second, all rays with cartilaginous distal portions. Eleven pterygiophores diagonally distributed along ventral portion of dorsal fin, each pterygiophore with with anterior, posterior and lateral laminar expansions and cartilaginous tips. First anterior pterygiophore largest with distinctive anterior laminar expansion, large and with spine-like margins intercalated with concave portions. Anterior three pterygiophores divided into proximal and distal radials, remaining eight pterygiophores divided into proximal, medial and radials. Dorsal-fin stay located posterior to last pterygiophore, with ossified dorsal portion and hook-shaped cartilage. Anal fin with eight branched and three unbranched rays, with unbranched rays increasing in size from anteriormost ray, branched rays with overall similar size, all rays with cartilaginous distal portions (Fig. 13B) Nine pterygiophores diagonally distributed along dorsal portion of anal fin, all with cartilaginous tips, anal pterygiophores with much less developed laminar expansions than dorsal ones.

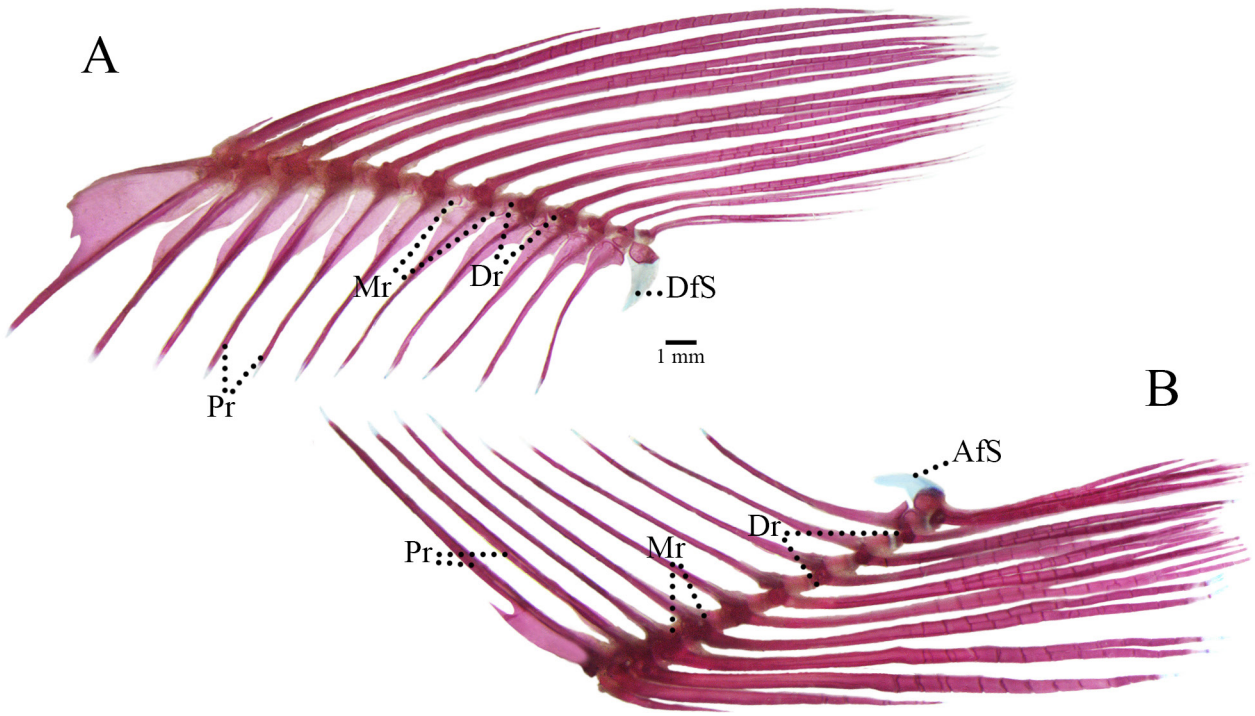

FIGURE 13 | Dorsal (**A**) and anal fin (**B**) of *Hypomasticus steindachneri*, MZUEL 16474, 99.78 mm SL. Pr: proximal radial, Mr: medial radial, Dr: distal radial, DFS: dorsal fin stay and AFS: anal fin stay.

First anterior pterygiophore with prominent anterior laminar expansion, convex anteroventrally and dorsally concave, with spine-like tip. First to fourth pterygiophores divided into proximal and distal radials, remaining five pterygiophores divided into proximal, medial and radials. Anal-fin stay located posterior to last pterygiophore, with ossified ventral portion and hook-shaped cartilage. Pelvic bones elongated and each parallel to its counterpart (Fig. 14A), its anterior portion slightly conical and with cartilaginous tip, posterior portion of bone with L-shaped margin with prominent ischiatic process, tip of ischiatic process also cartilaginous, radial closest to midline large and L-shaped, similar to ischiatic process, pelvic fin with one unbranched ray and eight branched rays. Caudal skeleton composed by one parhypural, six hypurals, three epurals, two uroneurals, a pleurostyle and a compound centrum formed by preural centrum 1 and ural centrum 1 (Fig. 14B). Ventral portion of hypural plate composed by parhypural and two hypurals. Parhypural with proximal ventral lamina and fused with compound centrum along with second hypural.

First hypural large and somewhat triangular, separated from compound central by gap. Dorsal portion of hypural plate with four hypurals that decrease in size ventrodorsally, with only third hypural in contact with compound centrum and the rest separated. First uroneural significantly larger than second and tightly attached to pleurostyle. Compound centrum with modified, plate-like neural spine, with concave posterodorsal portion that connects with epurals. Three epurals rod-like and smilar in size. Neural and haemal spines adjacent to caudal-fin skeleton with anterior bony projections. Dorsal lobe of caudal fin with nine branched rays, one unbranched ray and

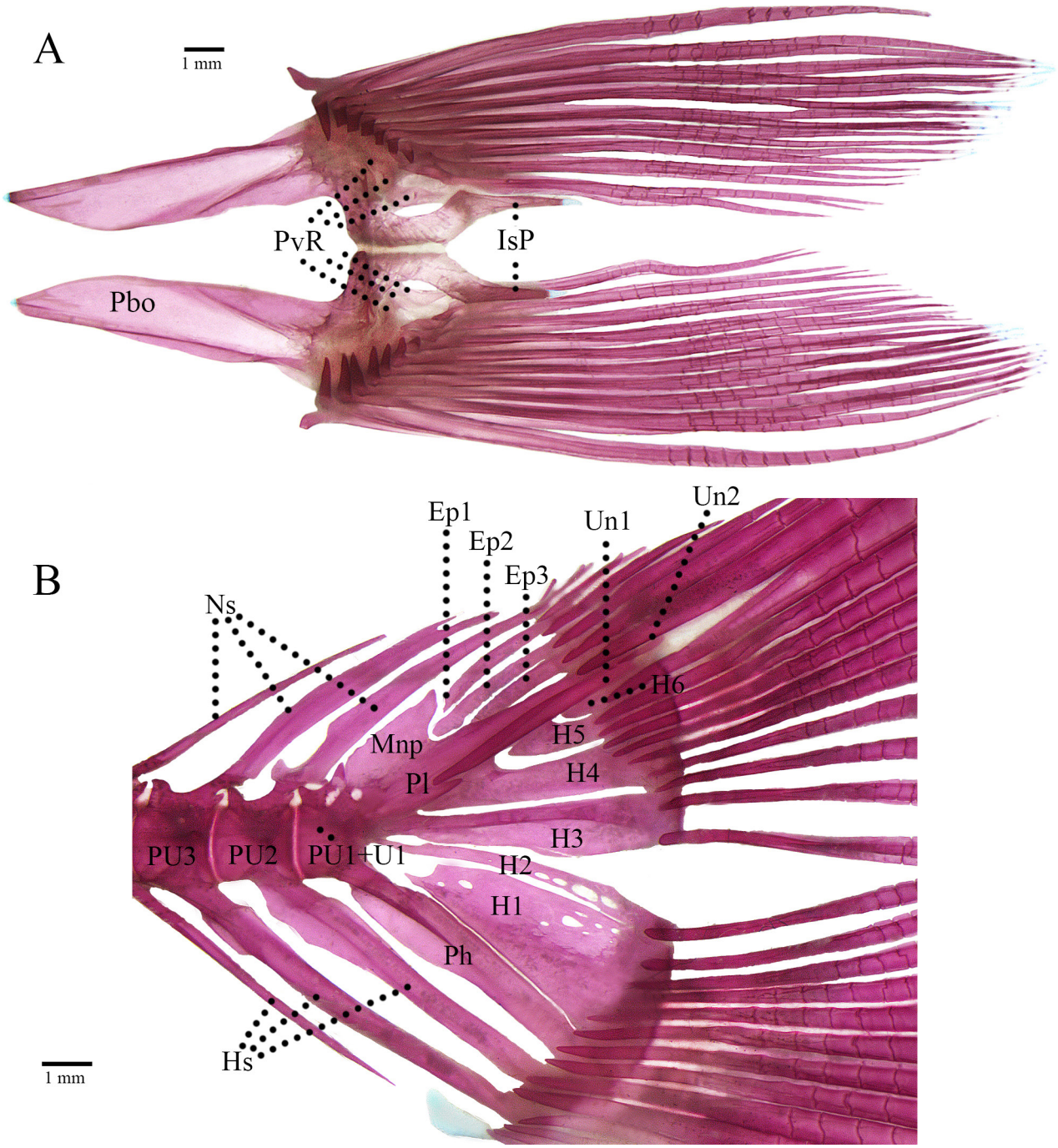

FIGURE 14 | Pelvic girdle in dorsal view (**A**) and caudal skeleton (**B**) of *Hypomasticus steindachneri*, MZUEL 16474, 99.78 mm SL. IsP: isquiatic process, PvR: pelvic-fin radials, Pbo: pelvic bone, PU2-3: preural centrum, PU1+U1: complex centrum formed by preural centrum 1 and ural centrum 1, Hs: haemal spine, Ns: neural spine, Mnp: modified neural process, Ph: parhypural, H1-6: hypurals, Un1-2: uroneurals and Ep1-3: epural.

seven procurrent rays. Third through sixth hypurals support principal rays of dorsal lobe of caudal fin, and distal tips of uroneurals, epurals and neural spine of second preural centrum support procurrent rays. Ventral lobe of caudal fin with eight branched rays, one unbranched ray and five procurrent rays. First and second hypurals and parhypural support ventral principal rays and tips of haemal spines of second and third preural centra support procurrent rays.

Coloration in alcohol. Ground color ranging from tan to dark brown (Figs. 5A, 15). Head and body gently countershaded. Smaller specimens with twelve transverse dark bars, extending from the dorsal portion of the body to the pectoral-fin insertion, partially interrupted by the lateral line. Bars fuse to form eight bars in gradually larger specimens and eventually disappear in adults. Dark spot located immediately posterior to sixth infraorbital, sometimes filling the entire bone. Opercle with conspicuous dark blotch that becomes less visible in large specimens, positioned below the lateral line and above the pectoral-fin insertion. Snout region more pigmented than remaining head. Trunk with three conspicuous dark midlateral blotches, first vertically aligned through base of last third of dorsal-fin base, second located between anal opening and anterior portion of anal fin and last on posterior portion of the caudal peduncle. Blotches somewhat uniform in size, decreasing in size posteriorly in smaller specimens. Ventral surfaces of head and body pale to cream, without chromophores. Adipose fin with dark distal margin. Remaining fins range from nearly hyaline to yellowish, with few chromophores along margins of rays.

Coloration in life. Coloration pattern like that of preserved specimens, midlateral blotches dark and well defined. Juveniles with head and body yellowish-silver, scales with dark yellow base and blueish silver tips. Adults with head and body pale gray, with the dorsal region darker than the rest of the body, and scales with dark yellow base and silver tips. Adipose fin scarlet red, remaining fins bright or dark yellow. Conspicuous red blotch above upper lip. Iris red or orange.

Sexual dimorphism. Two of the five radiographed individuals and one dry skeleton (MZUEL 16474), presumably mature males, exhibited hypertrophy of the first pair of ribs, which were curved, with the tips directed posteriorly and displaying a shovel-like shape. In this condition, the tips of the first pair of ribs nearly reach the tips of the second pair, in contrast to the typical parallel arrangement seen in most specimens.

Geographical distribution. *Hypomasticus steindachneri* is found in the Pardo, Jequitinhonha, Itanhém, Mucuri and Doce coastal river basins, extending from southern Bahia State to the eastern portion of Minas Gerais and Espírito Santo states, Brazil (Fig. 16).

Ecological notes. In the Doce River basin, specimens of *Hypomasticus steindachneri* are more frequently observed in lakes than in the main river channel and streams, where its congener *H. copelandii* is more frequently found. However, in the Jequitinhonha and Mucuri River basins, *H. steindachneri* is frequently observed in the main river channels. The migratory behavior of the species was documented in the Mucuri River, where specimens were observed using a fish passage at the Santa Clara Dam (Pompeu, Martinez,

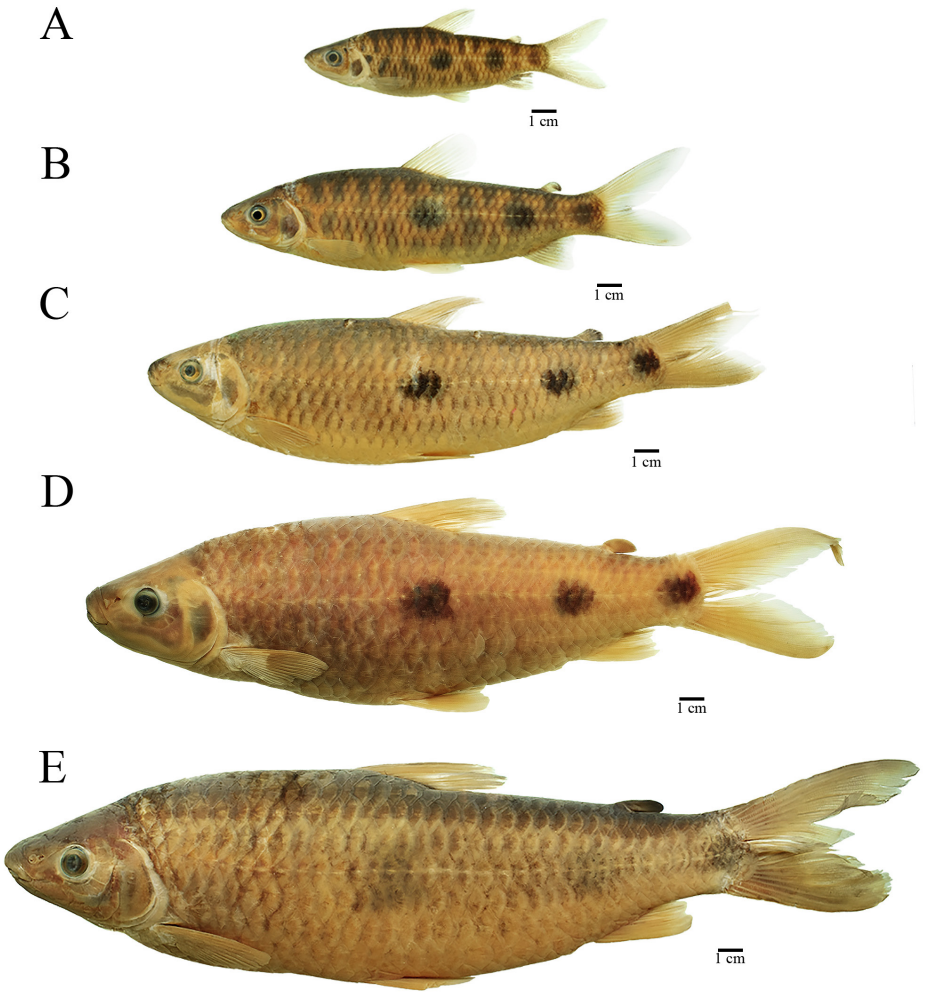

FIGURE 15 | *Hypomasticus steindachneri*: **A.** MZUSP 112707, 79.37 mm SL, rio Pardo. **B.** MZUEL 16474, 140.6 mm SL, rio Pardo. **C.** MZUEL 16474, 200.91 mm SL, rio Pardo. **D.** LISDEBE 7905, 241.2 mm SL, rio Araçuaí, tributary of rio Jequitinhonha. **E.** MZUEL 22537, 293.52 mm SL, rio Corrente Grande, tributary of rio Doce.

2007). In that study, it was reported that specimens of *H. steindachneri* sustained injuries and ultimately perished within the system of fish passage.

Conservation status. *Hypomasticus steindachneri* is widely distributed across four major drainages of the Northeastern Atlantic Forest ecoregion. The Atlantic Forest is the most deforested biome in Brazil, with over 85% of its original area lost. As a result, the coastal drainages have been significantly impacted by human activity since colonization, particularly given that the highest population density in the country is concentrated in this region. The Jequitinhonha basin faces numerous threats, including the deterioration of water quality resulting from unregulated land use, siltation of river channels, replacement of native vegetation with monocultures and the presence of high concentrations of toxic substances (Magalhães Júnior *et al*., 2019).

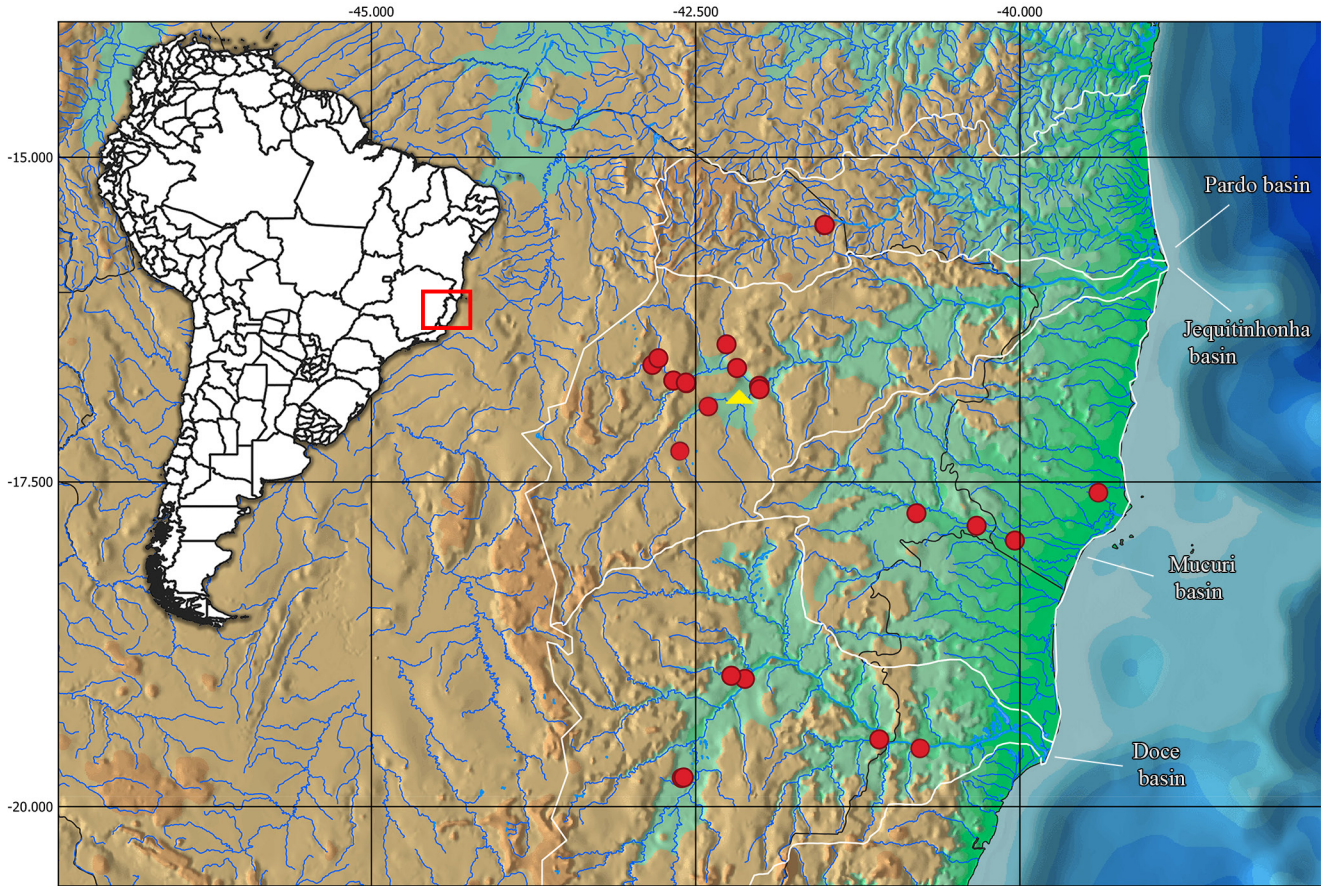

FIGURE 16 | Geographic distribution of *Hypomasticus steindachneri* in eastern Brazil, yellow triangle represents estimated type-locality.

In addition to the effects of pollution and an increase in droughts in recent decades, these coastal basins continue to experience the adverse impacts of large-scale mining. This sector was responsible for the destruction of the Mariana dam in the Doce River basin, which resulted in the largest environmental disaster in Brazilian history. The presence of numerous dams in the basins where the species is found (Silva *et al*., 2021) represents another potential factor that may negatively affect *H. steindachneri* populations, especially considering the migratory behavior exhibited by the species. Notwithstanding the significance of these factors, the species exhibits a broad distribution and is present in numerous protected areas, including Mata Escura Biological Reserve, Rio Doce State Park, Sempre Vivas National Park and Biribiri State Park. Accordingly, we recommend the classification of *Hypomasticus steindachneri* as Least Concern (LC) in accordance with the International Union for Conservation of Nature (IUCN) categories and criteria (IUCN Standards and Petitions Subcommittee, 2024).

Material examined. All from Brazil, river basins: **Jequitinhonha:** NMW 68405, 323 mm SL, holotype. ANSP 206697, 1, 320 mm SL. LISDEBE 7908, 1, 248.0 mm SL. LISDEBE 7909, 1, 237.1 mm SL. LISDEBE 7910, 1, 106.5 mm SL. LISDEBE 7911, 2, 209.7–248.5 mm SL. LISDEBE 7904, 4, 126.2–238.9 mm SL. LISDEBE 7905, 6, 203.1–241.7 mm SL. MZUSP 87849, 2, 186.5–222 mm SL. MZUSP 87850, 1, 169.2

mm SL. MZUSP 93781, 2, 109.2–137.6 mm SL. JEQUI 5895, 1, 120 mm SL. JEQUI 5964, 1, 60 mm SL. **Pardo:** MZUEL 17996, 8 alc, 1 c&s, 90.7–140.6 mm SL. MZUEL 16474, 8 alc, 2 sk, 99.7–223 mm SL. MZUSP 112707, 2, 78–79.37 mm SL. MZUSP 112108, 1 sk. MZUSP 93813, 2, 271.4–357.8 mm SL. **Mucuri:** MZUSP 87866, 1, 140.5 mm SL. MZUSP 87868, 1, 139 mm SL. MZUSP 1680, 1, 96.5 mm SL. **Doce:** MZUEL 22537, 2, 290.3–293.5 mm SL. MZUEL 20990, 2, 253–264.8 mm SL. MZUEL 22536, 1, 274.4 mm SL. MZUEL 12324, 3, 260–283.1 mm SL. LISDEBE 203, 3, 207.9–290.3 mm SL. MZUSP 28984, 5, 125–260 mm SL. MZUSP 36667, 1, 319.5 mm SL. MZUSP 45121, 1, 303.9 mm SL. MZUSP 48470, 2, 190.5-225 mm SL. MZUSP 107327, 2, 334.9–344.2 mm SL.

Hypomasticus australis, new species

urn:lsid:zoobank.org:act:C3FBCD92-298C-4347-8D98-41C8950CA08F

(Figs. 17–27; Tab. 5)

Leporinus steindachneri. —Santos, 2007:19, 37, 45, 49–51 (phylogenetic relationships based on molecular data: Rio de Janeiro coastal drainages, Brazil). —Garavello, Britski in Reis *et al*., 2003:78 (in part, catalog). —Camelier, Zanata, 2015 (distribution). —Guedes *et al*., 2015:1–06 (mention, Rio de Janeiro coastal drainages, Brazil). —Souza *et al*., 2017:507–516 (ontogeny, Rio de Janeiro coastal drainages, Brazil).

Leporinus copelandii. —Costa, 2018:39, 41, 56 (checklist, Juquiá River, Ribeira de Iguape River basin).

Hypomasticus cf. *steindachneri*. —Birindelli *et al*., 2020:423 (in part, comparative material, Rio de Janeiro coastal drainages, Brazil).

Hypomasticus steindachneri. —Toledo-Piza *et al*., 2024:48 (in part, catalog).

Hypomasticus thayeri. —Birindelli *et al*., 2020: fig. 5 and supplemental material (in part, material used for molecular analysis erroneously identified as *Hypomasticus thayeri*, Rio de Janeiro coastal drainages, Brazil). —Sidlauskas *et al*., 2025:27, fig. 5 and supplemental material (in part, material used for molecular analysis erroneously identified as *Hypomasticus thayeri*, Rio de Janeiro coastal drainages, Brazil).

Holotype. MZUSP 125891, 273.4 mm SL, Brazil, São Paulo State, municipality of Registro, rio Ribeira de Iguape, near the confluence with rio Juquiá 24°24'13.5"S 47°49'29.7"W, 18 Sep 2021, O. T. Oyakawa, J. C. Nolasco, D. Garrone-Neto & E. O. Santinelli.

Paratypes. All from Brazil, São Paulo State, Ribeira de Iguape River basin. MZUSP 129599, 1 alc, 233.1 mm SL, municipality of Registro, rio Jacupiranga, tributary of rio Ribeira de Iguape, 24°35'36.3"S 47°52'39.6"W, 1995, M. R. Santos & M. Morato. MZUSP 38608, 1 alc, 100.3 mm SL, municipality of Juquiá, ribeirão Poço Grande, tributary of rio Juquiá, 24°20'00"S 47°38'00"W, 29 Mar 1987, MZUSP staff. MZUSP 45191, 2 alc, 205.3–207 mm SL, municipality of Eldorado, rio Ribeira de Iguape, 24°32'00"S 48°07'00"W, 5 Mar 1993, M. Damato. MZUSP 101241, 1 alc, 240.8 mm SL, municipality of Registro, rio Ribeira de Iguape, near the confluence with rio Juquiá, 24°24'10.8"S 47°49'22.8"W, 19 Nov 2008, C. Oliveira, O. T. Oyakawa, R. Devidé, F. Roxo, J. M. Henriques & P. Hollanda. LISDEBE 3, 7 alc, 135-168.5 mm SL, municipality of Juquiá, rio Quilombo, tributary of rio Juquiá, 24°21'19.8"S 47°50'57.0"W, 1–5 Sep

FIGURE 17 | *Hypomasticus australis*, holotype, MZUSP 125891, 273.4 mm SL, preserved (**A**) and live specimen (**B**), Brazil, São Paulo State, municipality of Registro, rio Ribeira de Iguape.

1980, UFSC staff. LISDEBE 25, 11 alc, 134.6–183.5 mm SL, municipality of Juquiá, rio Juquiá, tributary of rio Ribeira de Iguape, 24°19'19.2"S 47°37'04.8"W, 14 Jun 1981, J. C. Garavello. LISDEBE 45, 5 alc, 94.6–206.6 mm SL, municipality of Registro, rio Juquiá, tributary of rio Ribeira de Iguape, 24°24'11.8"S 47°49'21.7"W, 23–26 Apr 1979, UFSC staff. LBP 7502, 1 alc, 191.3 mm SL, municipality of Registro, rio Ribeira de Iguape, near the confluence with rio Juquiá, 24°24'10.8"S 47°49'22.8"W, 19 Nov 2008, C. Oliveira, O. T. Oyakawa, R. Devidé, F. Roxo, J. M. Henriques & P. Hollanda. MZUEL 23978, 1 alc, 90 mm SL, municipality of Juquiá, ribeirão Poço Grande, tributary of rio Juquiá, 24°20'00"S 47°38'00"W, 29 Mar 1987, MZUSP staff. MZUEL 23979, 1 alc, 193.1 mm SL, municipality of Eldorado, rio Ribeira de Iguape, 24°32'00"S 48°07'00"W, 5 Mar 1993, M. Damato. MZUEL 23980, 2 alc, 1 c&s, 97–147.2 mm SL, municipality of Registro, rio Juquiá, tributary of rio Ribeira de Iguape, 24°24'11.8"S 47°49'21.7"W, 23–26 Apr 1979, UFSC staff. MZUEL 23981, 3 alc, 137.2–149.1 mm SL, municipality of Juquiá, rio Quilombo, tributary of rio Juquiá, 24°21'19.8"S 47°50'57.0"W, 1–5 Sep 1980, exp. dcb. UFSC.

Non-types. Ribeira de Iguape basin: São Paulo State. MZUSP 47895, 1 alc, 114.3 mm SL, municipality of Registro, rio Ribeira de Iguape, 24°29'23.3"S 47°50'09.6"W, 21 Jan 1955, M. R. Cuocolo. MZUSP 1786, 1 alc, 115.4 mm SL, ribeirão Poço

Grande, tributary of rio Juquiá, 24°15'16"S 47°37'21"W, A. Hempel. MZUSP 63681, 1 alc, 180.5 mm SL, municipality of Iporanga, rio Ribeira de Iguape, 24°35'13.2"S 48°35'27.6"W, 1944, Vieira & Lima. MZUSP 3456, 1 alc, 244.9 mm SL, municipality of Juquiá, rio Juquiá, tributary of rio Ribeira de Iguape, precise location unknow, L. P. Travassos Filho. **Rio de Janeiro coastal basins: Rio de Janeiro State.** MZUSP 1354, 6, 109–175.1 mm SL, municipality of Campos dos Goytacazes, Lagoa Feia, 22°00'00"S 41°20'00"W, Dec 1911, E. Garbe. MZUSP 3614, 2, 160–160.5 mm SL, municipality of Itaboraí, rio Itaboraí, tributary of rio Caceribu, 22°44'58.8"S 42°51'01.4"W, 1909, E. Garbe. MZUSP 80297, 1 alc, 95.5 mm SL, municipality of Silva Jardim, rio São João, 22°34'00"S 42°34'00"W, 12 Oct 2002, M. de Pinna, M. I. Landim & C. R. Moreira. MZUSP 86775, 1 alc, 315.9 mm SL, municipality of Campos dos Goytacazes, Lagoa Feia, 22°00'00"S 41°20'00"W, 3 Sep 2004, C. Oliveira, O. T. Oyakawa, A. L. Alves, M. Chiachio & M. S. Ghazzi. MZUSP 129181, 1 alc, 224 mm SL, Rio de Janeiro State, municipality of Campos dos Goytacazes, rio Mocotó, tributary of rio Imbé, 21°50'10"S 41°44'22"W, 30 Apr 2014, O. T. Oyakawa, P. Camelier, M. Melo, J. C. Nolasco. LBP 2380, 2 alc, 197.1–208.8 mm SL, municipality of Campos dos Goytacazes, Lagoa Feia, 22°00'00"S 41°20'00"W, 3 Sep 2004, C. Oliveira, O. T. Oyakawa, A. L. Alves, M. Chiachio & M. S. Ghazzi. LBP 10727, 1 alc, 108.3 mm SL, municipality of Conceição do Macabu, rio Macabu, 22°04'05.9"S 41°54'35.4"W, 20 Oct 2010, C. Oliveira, G. J. C. Silva, K. T. Abe & A. O. Ribeiro. LBP 10833, 1 alc, 118.69 mm SL, municipality of Conceição do Macabu, rio Macabu, 22°04'05.9"S 41°54'35.4"W, 20 Oct 2010, C. Oliveira, G. J. C. Silva, K. T. Abe & A. O. Ribeiro.

Diagnosis. *Hypomasticus australis* can be distinguished from *Hypomasticus arcus*, *H. despaxi*, *H. granti*, *H. lebaili*, *H. lineomaculatus*, *H. melanostictus*, *H. megalepis*, *H. santosi* and *H. torrenticola* by possessing 12 scale rows around the caudal peduncle (*vs*. 16); from *H. mormyrops*, *H. copelandii* and *H. steindachneri* by possessing a subterminal mouth (*vs*. inferior mouth in *H. mormyrops* or terminal mouth in *H. copelandii* and *H. steindachneri*), can be distinguished from *H. gomesi*, *H. nijsseni* and *H. tepui* by possessing three midlateral blotches (*vs*. additional smaller blotches formed by dermal pigment, five of which form an interrupted "X" in *H. gomesi* and *H. nijsseni* and four dark longitudinal stripes in *H. tepui*), from *H. santanai* by possessing diffuse midlateral blotches (*vs*. conspicuous midlateral blotches), from *H. thayeri* by possessing thinner lips and a larger size, with the largest specimen analyzed measuring 315.9 mm SL (*vs*. thicker lips and smaller size, with the largest specimen analyzed measuring 240.2 mm SL). Additionally, it further differs from *H. steindachneri* by possessing the mouth cleft longitudinally aligned with the ventral margin of second infraorbital bone (*vs*. mouth cleft longitudinally aligned with the ventral margin of the eye orbit) and three diffuse midlateral blotches, extending through 4–5 scales horizontally and 2–3 scale rows vertically (*vs*. 3 conspicuous midlateral blotches, extending through 2–3 scales horizontally and 1–2 scale rows vertically).

Description. Morphometric data of examined specimens in Tab. 5. Large-sized species of *Hypomasticus*, largest examined specimen 315.9 mm SL. Body tall, elongated and laterally compressed. Dorsal profile almost straight from snout to tip of supraoccipital and gently convex from tip of supraoccipital to dorsal-fin origin, straight to slightly convex in dorsal-fin base, slightly convex from posterior insertion of dorsal

TABLE 5 | Morphometric data of *Hypomasticus australis* (52 specimens). SD = Standard deviation.

	Holotype	Mean	Min-Max	SD
Standard length (mm)	273.4	162.4	90–315.9	–
Percentages in standard length				
Snout tip to dorsal-fin origin	45.9	47.8	45.5–50.5	1.1
Snout tip to adipose-fin origin	83.4	84.4	82.2–86.7	0.9
Snout tip to pelvic-fin origin	49.5	49.7	46.6–53.3	1.3
Snout tip to anal-fin origin	76.9	77.1	72.4–83.7	1.8
Dorsal-fin origin to caudal-fin origin	51.8	53.4	48.8–56.9	1.6
Dorsal-fin origin to adipose-fin origin	38.9	39	36.2–41.4	1.1
Caudal peduncle length	11.7	11.4	9–13.4	0.9
Caudal peduncle depth	10.2	10.3	8.8–11.2	0.4
Body depth at dorsal-fin origin	27.8	27.8	25.3–31.8	1.4
Body width at dorsal-fin origin	15.7	15	12–17.8	1.3
Head length	21.7	23.7	20.8–25.7	0.9
Percentages in head length				
Preopercle length	75.4	75.7	72.4–79.2	1.6
Snout length	41.2	40.5	36.9–53.6	2.3
Eye diameter	16.6	18.2	14.5–21.7	1.5
Snout depth at anterior eye margin	59.9	52.6	45.9–59.9	3
Head depth at tip of supraoccipital	87.3	80.4	73.8–93.3	3.4
Head width at opercle	60.5	54.9	48.1–64.3	3.5
Interorbital distance	41.5	39.3	35.1–47.3	2.1

fin to adipose fin origin, broadly convex in adipose-fin base and gently concave from posterior insertion of adipose-fin to origin of upper lobe of caudal fin. Ventral profile slightly convex from lower jaw to end of branchiostegal rays, broadly convex from end of branchiostegal rays to posterior insertion of anal-fin rays and gently concave from this point to origin of lower lobe of caudal-fin. Greatest body depth at dorsal-fin origin. Mouth subterminal, its cleft longitudinally aligned with ventral margin of second infraorbital bone in specimens larger than 90 mm SL. Upper lip distinctly large, thicker than lower, both covered with small papillae. Snout rounded, anteriorly blunt. Teeth incisiform, compressed, unicuspid and with blunt cutting edge.

Vertebrae 36 (6), with ribs present on vertebrae 5 to 18 (6). Supraneurals 7 (2) or 8 (4). First dorsal-fin pterygiophore inserted posterior to neural spine of vertebra 11 (5) or 10 (1). First anal-fin pterygiophore inserted posterior to haemal spine of vertebra 25 (5) or 24 (1). Premaxillary bone with 4*(47) teeth arranged side-by-side and gently decreasing in size from symphyseal tooth. Dentary bone with 4 (47) teeth arranged side by side, and gently decreasing in size from symphyseal tooth.

Scales large and cycloid, with 8–9 radii (3). Lateral line complete with 36* (11), 37 (37) or 38 (4) perforated scales. Transverse series with 4* (52) scales from dorsal-fin origin to lateral line and 3.5* (50) or 3 (2) scales from lateral line to pelvic-fin base. 10 (19), 11*(21) or 12 (7) predorsal scales. 12* (52) horizontal scale rows around caudal peduncle.

Dorsal fin ii,9 (1) or 10*(51), origin slightly anterior of vertical through pelvic-fin origin, distal margin rounded. Pectoral fin i,13 (15), 14* (27), 15 (6) or 16 (4), base located posterior to gill opening, distal margin rounded. Pelvic fin i,8* (52), distal margin rounded. Anal fin iii,8* (52), distal margin straight or slightly concave. Caudal fin rays i,9,8,i* (52), caudal fin forked, upper lobe slightly more elongated than lower lobe.

Osteology. In this section only the differences between the osteology of *H. australis* and *H. steindachneri* (see above) are described, due to their overall osteological similarity. Eight supraneurals along dorsal midline, each associated with anterodorsal margin of neural spine of fourth to eleventh vertebrae (Fig. 18A), eighth supraneural small and comma-shaped, relatively further away from anterodorsal margin of neural spine. Second infraorbital with dorsal margin distinctly convex, almost triangular (Fig. 18B). Third infraorbital with irregular ventral margin, with third pore further away from posterior margin. Fourth infraorbital with irregular posterior margin.

Fifth infraorbital with rounded posterodorsal margin. Sixth infraorbital ovoid, sensory canal bearing three pores, one on each tip of sensory canal. Supraorbital comma-shaped. Nasal plate-like, with somewhat triangular anteroventral margin and slightly rounded dorsal margin. Premaxillary bone gently vertically oriented, anterodorsal margin with distinct protuberance, significantly larger than in most anostomids (Fig. 19). Maxillary bone slightly leaning forward. Lower jaw trapezoidal.

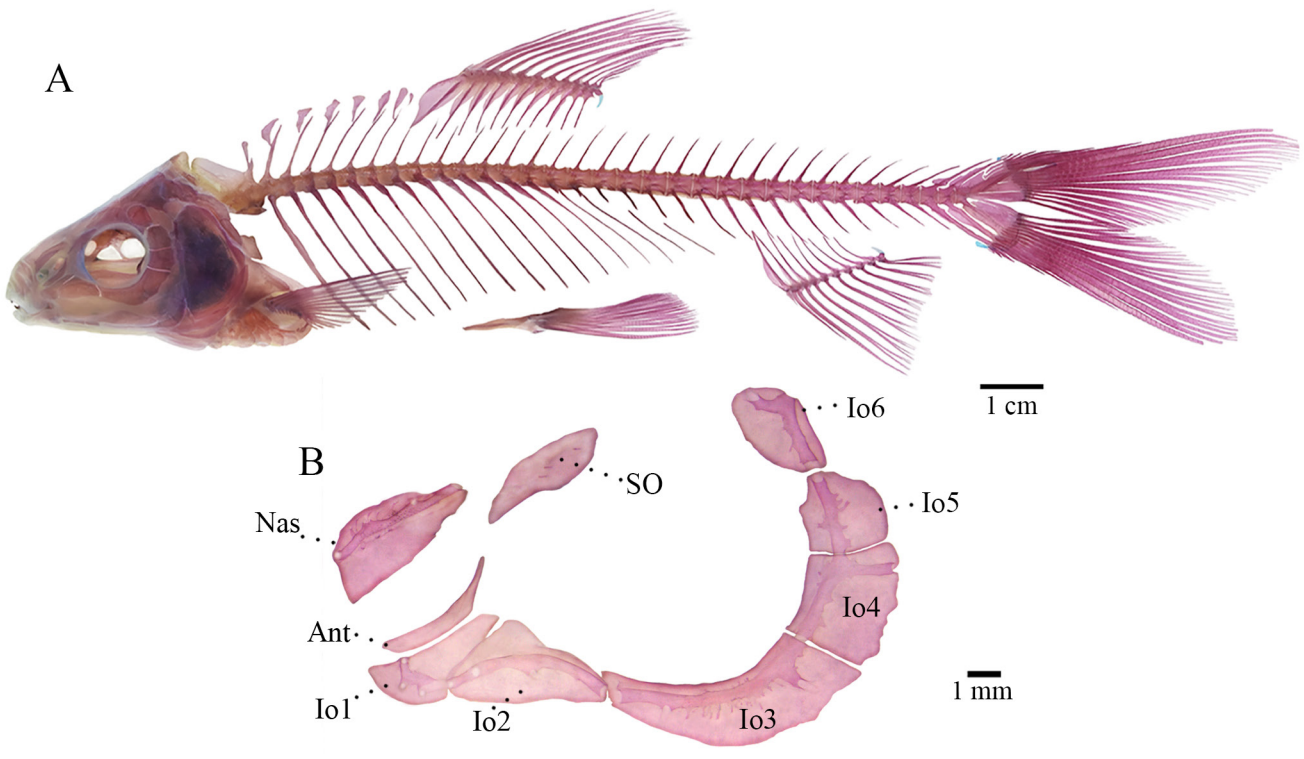

FIGURE 18 | *Hypomasticus australis*, MZUEL 23980, 94.61 mm SL, lateral view of the body skeleton (**A**) and infraorbital bones and associated elements (**B**). Nas: nasal, Ant: antorbital, Io1-6: infraorbital and SO: supraorbital.

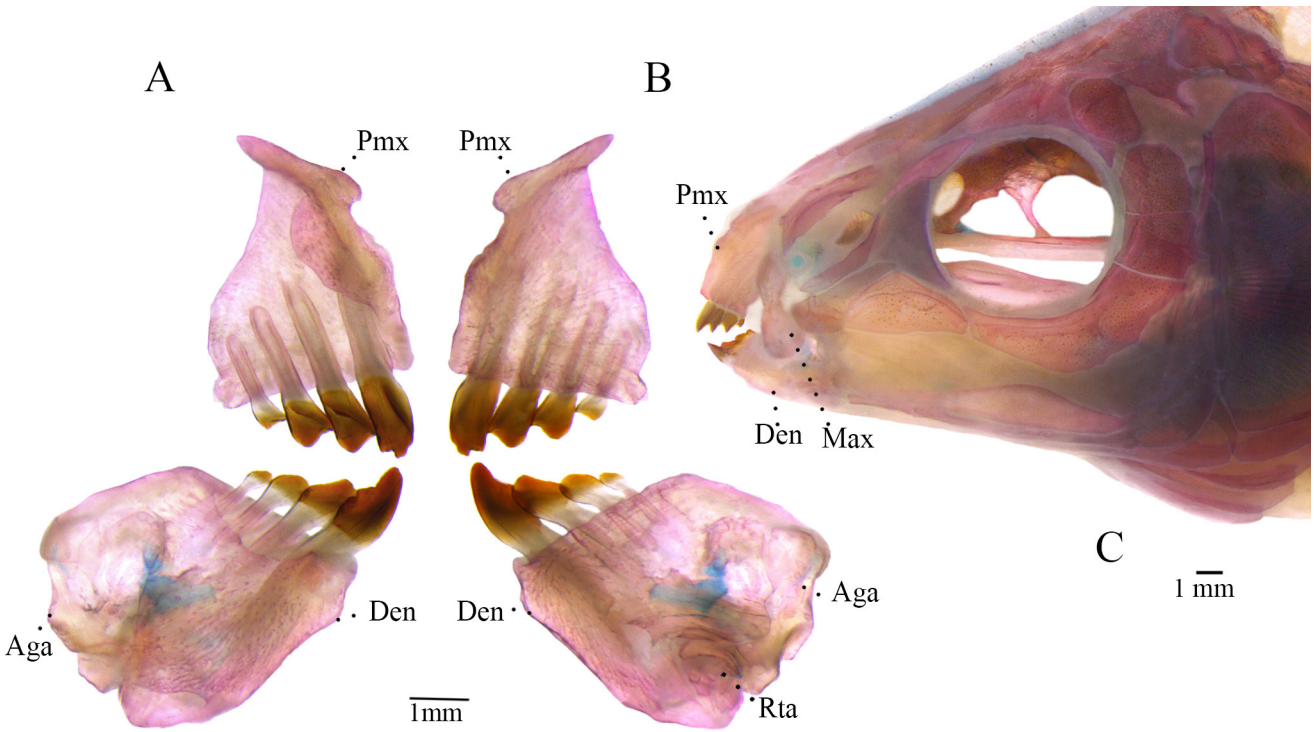

FIGURE 19 | Medial (**A**) and lateral (**B**) view of the jaws and lateral view of the head (**C**) of *Hypomasticus australis*, MZUEL 23980, 94.61 mm SL. Pmx: premaxilla, Max: maxilla, Den: dentary, Aga: anguloarticular and Rta: retroarticular.

Lateral shelf of the quadrate large and with slightly rounded edge, beginning at condyle and extending to preopercle (Fig. 20) Metapterygoid-quadrate fenestra medium sized and bean-shaped, with dorsal portion somewhat ovoid. Ectopterygoid with slightly convex anteroventral margin and somewhat straight posterior portion. Autopalatine elongated, with distinct rounded process extending anteroventrolaterally from main body of bone and cartilaginous anteroventral tip.

Urohyal relatively short and with a developed laminar process on ventral branch (Fig. 21). Urohyal almost triangular in shape, with dorsal branch longer than ventral branch, forming a slightly convex posterior margin. Condyle compressed dorsoventrally. Basihyal relatively short and laterally enlarged. Fourth branchiostegal ray significantly smaller than remaining rays. Basibranchials vertically interconnected without visible ossified connection (Fig. 22B). Fifth ceratobranchial with bony expansion on posterior margin bearing four rows of conical teeth. Four pairs of small pharyngobranchials, pharyngeal tooth plate bearing three rows of small conical teeth.

Mesethmoid with prominent anterior tip, with convex margin and clearly pointing downwards (Fig. 22A). Lateral ethmoid with gently compressed lateral process directed posteroventrally, which composes anterior margin of orbit. (Fig. 23A). Vomer with anterior downwards pointing process that articulates with autopalatine (Figs. 22A, 23B). Orbitosphenoid with a very distinct process that runs posteroventrally and connects with dorsal process of parasphenoid, forming column separating contralateral optic chambers. Parasphenoid with dorsal process that runs anterodorsally and connects with

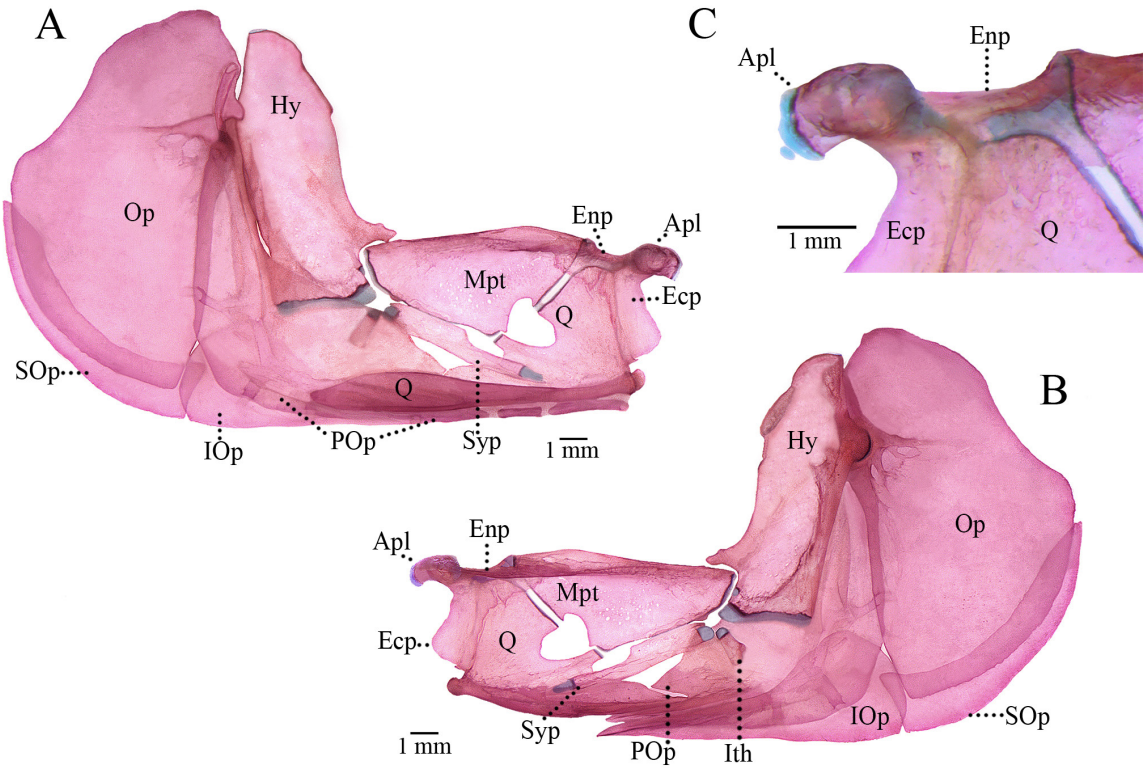

FIGURE 20 | Lateral (**A**) and medial (**B**) view of suspensorium with detail of autopalatine in lateral view (**C**) of *Hypomasticus australis*, MZUEL 23980, 94.61 mm SL. Ecp: ectopterygoid, Enp: entopterygoid, Hy: hyomandibular, IOp: interopercle, Mpt: metapterygoid, Op: opercle, Apl: autopalatine, POp: preopercle, Q: quadrate, SOp: subopercle, Syp: symplectic and Ith: interhyal.

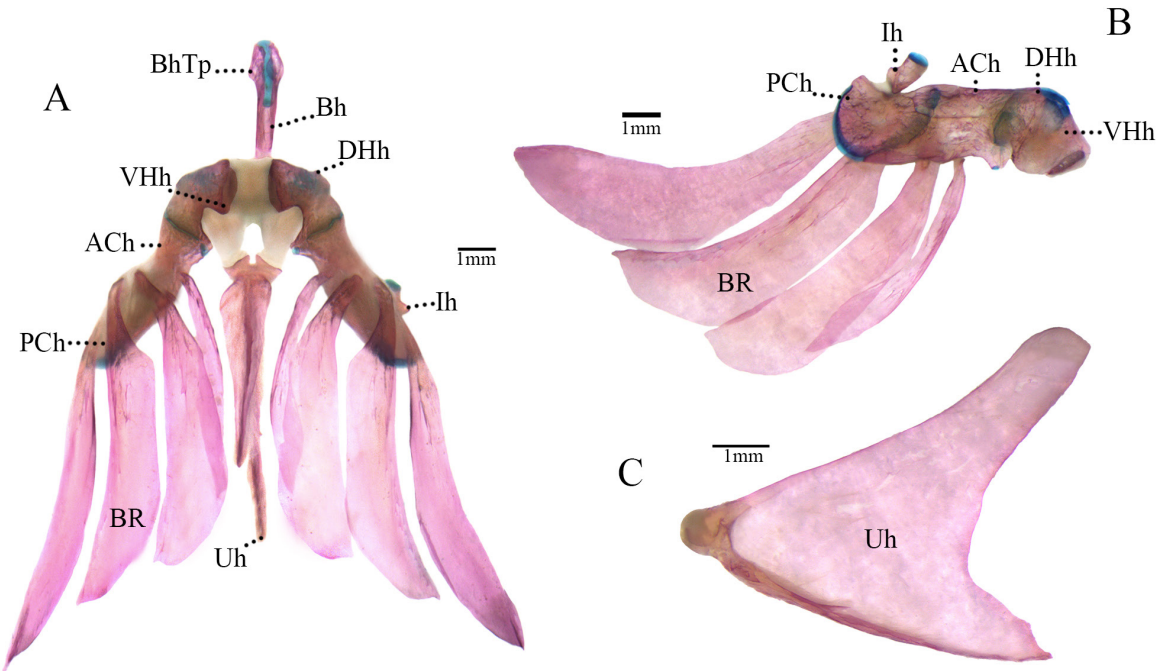

FIGURE 21 | Dorsal (**A**) and ventral (**B**) view of hyoid arch with detail of the urohyal in lateral view (**C**) of *Hypomasticus australis*, MZUEL 23980, 94.61 mm SL. BR: branchiostegal rays, Uh: urohyal, DHh: dorsal hypohyal, VHh: ventral hypohyal, ACh: anterior ceratohyal, PCh: posterior ceratohyal, Ih: interhyal, Bh: basihyal and Bhtp: basihyal toothplate.

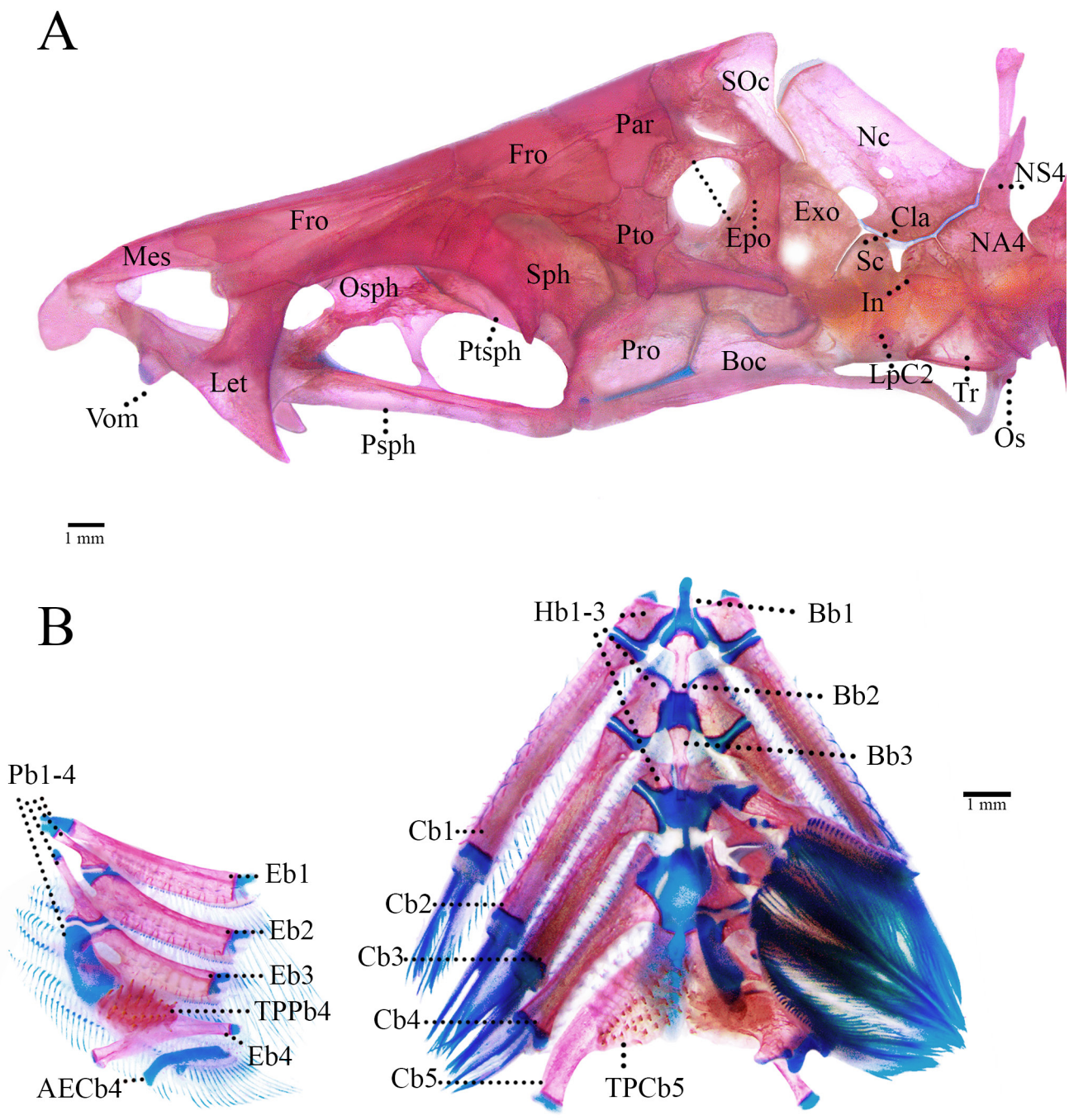

FIGURE 22 | Neurocranium in lateral view (**A**) and branchial apparatus (**B**) of *Hypomasticus australis*, MZUEL 23980, 94.61 mm SL. Mes: mesethmoid, Vom: vomer, Let: lateral ethmoid, Fro: frontal, Osph: orbitosphenoid, Ptsph, pterosphenoid, Psph: parasphenoid, Sph: sphenotic, Pto: pterotic, Pro: prootic, Par: parietal, Epo: epiotic, SOc: supraoccipital, Boc: basioccipital, Exo: exoccipital, Nc: neural complex, Cla: claustrum, Sc: scaphium, In: intercalarium, LpC2: lateral process of centrum 2, Tr: tripus, NA4: neural arch of centrum 4, NS4: neural spine of centrum 4, Os: os suspensorium, Bb1-3: basibranchial, Hb1-3: hypobranchial, Cb1-5: ceratobranchial, TPCb5: tooth plate of fifth ceratobranchial, Pb1-4: pharyngobranchial, Ep1-4: epibranchial, AECb4: accessory element of ceratobranchial 4 and TPPb4: tooth plate of fourth pharyngobranchial.

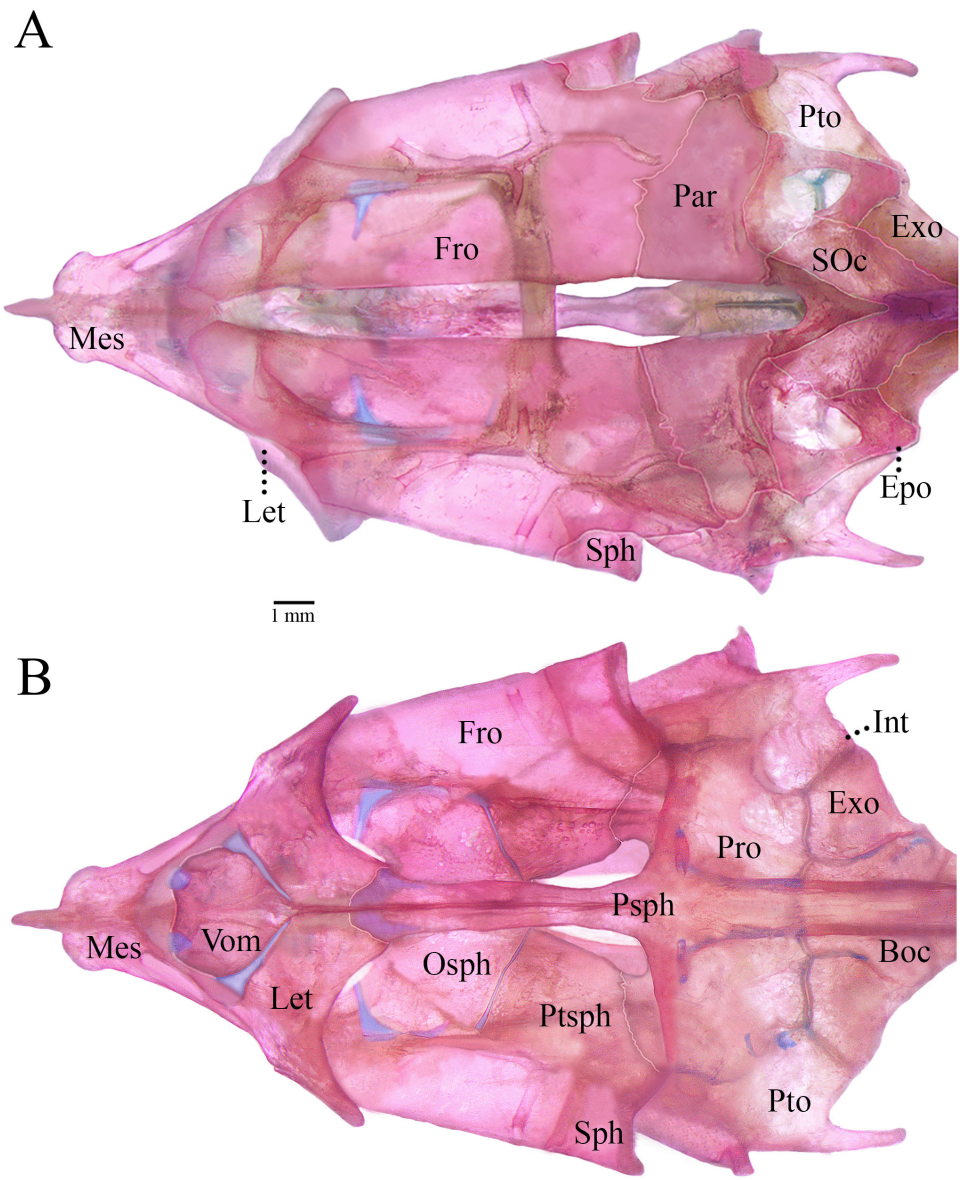

FIGURE 23 | Neurocranium in dorsal (**A**) and ventral view (**B**) of *Hypomasticus australis*, MZUEL 23980, 94.61 mm SL. Mes: mesethmoid, Let: lateral ethmoid, Fro: frontal, Sph: sphenotic, Par: parietal, SOc: supraoccipital, Pto: pterotic, Epo: epiotic, Exo: exoccipital, Vom: vomer, Osph: orbitosphenoid, Ptsph, pterosphenoid, Psph: parasphenoid, Pro: prootic, Boc: basioccipital and Int: intercalar.

ventral process of orbitosphenoid. Neural complex with rounded anterodorsal margin, somewhat straight posterodorsal margin and anteroventral margin with broad concave invagination creating fossa between neural complex and exoccipital.

Supracleithrum large, vertically elongated and divided in two separated ossifications, with dorsal portion largest and posteriorlly convex and ventral portion smaller and ovoid (Fig. 24). Posteroventral portion of coracoid with slightly triangular laminar process. First postcleithrum small and shaped like inverted teardrop, located between ventral section of supracleithrum and posteromedial portion of cleithrum. Pectoral fin with one unbranched ray and fourteen branched rays.

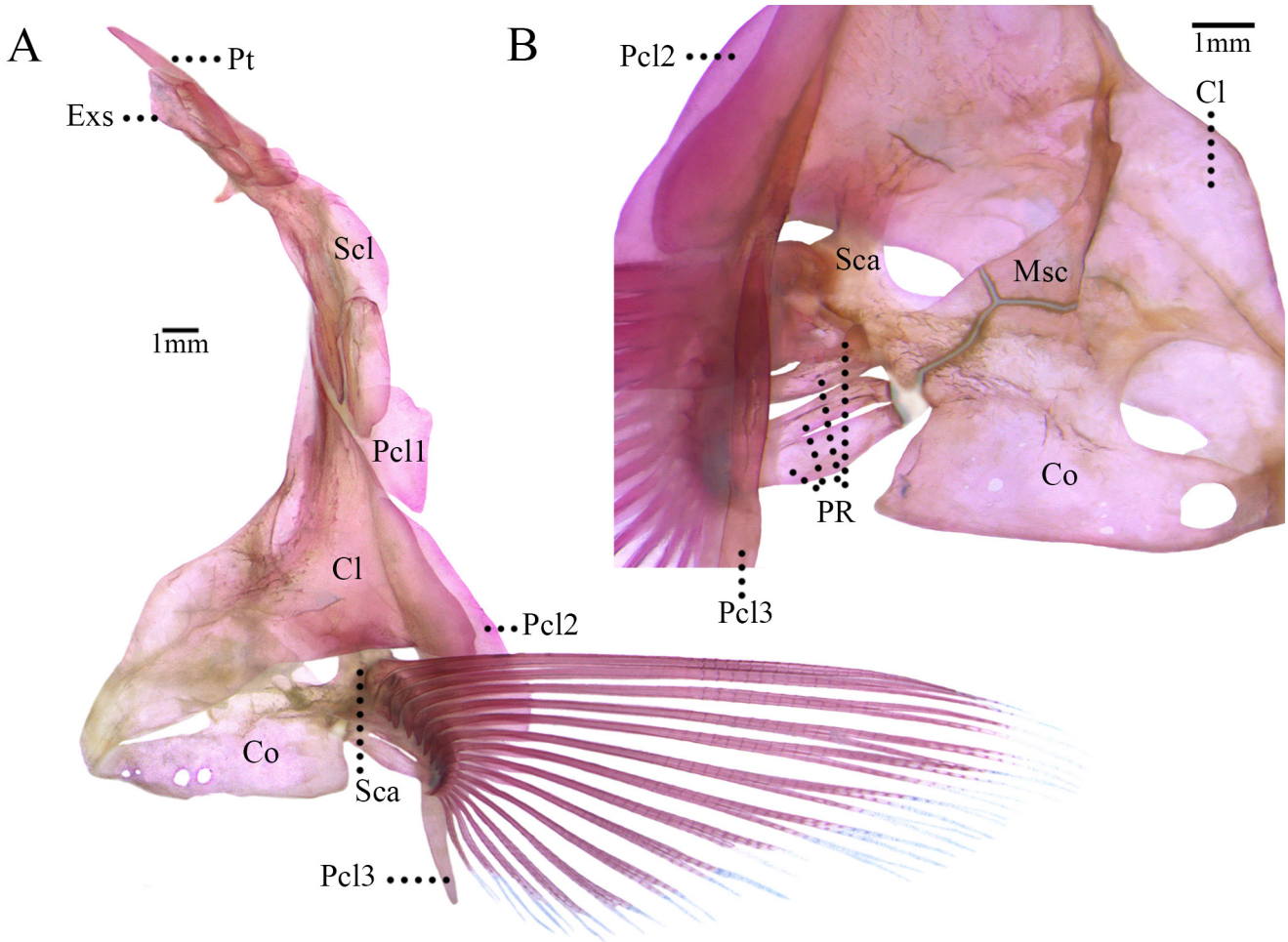

FIGURE 24 | Pectoral girdle in lateral (**A**) and medial view (**B**) of *Hypomasticus australis*, MZUEL 23980, 94.61 mm SL. Pt: posttemporal, Exs: extrascapular, Scl: supracleithrum, Cl: cleithrum, Co: coracoid, Sca: scapula, Msc: mesocoracoid, Pcl 1-3: postcleithra and PR: proximal radials.

First anterior pterygiophore of dorsal fin largest, with distinctly convex anterior laminar expansion and posterior laminar expansion relatively well developed (Fig. 25A). First anterior pterygiophore of anal fin with distinctly convex anterior laminar expansion and posterior laminar expansion relatively small (Fig. 25B).

Pelvic bones elongate, each with gently convex lateral margin and parallelling its counterpart (Fig. 26A), Neural spines of second and third preural centrum with distinct dorsal and ventral laminar process (Fig. 26B).

Coloration in alcohol. Ground color ranging from light beige to tan (Figs. 17, 27). Head and body gently countershaded. Smaller specimens with twelve transverse bars, extending from dorsal portion of body to horizontal through pectoral fin, partially interrupted by lateral line. Bars faint or absent in larger specimens. Dark spot located immediately posterior to sixth infraorbital, sometimes filling entire bone. Opercle with dark blotch, filled with white or silver pigmentation, positioned below lateral line and above pectoral-fin insertion. Some specimens with light coloration around the eye and

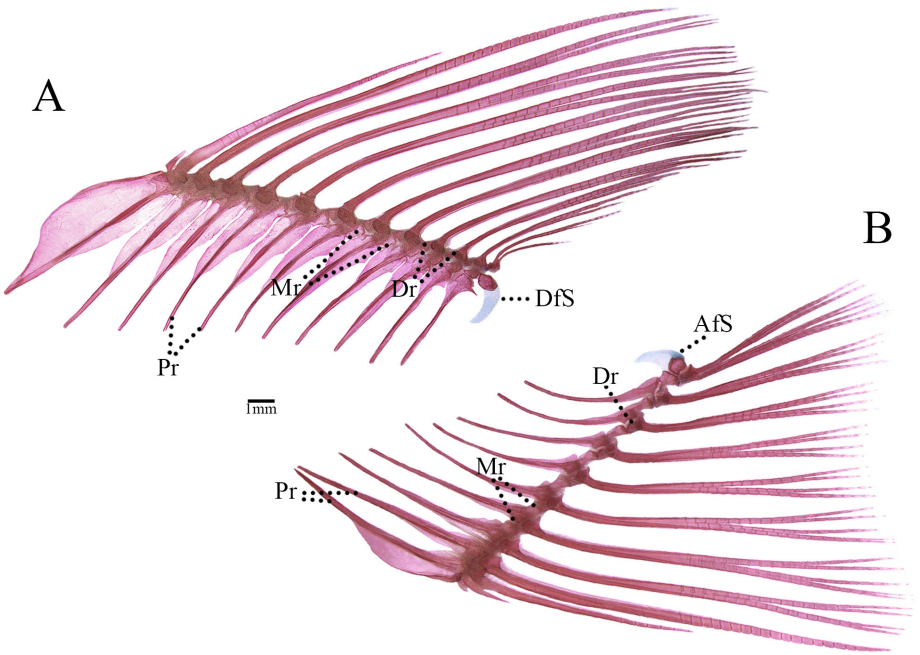

FIGURE 25 | Dorsal (**A**) and anal fin (**B**) of *Hypomasticus australis*, MZUEL 23980, 94.61 mm SL. Pr: proximal radial, Mr: medial radial, Dr: distal radial, DFS: dorsal fin stay and AFS: anal fin stay.

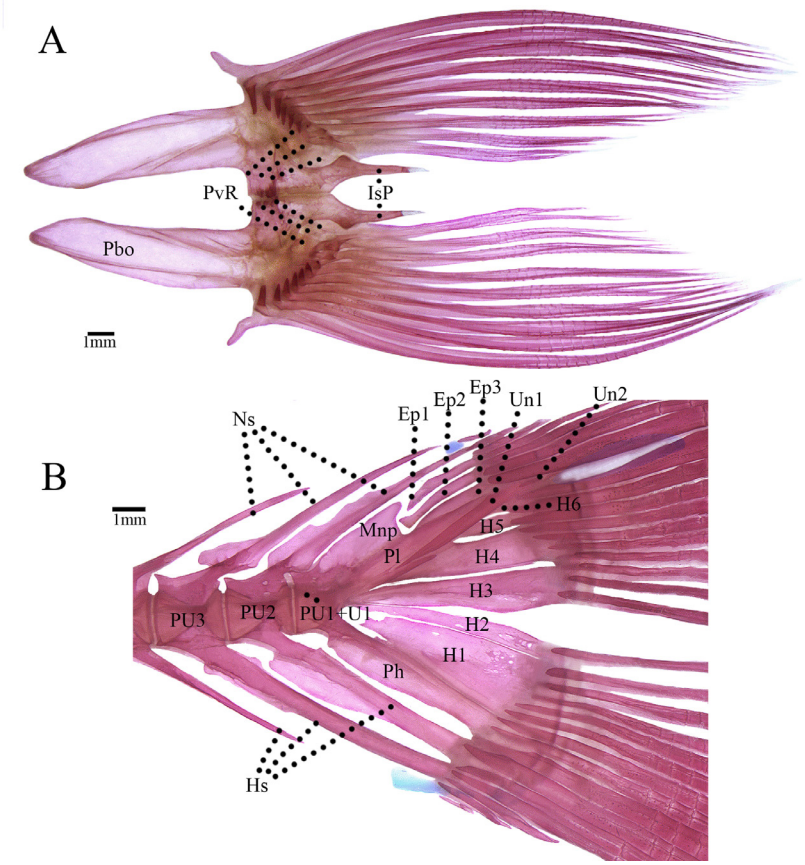

FIGURE 26 | Pelvic girdle in dorsal view (**A**) and caudal skeleton (**B**) of *Hypomasticus australis*, MZUEL 23980, 94.61 mm SL. IsP: isquiatic process, PvR: pelvic-fin radials, Pbo: pelvic bone, PU2-3: preural centrum, PU1+U1: complex centrum formed by preural centrum 1 and ural centrum 1, Hs: haemal spine, Ns: neural spine, Mnp: modified neural process, Ph: parhypural, H1-6: hypurals, Un1-2: uroneurals and Ep1-3: epural.

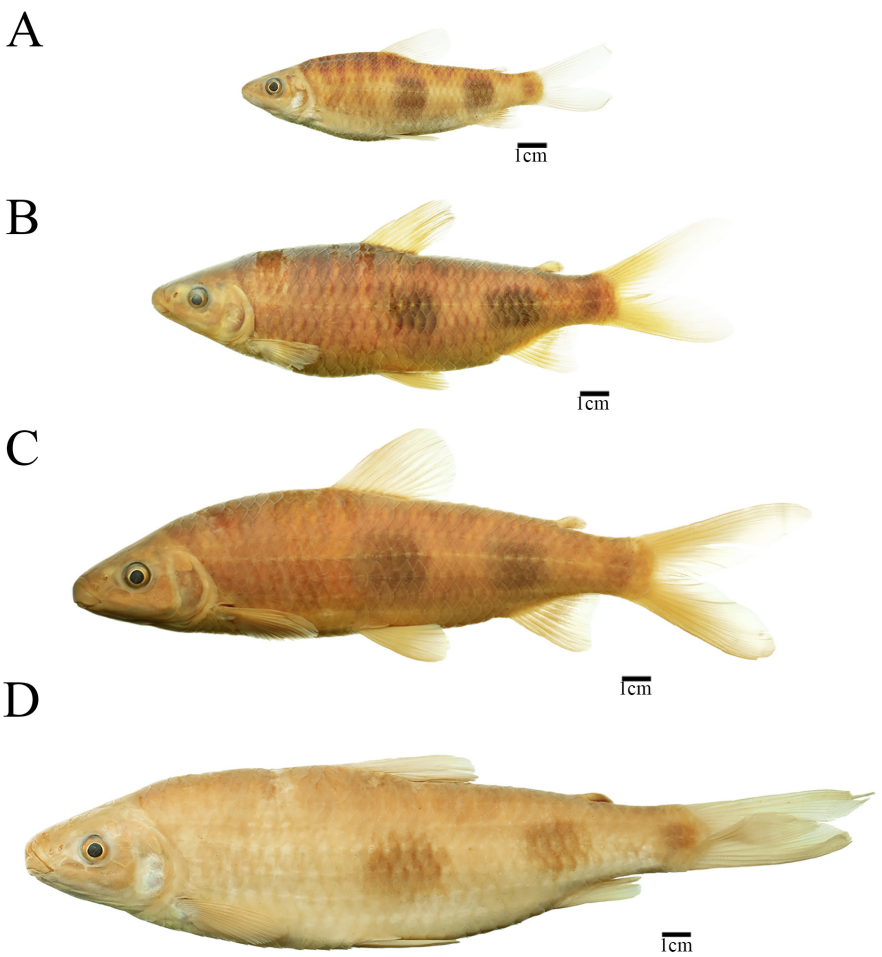

FIGURE 27 | *Hypomasticus australis*: **A.** MZUEL 23978, 90 mm SL, rio Poço Grande, tributary of rio Juquiá. **B.** LISDEBE 25, 134.6 mm SL, rio Juquiá, tributary of rio Ribeira de Iguape. **C.** LISDEBE 3, 168.5 mm SL, rio Quilombo, tributary of rio Juquiá. **D.** MZUEL 23979, 193.1 mm SL, rio Ribeira de Iguape.

in pre-opercular region. Snout region more pigmented than remaining head. Trunk with three large, diffuse midlateral blotches, first vertically aligned through base of last third of dorsal-fin base, second located between anal opening and posterior portion of anal fin, and last on posteriormost portion of caudal peduncle. Blotches somewhat uniform in size, decreasing in size posteriorly in smaller specimens. Ventral surfaces of head and body pale to cream, without chromophores. Fin coloration ranges from nearly hyaline to yellowish, with few chromophores along margins of rays.

Coloration in life. Coloration pattern like that of preserved specimens, midlateral blotches dark and diffuse. Head and body pale gray, with the dorsal region darker than the rest, and scales with dark yellow or reddish base and silver tips. Adipose fin scarlet red. Remaining fins bright or dark yellow. Conspicuous red blotch above the upper lip. Iris red or orange.

Sexual dimorphism. Two of the five radiographed individuals, presumably mature males, exhibited hypertrophy of the first pair of ribs, which were curved, with the tips directed posteriorly and displaying a shovel-like shape. In this condition, the tips of the first pair of ribs nearly reach the tips of the second pair, in contrast to the typical parallel arrangement seen in most specimens.

Geographical distribution. *Hypomasticus australis* is found across the Ribeira de Iguape, Una do Prelado and Rio de Janeiro coastal River basins, including the Lagoa Feia system, extending from the State of Rio de Janeiro to eastern São Paulo, and northeastern Paraná, Brazil (Fig. 28).

Ecological notes. *Hypomasticus australis* was not observed in the Paraíba do Sul river and its tributaries, it was instead found exclusively in the Rio de Janeiro coastal basins, including the Macabu, Caceribu and the Lagoa Feia. *Hypomasticus australis* is the only species of the genus found in the Ribeira de Iguape and in the Rio de Janeiro coastal drainages.

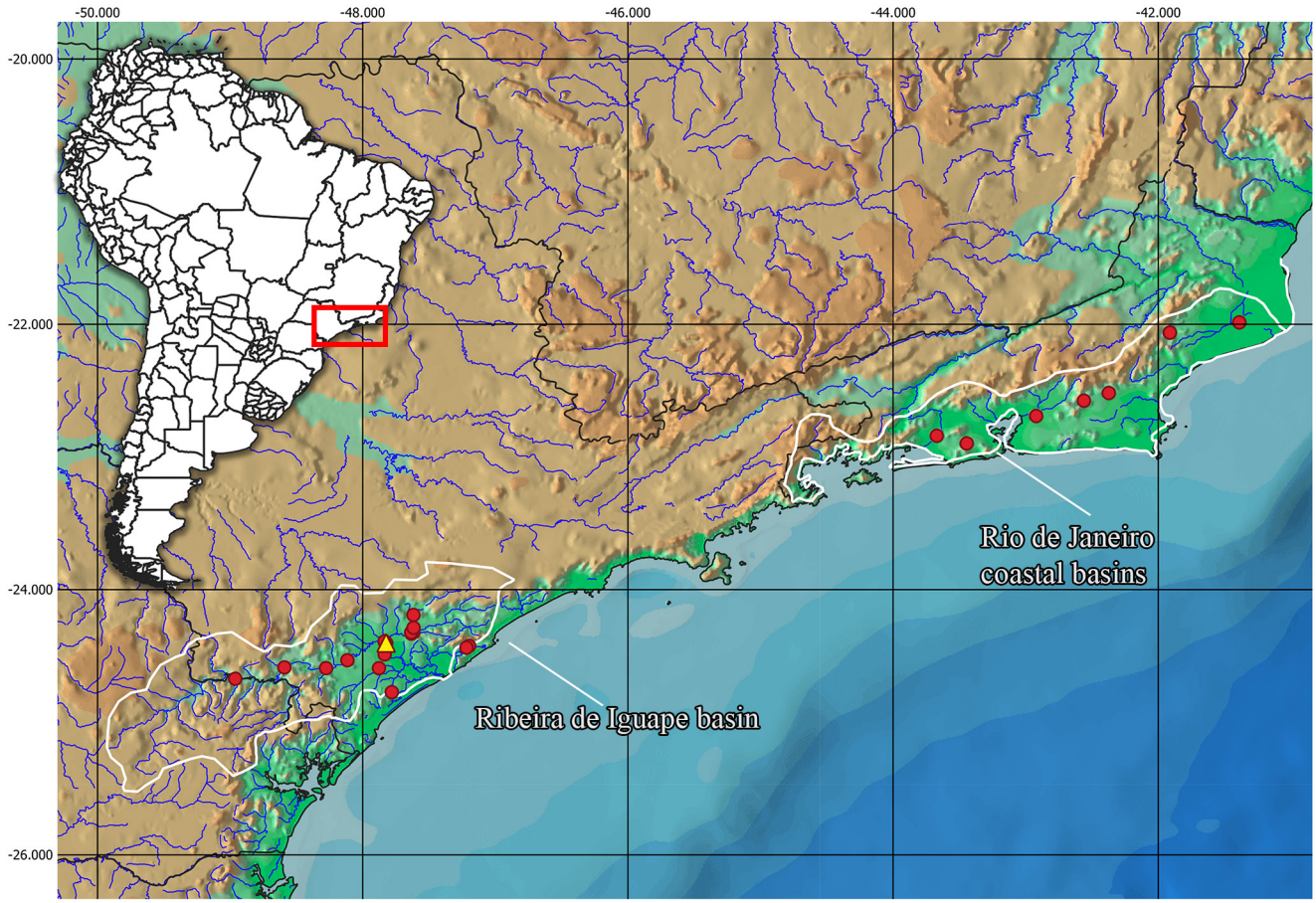

FIGURE 28 | Geographic distribution of *Hypomasticus australis* in eastern Brazil, yellow triangle represents type-locality.

Etymology. The species name *australis* is derived from the Latin term "austrālis," meaning "of the south," in reference to the distribution of the species. Members of the genus *Hypomasticus* are known to inhabit the Guiana Shield, the Amazon basin, and several coastal drainages in Brazil. This new species, found in the Ribeira de Iguape basin, marks the southernmost occurrence of the genus. An adjective.

Conservation status. *Hypomasticus australis* is distributed across the Fluminense and Ribeira de Iguape ecoregions of the Atlantic Forest, where it faces similar threats to those affecting *H. steindachneri.* These include high human population density, pollution, deforestation, mining and the construction of dams. The Rio de Janeiro coastal drainages, which drains heavily industrialized and populated urban areas, has notably compromised habitat integrity, potentially placing populations of the new species in this area at risk. However, as in *H. steindachneri*, the wide distribution of the species and his occurrence in relatively well-protected areas, such as the Ribeira de Iguape River basin, indicates that the existence of the new species is unlikely to face immediate threats. Therefore, we recommend the classification of *H. australis* as Least Concern (LC) according to the International Union for Conservation of Nature (IUCN) categories and criteria (IUCN Standards and Petitions Subcommittee, 2024).

Remarks. One of the *Hypomasticus australis* specimens analyzed (MZUSP 1786, Fig. **S1**) was collected in 1898, 126 years ago, in a tributary of the Juquiá River. The collector's name on the label appears as "Hempel", almost certainly referring to the entomologist Adolph Hempel (1870–1949). Born in the United States and later naturalized as a Brazilian citizen, Hempel worked for many years at the Ipiranga Museum (Museu Paulista da Universidade de São Paulo), collecting and describing several species. Photographs of this historical specimen are available in the supplementary material.

DISCUSSION

Many species of anostomids were historically identified and recognized based on a set of distinctive external traits including body coloration, scale counts, tooth number and shape, and mouth position. This approach to species identification has been especially prevalent among the *Hypomasticus* species from the coastal drainages. For instance, the inferior mouth is a distinctive feature of *H. mormyrops*, whereas the subinferior mouth characterizes *H. thayeri*. Additionally, *H. copelandii* is recognized by the numerous scales along the lateral line and its red fins, whereas *H. steindachneri* is differentiated by having fewer scales and yellow fins. The phylogenetic and species delimitation analyses conducted in this study demonstrated that these tradicional diagnostic traits often grouped multiple taxonomic entities under the same species name, indicating that such traits are clearly homoplastic within the group. The clear identification of undescribed new species, particularly within the populations of *H. copelandii* and *H. mormyrops*, highlights the need for a taxonomic review of the genus *Hypomasticus,* employing a novel array of molecular data.

Two recent studies presented phylogenetic trees that included sequences of *H. australis* (Birindelli *et al*., 2020; Sidlauskas *et al*., 2025). In both studies, the specimens were misidentified as *H. thayeri*. Birindelli *et al*. (2020) included five species of the *H. mormyrops* clade in an analysis based solely on the COI gene. They recovered *H. australis* as the sister group of *H. copelandii* from the Doce River; this clade was found to be the sister group of *H. steindachneri* plus *H. santanai*, and these four species together formed the sister group of *H. mormyrops* from the Paraíba do Sul River. Sidlauskas *et al*. (2025) included four species of the *H. mormyrops* clade in a multilocus analysis using both mitochondrial and nuclear genes. They recovered *H. australis* as the sister group of *H. copelandii* from the Doce River; this clade was found to be the sister group of *H. mormyrops* from the Paraíba do Sul, and these three species were recovered as the sister group of *H. steindachneri*. Our study corroborated the close relationship between *H. australis* and *H. copelandii*; however, our tree indicates a closer relationship between the new species and *H. thayeri*, with this clade forming the sister group to *H. copelandii* from the Paraíba do Sul River. Our analysis also recovered two previously unobserved relationships: *H. mormyrops* from the Paraíba do Sul as the sister group of *H. copelandii* from the Doce River, and *H. mormyrops* from the Doce River as the sister group of *H. steindachneri*. The close relationship between *H. santanai* and *H. steindachneri*, previously observed by Birindelli *et al*. (2020), was also corroborated in our analysis.

Delimitation of species in Anostomidae. The specimens from the Doce and Mucuri River basins are herein recognized as part of *H. steindachneri* based on their morphological similarity and phylogenetic proximity to the specimens from the type-locality in the Rio Jequitinhonha, despite exhibiting significant genetic divergence and current geographic isolation. This taxonomic decision is primarily due to the lack of sufficient diagnostic data that would allow for the clear differentiation of these populations from those of the Jequitinhonha and Pardo basins, or for the confident recognition and description of the Doce and Mucuri populations as a single distinct species. Considering the available evidence, and despite the molecular and geographic distinctions, we interpret these populations as being in an early stage of speciation that has not yet resulted in evident morphological traits allowing their visual distinction from the other populations. The acquisition of additional data in the future may lead to a shift in perspective, potentially supporting the recognition of one or more distinct species within these populations.

The use of 2% divergence threshold of the Barcode DNA as a parameter for species delimitations has been demonstrated to be a generally effective approach for freshwater fishes' delimitation (Ward *et al*., 2009; Pereira *et al*., 2013), as has been frequently employed in the description of new anostomid species (Ito *et al*., 2023; Britski *et al*., 2024). However, anostomids are ecomorphologically diverse, occupy a range of ecological niches, display varied morphologies, and exhibit a notably accelerated rate of speciation (Melo *et al*., 2022). Genetic sequencing of several anostomid species has demonstrated that, in some instances, morphologically distinct species exhibit a genetic divergence of less than 2% from their closest congener (Ramirez, Galetti Jr., 2015; Ramirez *et al*., 2020; Garavello *et al*., 2021). On the other hand, there are cases in which single species exhibit an intraspecific distance greater than 2% (Ramirez *et al*., 2017). These results highlight the need to carefully evaluate each taxonomic group separately, considering

their specific set of morphological diagnostic traits combined with their molecular delimitation (Pereira *et al*., 2013; Gomes *et al*., 2015). In the family Anostomidae, easily verifiable meristic counts with minimal intraspecific polymorphism, such as the number of teeth on the jaws, the number of scales on the lateral line, and the number of scales around the caudal peduncle can be extremely useful for species recognition, diagnoses and delimitation (Britski *et al*., 2012; Burns *et al*., 2017; Britski, Birindelli, 2019).

Sexual dimorphism in *Hypomasticus*. The hypertrophy of the first pair of ribs and associated musculature has long been documented in the families Curimatidae and Prochilodontidae, where it is frequently associated with sound production during the mating season (Schaller, 1971; Dorn, 1972; Schaller, 1974; Godoy, 1975; Castro, Vari, 2004). This trait was only recently recorded in the Anostomidae, initially in the genus *Megaleporinus* (Ramirez *et al*., 2017), alongside the first report of sound production in this genus (Muñoz-Duque *et al*., 2021), and later in *Leporinus* (Ito *et al*., 2023). Now, it has been identified in two species of *Hypomasticus* (Fig. 29). The presence of this feature in these three phylogenetically distinct clades suggests that it may be widely distributed within the family. Additional studies, including *in vivo* experiments, are required to gain a deeper understanding of the presence and functions of sound production in these species.

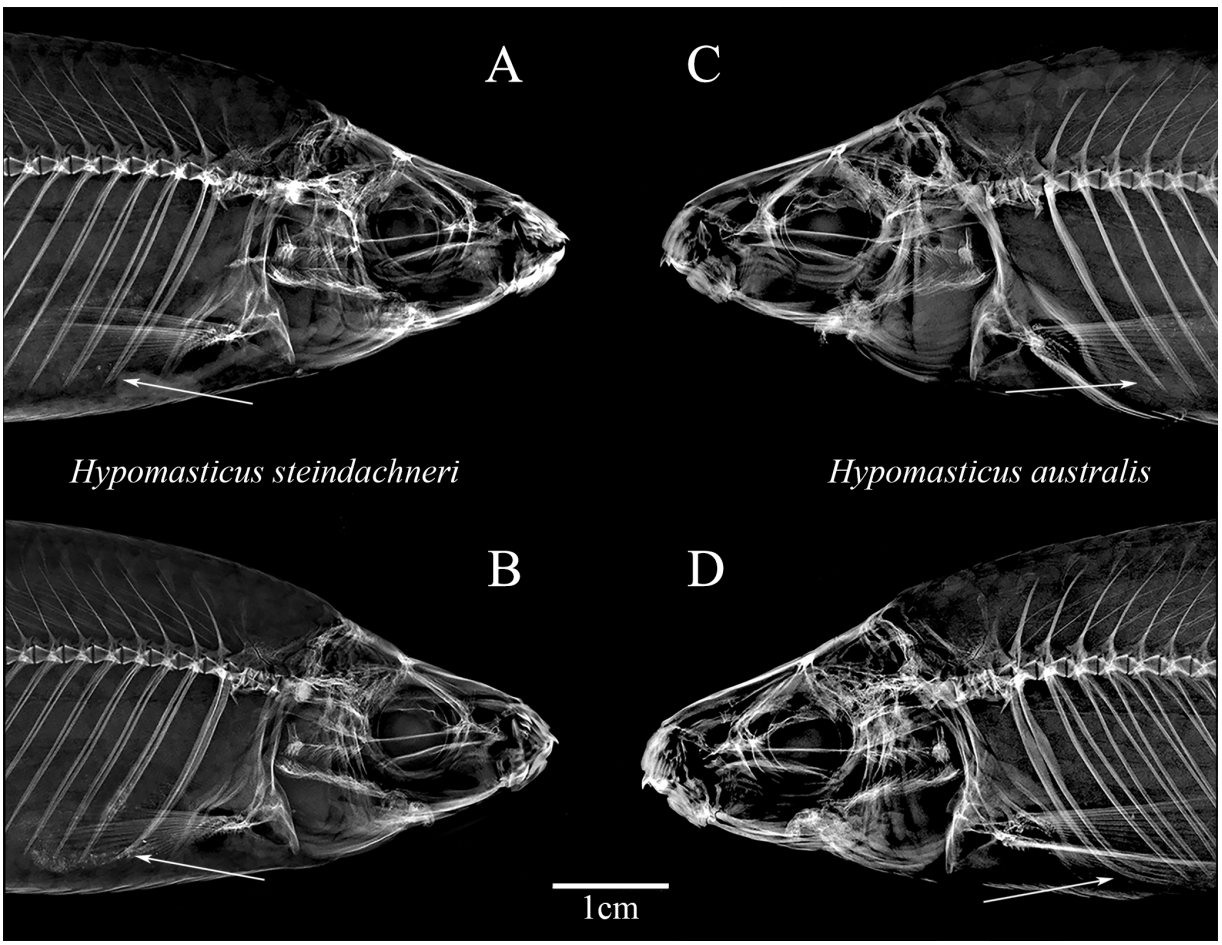

FIGURE 29 | Radiographed specimens of *Hypomasticus steindachneri* and *H. australis* with regular (**A**, **C**) and hypertrophied (**B**, **D**) first pair of ribs. **A.** MZUEL 17996, 114.8 mm SL. **B.** MZUEL 17996, 112.8 mm SL. **C.** LISDEBE 3, 137.9 mm SL. **D.** LISDEBE 3, 136.3 mm SL.

Orbitosphenoid-parasphenoid bar. An unexpected osteological finding was a bar formed by processes of the orbitosphenoid and parasphenoid bones (Figs. 7C, 10A, 19C, 22A). This columnar bony feature was observed in the c&s specimens of *H. australis* and *H. steindachneri,* as well as partially ossified in a dry skeleton of *H. steindachneri*, though identifying this feature in radiographed specimens proved difficult due to the overlapping of the head bones. This osteological trait has not been previously documented in Anostomidae, although a similar process was observed in the orbitosphenoid of *Insperanos* (Sidlauskas *et al*., 2021), which was described as "posteroventral margin concave, with distinct ventral processes". It is plausible that this ossification serves the function, as described by the authors, of a barrier between the contralateral optic chambers. This ossification has been previously described in the family Prochilodontidae, specifically in the genus *Semaprochilodus* Fowler, 1941 (Castro, Vari, 2004) where it was noted that the presence and the morphology of this trait distinguished the genera within the family. For instance, *Prochilodus* Agassiz, 1829 exhibits an orbitosphenoid with an extensive ventromedial wing that contacts the dorsomedial portion of the parasphenoid, creating a broad area of connection between these bones. This condition is also present in all species of Curimatidae. In *Semaprochilodus*, as well as in *Hypomasticus australis* and *H. steindachneri*, this process is reduced to a bar-like structure that extends ventrally from the orbitosphenoid to contact the dorsomedial process of the parasphenoid. In *Ichthyoelephas* Posada, 1909, the orbitosphenoid and parasphenoid processes are completely absent, condition that has also been consistently observed in all anostomids whose osteology has been documented to date. The presence of the bar in *Hypomasticus* and in several outgroup families may represent either an evolutionary convergence or a plesiomorphic condition. Further analyses, such as ancestral state reconstruction including additional species representing the remaining genera of Anostomidae, are necessary to clarify the evolutionary history of this trait.

Comparative material examined. All from Brazil. *Hypomasticus copelandii*: Doce: MZUEL 20991, 1, 304.37 mm SL. NUP 15470, 1, 279.51 mm SL. NUP 15505, 1, 235,22 mm SL. NUP 15041, 2, 440.21–450 mm SL. LISDEBE 6698, 1, 110.54 mm SL. LISDEBE 6675, 1, 98.54. MZUSP 81004, 1, 146.98 mm SL. Mucuri: LBP 8098, 3, 224.77-315.72 mm SL. LBP 8102, 2, 179.01–190.03 mm SL. Paraíba do Sul: MZUEL 17712, 1, 288.13 mm SL. MNRJ 13485, 2, 209.35–218.53 mm SL. LISDEBE 4603, 1, 171.67 mm SL. MZUSP 87854, 1, 301.89 mm SL. MZUSP 3045, 2, 208.73–215.01 mm SL. LBP 30201, 1, 274.08 mm SL. *Hypomasticus mormyrops*: Doce: MZUEL 20989, 1, 236.5 mm SL. MZUEL15901, 6, 88.69–180.23 mm SL. LISDEBE 176, 5, 134.72–170.36 mm SL. LISDEBE 6696, 2, 115.02–134.68 mm SL. MZUSP 66180, 1, 101.88 mm SL. MZUSP 100734, 1, 167.28 mm SL. MZUSP 87877, 1, 145.48 mm SL. Paraíba do Sul: MZUEL14127, 2, 139.13–170.14 mm SL. MZUEL 8022, 1, 103.47 mm SL. MZUSP 110150, 1, 176.47 mm SL. MZUSP 107896, 1, 160.25 mm SL. LBP 8103, 2, 160.25–160.31 mm SL. LBP 6448, 5, 109.78–149.47 mm SL. LISDEBE 154, 20, 127.91–172.95 mm SL. *Hypomasticus santanai*: All from Rio das Contas: MZUEL 18604, 208.32 mm SL, holotype. MZUEL 18605, 1, 178 mm SL, paratype. MZUEL 20020, 1, 159.24 mm SL, paratype. LBP 25152, 2, 191.89–237.99 mm SL, paratype. LBP 28094, 2, 182.28-212.01 mm SL, paratype. *Hypomasticus thayeri*: Doce: MZUEL 10561, 1, 162.48 mm SL. MZUSP 1557, 1, 100.3 mm SL. MZUSP 87900, 2, 79.62–101.81 mm SL. MZUSP 109968, 4, 98.04–134.97 mm SL. MZUSP 87811, 4, 72.28–114.72 mm SL. MZUSP 87899, 4, 94.01–111.09 mm SL. Paraíba do Sul: MNRJ 13484, 13, 125.56–210.22 mm SL. MZUSP 107911, 1, 168.44 mm SL. MZUSP 87897, 1, 201.09 mm SL. MZUSP 62747, 2, 194.84–234.11 mm SL. MZUSP 87896, 2, 211.52–239.27 mm SL. MZUSP 87898, 1, 140.39 mm SL.

ACKNOWLEDGMENTS

We would like to express our gratitude to Brian Sidlauskas (Tulane University), Fernando Jerep and Oscar Shibatta (UEL) for insights during the investigation of these species. To Alexandre Kannebley de Oliveira (UFSCAR), Carla Pavanelli and Weferson Graça (UEM), Mario de Pinna and Michel Gianeti (USP) Mark Sabaj, John Lundberg, Kyle Luckenbill and Mariangeles Arce (ANSP), Paulo Buckup, Cristiano Moreira, Marcelo Britto (MNRJ) and Claudio Oliveira (UNESP) for receiving us in their institution and providing access and information for specimens under their care. To Domingos Garrone-Neto and Eduardo Santinelli for help in the fieldwork.

REFERENCES

- **Abell R, Thieme ML, Revenga C, Bryer M, Kottelat M, Bogutskaya N *et al.*** Freshwater ecoregions of the World: a new map of biogeographic units for freshwater biodiversity conservation. BioScience. 2008; 58:403–14. https://doi.org/10.1641/B580507
- **Andrade Neto FR.** Estado atual do conhecimento sobre a fauna de peixes da bacia do Jequitinhonha. MG.Biota. 2010; 2(5):23–35.
- **Assega FM, Birindelli JLO.** Taxonomic revision of the genus *Anostomoides* (Characiformes: Anostomidae). Zootaxa. 2019; 4646(1):124–44. https://doi.org/10.11646/zootaxa.4646.1.7
- **Bemis PL, Hilton EJ, Brown B, Arrindell R, Richmond AM, Little CD *et al.*** Methods for preparing dry, partially articulated skeletons of Osteichthyans, with notes on making ridewood dissections of the cranial skeleton. Copeia. 2004; 2004(3):603–09. https://doi.org/10.1643/CI-03-054R1
- **Birindelli JLO, Britski HA.** Two new species of *Leporinus* (Characiformes: Anostomidae) from the Brazilian Amazon, and redescription of *Leporinus striatus* Kner 1858. J Fish Biol. 2013; 83(5):1128–60. https://doi.org/10.1111/jfb.12206
- **Birindelli JLO, Melo BF, Ribeiro-Silva LR, Diniz D, Oliveira C.** A new species of *Hypomasticus* from eastern Brazil based on morphological and molecular data (Characiformes, Anostomidae). Copeia. 2020; 108(2):416–25. https://doi.org/10.1643/CI-19-335
- **Borodin NA.** Notes on some species and subspecies of the genus *Leporinus* Spix. Mem Mus Comp Zool Harvard Coll. 1929; 50(3):269–90.
- **Britski HA, Birindelli JLO.** A new species of *Leporinus* Agassiz, 1829 (Characiformes: Anostomidae) from the rio Tocantins, Brazil. Neotrop Ichthyol. 2013; 11(1):25–32. https://doi.org/10.1590/S1679-62252013000100003
- **Britski HA, Birindelli JLO.** Description of a new species of *Leporinus* (Characiformes: Anostomidae) from the rio Tapajós basin, Brazil. Zootaxa. 2019; 4603(1):183–91. https://doi.org/10.11646/zootaxa.4603.1.10
- **Britski HA, Birindelli, JLO, Garavello JC.** A new species of *Leporinus* Agassiz, 1829 from the upper rio Paraná basin (Characiformes, Anostomidae) with redescription of *L. elongatus* Valenciennes, 1850 and *L. obtusidens* (Valenciennes, 1837). Pap Avulsos Zool. 2012; 52(37):441–75. https://doi.org/10.1590/S0031-10492012021700001
- **Britski HA, Garavello JC, Oliveira C, Birindelli JL.** Bisecting the type series of *Leporinus paranensis* Garavello & Britski, 1987 (Characiformes, Anostomidae). Pap Avulsos Zool. 2024; 64:e202464023. https://doi.org/10.11606/1807-0205/2024.64.023
- **Britski HA, Garavello JC, Ramirez JL.** Description of a new species of *Schizodon* (Characiformes: Anostomidae) from the upper rio Tapajós basin, Brazil. Zootaxa. 2023; 5330(1):135–40. https://doi.org/10.11646/zootaxa.5330.1.8
- **Burns MD, Chatfield M, Birindelli JLO, Sidlauskas BL.** Systematic assessment of the *Leporinus desmotes* species complex, with a description of two new species. Neotrop Ichthyol. 2017; 15(2):e160166. http://dx.doi.org/10.1590/1982-0224-20160166

- **Calegari BB, Delapieve MLS, Sousa LM.** Tutorial para preparação de mapas de distribuição geográfica. Bol Soc Bras Ictiol. 2016; 118:15–30.
- **Camelier P, Zanata AM.** Biogeography of freshwater fishes from the Northeastern Mata Atlântica freshwater ecoregion: distribution, endemism, and area relationships. Neotrop Ichthyol. 2015; 12(4):683–98. https://doi.org/10.1590/1982-0224-20130228
- **Carvalho TP.** Distributional patterns of freshwater fishes in coastal atlantic drainages of eastern Brazil: a preliminary study applying parsimony analysis of endemism. Darwiniana. 2007; 45(2):65–67.
- **Castro RMC, Vari RP.** Detritivores of the South American fish family Prochilodontidae (Teleostei: Ostariophysi: Characiformes): a phylogenetic and revisionary study. Smithson Contrib Zool. 2004; 622:1–189. https://doi.org/10.5479/si.00810282.622
- **Costa RMD.** Composição e diversidade da ictiofauna do Ribeirão Poço Grande, afluente do rio Juquiá, bacia do rio Ribeira de Iguape, estado de São Paulo. [Ph.D. Dissertation]. São Carlos: Universidade Federal de São Carlos; 2018. Available from: https://repositorio.ufscar.br
- **Dorn E.** Über den Lautapparat von Amazonasfischen, II. Die Naturwissenschaften. 1972; 59:169–70.
- **Edgar RC.** MUSCLE v5 enables improved estimates of phylogenetic tree confidence by ensemble bootstrapping. BioRxiv. 2021. https://doi.org/10.1101/2021.06.20.449169
- **Eigenmann CH, Ogle F.** An annotated list of characin fishes in the United States National Museum and the Museum of Indiana University, with descriptions of new species. Proc U S Nat Mus. 1907; 33(1556):1–38.
- **Ezard T, Fujisawa T, Barraclough TG.** SPLITS: species' limits by threshold statistics. 2009. R package version 1.0-18/r45. Available from: http://R-Forge.R-project.org/projects/splits
- **Garavello JC.** Revisão taxonômica do gênero *Leporinus* Spix, 1829 (Ostariophysi, Anostomidae). [Ph.D. Dissertation]. São Paulo: Universidade de São Paulo; 1979.
- **Garavello JC, Britski HA.** Family Anostomidae. In: Reis RE, Kullander SO, Ferraris CJ, editors. Check list of the freshwater fishes of South and Central America. Porto Alegre: Edipucrs; 2003. p.71–84.
- **Garavello JC, Ramirez JL, Oliveira AKD, Britski HA, Birindelli JL, Galetti Jr PM.** Integrative taxonomy reveals a new species of neotropical headstanding fish in genus *Schizodon* (Characiformes: Anostomidae). Neotrop Ichthyol. 2021; 19(4):e210016. https://doi.org/10.1590/1982-0224-2021-0016
- **Géry J.** Characoids of the world. New Jersey: TFH Publications; 1977.
- **Géry J, Planquette P, Le Bail PY.** Nomenclature des espèces du groupe *Leporinus maculatus* et formes affines des Guyanes (Pisces, Characoidei, Anostomidae). Rev Suisse Zool. 1988; 95(3):699–713.
- **Godoy MP.** Peixes do Brasil – Subordem Characoidei: bacia do rio Mogi Guassu. Piracicaba: Editora Franciscana; 1975.
- **Gomes LC, Pessali TC, Sales NG, Pompeu PS, Carvalho DC.** Integrative taxonomy detects cryptic and overlooked fish species in a neotropical river basin. Genetica. 2015; 143:581–88. https://doi.org/10.1007/s10709-015-9856-z
- **Günther A.** Catalogue of the fishes in the British Museum. Catalogue of the Physostomi, containing the families Siluridae, Characinidae, Haplochitonidae, Sternoptychidae, Scopelidae, Stomiatidae in the collection of the British Museum. 1864; 5:1–455.
- **Hammer Ø, Harper DA, Ryan PD.** PAST: paleontological statistics software package for education and data analysis. Palaeontol Electron. 2001; 4(1):1–09.
- **Hebert PD, Cywinska A, Ball SL, Dewaard JR.** Biological identifications through DNA barcodes. P R Soc London. 2003; 270(1512):313–21. https://doi.org/10.1098/rspb.2002.2218
- **Ito ISB, Souza-Shibatta L, Venturieri M, Birindelli JLO.** A new species of *Leporinus* (Characiformes: Anostomidae) from the Serra do Cachimbo, Pará State, Brazil. Neotrop Ichthyol. 2023; 21(3):e230058. https://doi.org/10.1590/1982-0224-2023-0058

- **International Union for Conservation of Nature (IUCN). Standards and petitions committee.** Guidelines for using the IUCN Red List categories and criteria. Version 16 [Internet]. Gland; 2024. Available from: http://www.iucnredlist.org/documents/RedListGuidelines.pdf
- **Latini AO, Petrere Jr. M.** Reduction of a native fish fauna by alien species: an example from Brazilian freshwater tropical lakes. Fisheries Manag Ecol. 2004; 11(2):71–79. https://doi.org/10.1046/j.1365-2400.2003.00372.x
- **Magalhães Júnior H, Lopes FA, Macedo DR.** Diagnóstico multitemporal do uso e cobertura da terra e qualidade das águas na bacia do rio Jequitinhonha em Minas Gerais como subsídio à gestão dos recursos hídricos superficiais. Rev Espinhaço. 2019; 8(2):15. https://doi.org/10.5281/zenodo.3583328
- **Melo BF, Sidlauskas BL, Near TJ, Roxo FF, Ghezelayagh A, Ochoa LE *et al*.** Accelerated diversification explains the exceptional species richness of tropical characoid fishes. Syst Biol. 2022; 71(1):78–92. https://doi.org/10.1093/sysbio/syab040
- **Mendes IS, Melo BF, Damasceno JS, Teixeira DF, Carvalho DC.** Phylogeography of *Hypomasticus copelandii* (Teleostei, Anostomidae) reveals distinct genetic lineages along Atlantic coastal drainages of Eastern Brazil. Diversity. 2022; 14(1):29. https://doi.org/10.3390/d14010029
- **Meireles WA.** Comparações no desenvolvimento ontogenético dos Characiformes: curimbatá (*Prochilodus hartii*), piabanha (*Brycon* sp.) e piau (*Leporinus steindachneri*) da bacia do rio Pardo. [Ph.D. Dissertation]. São Paulo: Universidade de São Paulo; 2012. Available from: https://www.teses.usp.br/teses/disponiveis/10/10132/tde-12062013-140600/pt-br.php
- **Muñoz-Duque S, López-Casas S, Rivera-Gutiérrez H, Jiménez-Segura L.** Bioacoustic characterization of mating calls of a freshwater fish (*Prochilodus magdalenae*) for passive acoustic monitoring. Biota Colomb. 2021; 22(1):108–21.
- **Nascimento MHS, Aragão DG, Silva JLN, Lima RC, Birindelli JLO, Fraga EC *et al*.** The DNA barcode reveals cryptic diversity and a new record for the genus *Leporinus* (Characiformes, Anostomidae) in the hydrographic basins of central northern Brazil. PeerJ. 2023; 11:e15184. https://doi.org/10.7717/peerj.15184
- **Pereira LHG, Hanner R, Foresti F, Oliveira C.** Can DNA barcoding accurately discriminate megadiverse Neotropical freshwater fish fauna? BMC Genet. 2013; 14(20). https://doi.org/10.1186/1471-2156-14-20
- **Pereira LHG, Maia GMG, Hanner R, Foresti F, Oliveira C.** DNA barcodes discriminate freshwater fishes from the Paraíba do Sul River basin, São Paulo, Brazil. Mitochondrial Dna. 2011; 22(sup1):71–79. https://doi.org/10.3109/19401736.2010.532213
- **Pompeu PDS, Martinez CB.** Efficiency and selectivity of a trap and truck fish passage system in Brazil. Neotrop Ichthyol. 2007; 5(2):169–76. https://doi.org/10.1590/S1679-62252007000200011
- **Pons J, Barraclough T, Gomez-Zurita J, Cardoso A, Duran D, Hazell S *et al*.** Sequence-based species delimitation for the DNA taxonomy of undescribed insects. Syst Biol. 2006. 55(4):595–610. https://doi.org/10.1080/10635150600852011
- **Posit team.** RStudio: integrated development environment for R. Posit Software, PBC, Boston, MA. 2024. Available from: http://www.posit.co/
- **Pugedo ML, Andrade Neto FR, Pessali TC, Birindelli JLO, Carvalho DC.** Integrative taxonomy supports new candidate fish species in a poorly studied neotropical region: the Jequitinhonha River basin. Genetica. 2016; 144(3):341–49. https://doi.org/10.1007/s10709-016-9903-4
- **Puillandre N, Brouillet S, Achaz G.** ASAP: assemble species by automatic partitioning. Mol Ecol Resour. 2021; 21(2):609–20. https://doi.org/10.1111/1755-0998.13281
- **Ramirez JL, Birindelli JLO, Galetti Jr. PM.** A new genus of Anostomidae (Ostariophysi: Characiformes): diversity, phylogeny and biogeography based on cytogenetic, molecular and morphological data. Mol Phylogenet Evol. 2017; 107:308–23. https://doi.org/10.1016/j.ympev.2016.11.012

- **Ramirez JL, Carvalho-Costa LF, Venere PC, Carvalho DC, Troy WP, Galetti Jr. PM.** Testing monophyly of the freshwater fish *Leporinus* (Characiformes, Anostomidae) through molecular analysis. J Fish Biol. 2016. 88(3):1204–14. https://doi.org/10.1111/jfb.12906
- **Ramirez JL, Galetti Jr. PM.** DNA barcode and evolutionary relationship within *Laemolyta* Cope 1872 (Characiformes: Anostomidae) through molecular analyses. Mol Phylogenet Evol. 2015; 93:77–82. https://doi.org/10.1016/j.ympev.2015.07.021
- **Ramirez JL, Santos CA, Machado CB, Oliveira AK, Garavello, JC, Britski HA *et al*.** Molecular phylogeny and species delimitation of the genus *Schizodon* (Characiformes, Anostomidae). Mol Phylogenet Evol. 2020; 153:106959. https://doi.org/10.1016/j.ympev.2020.106959
- **Reis RE, Kullander SO, Ferraris Jr. CJ.** Check list of the freshwater fishes of South and Central America. Porto Alegre: Edipucrs; 2003.
- **Sabaj Pérez MH.** Photographic atlas of fishes of the Guiana Shield. Bull Biol Soc Wash. 2009; 17(1):52–59. https://doi.org/10.2988/0097-0298-17.1.52
- **Salgado FS, Cunha MS, Melo S, Dergam JA.** Cytogenetic analysis of *Hypomasticus copelandii* and *H. steindachneri*: relevance of cytotaxonomic markers in the Anostomidae family (Characiformes). Comp Cytogenet. 2021; 15(1):65–76. https://doi.org/10.3897/compcytogen.v15.i1.61957
- **Santos GSA.** Análise filogenética das espécies de *Leporinus* (Ostariophysi: Characiformes: Anostomidae) das bacias do Prata e São Francisco. [Ph.D. Dissertation]. Universidade Estadual Paulista; 2007. Available from: https://www2.ibb.unesp.br/posgrad/teses/zoologia_me_2007_gleisy_santos.pdf
- **Sarmento-Soares LM, Mazzoni R, Martins-Pinheiro RF.** A fauna de peixes na bacia do rio Itanhém, leste de Minas Gerais e extremo Sul da Bahia. PANAMJAS. 2010; 5(1):47–61.
- **Schaller F.** Übern den lautapparat von Amazonas-Fische. Die Naturwissenschaften. 1971; 58:573–74.
- **Schaller F.** Wie trommeln Amazonasfische? Umschau Wissenschaften Tech. 1974; 74:249.
- **Souza G, Caramaschi EP, Monteiro LR.** Morphometrics and allometry of the larvae of five Characiformes species in the Paraíba do Sul River basin. Zygote. 2017; 25(4):507–18. https://doi.org/10.1017/S096719941700034X
- **Sidlauskas BL, Assega FM, Melo BF, Oliveira C, Birindelli JLO.** Total evidence phylogenetic analysis reveals polyphyly of *Anostomoides* and uncovers an unexpectedly ancient genus of Anostomidae fishes (Characiformes). Zool J Linn Soc-Lond. 2021; 194(2):626–69. https://doi.org/10.1093/zoolinnean/zlab016
- **Sidlauskas BL, Melo BF, Birindelli JL, Burns MD, Frable BW, Hoekzema K *et al.*** Molecular phylogenetics, a new classification, and a new genus of the Neotropical fish family Anostomidae (Teleostei: Characiformes). Neotrop Ichthyol. 2025; 23(1):e240076. https://doi.org/10.1590/1982-0224-2024-0076
- **Sidlauskas BL, Vari RP.** Phylogenetic relationships within the South American fish family Anostomidae (Teleostei, Ostariophysi, Characiformes). Zool J Linn Soc-Lond. 2008; 154(1):70–210. https://doi.org/10.1111/j.1096-3642.2008.00407.x
- **Silva AT, Chagas RJ, Santos ACDA, Zanata AM, Rodrigues BK, Polaz CNM *et al.*** Freshwater fishes of the Bahia State, northeastern Brazil. Biota Neotrop. 2020; 20(4):e20200969. https://doi.org/10.1590/1676-0611-BN-2020-0969
- **Silva FO, Kalapothakis E, Silva LGM, Pelicice FM.** The sum of multiple human stressors and weak management as a threat for migratory fish. Biol Conserv. 2021; 264:109392. https://doi.org/10.1016/j.biocon.2021.109392
- **Steindachner F.** Die Süsswasserfische des südöstlichen Brasilien (II). Sitzungsberichte der Kaiserlichen Akademie der Wissenschaften. Mathematisch-Naturwissenschaftliche Classe. 1875; 71(3):211–45.
- **Tamura K.** Estimation of the number of nucleotide substitutions when there are strong transition-transversion and G + C-content biases. Mol Biol Evol. 1992; 9(4):678–87. https://doi.org/10.1093/oxfordjournals.molbev.a040752
- **Tamura K, Stecher G, Kumar S.** MEGA11: molecular evolutionary genetics analysis version 11. Mol Biol Evol. 2021; 38(7):3022–27. https://doi.org/10.1093/molbev/msab120

- **Taphorn DC.** The characiform fishes of the Apure River drainage, Venezuela. [Ph.D. Dissertation]. Florida: University of Florida; 1990.
- **Taylor WR, Van Dyke GG.** Revised procedures for staining and clearing small fishes and other vertebrates for boné and cartilage study. Cybium. 1985; 9(2):107–19.
- **Toledo-Piza M, Baena EG, Dagosta FC, Menezes NA, Ândrade M, Benine RC *et al*.** Checklist of the species of the Order Characiformes (Teleostei: Ostariophysi). Neotrop Ichthyol. 2024; 22(1):e230086. https://doi.org/10.1590/1982-0224-2023-0086
- **Ward RD, Hanner R, Hebert PD.** The campaign to DNA barcode all fishes, FISH-BOL. J Fish Biol. 2009; 74(2):329–56.
- **Ward RD, Zemlak TS, Innes BH, Last PR, Hebert PDN.** DNA barcoding Australia's fish species. Philos Trans R Soc. 2005; 360(1462):1847–57. https://doi.org/10.1098/rstb.2005.1716
- **Weitzman SH.** The osteology of *Brycon meeki*, a generalized characid fish, with an osteological definition of the family. Stanford Ichthyol Bull. 1962; 8(1):3–77.

AUTHORS' CONTRIBUTION

Ian Solon B. Ito: Conceptualization, Data curation, Formal analysis, Investigation, Methodology, Validation, Visualization, Writing-original draft, Writing-review and editing.

Lenice Souza-Shibatta: Data curation, Methodology, Writing-review and editing.

Osvaldo T. Oyakawa: Investigation, Methodology, Writing-review and editing.

Júlio C. Garavello: Data curation, Investigation, Writing-review and editing.

Heraldo A. Britski: Data curation, Investigation, Writing-review and editing.

José L. O. Birindelli: Conceptualization, Data curation, Funding acquisition, Methodology, Project administration, Resources, Software, Supervision, Validation, Visualization, Writing-review and editing.

ETHICAL STATEMENT

Not applicable.

DATA AVAILABILITY STATEMENT

The authors confirm that the data supporting the findings of this study areavailable within the article.

COMPETING INTERESTS

The authors declare no competing interests.

FUNDING

This study was financed by the Coordenação de Aperfeiçoamento de Pessoal de Nível Superior (CAPES proc. 88887.827323/2023-00). JLB received grant from CNPq (process 08846/2023-0). This study received financial support from Fundação Araucária (processes CP 23/2024, NAPI Taxonline 68/2024), and FINEP (process 3086-24).

HOW TO CITE THIS ARTICLE

- **Ito ISB, Souza-Shibatta L, Oyakawa OT, Garavello JC, Britski HA, Birindelli JLO.** Systematic assessment of the *Hypomasticus steindachneri* (Characiformes: Anostomidae) species complex, with the description of a new species. Neotrop Ichthyol. 2025; 23(3):e250003. https://doi.org/10.1590/1982-0224-2025-0003

Neotropical Ichthyology

OPEN ACCESS

This is an open access article under the terms of the Creative Commons Attribution License, which permits use, distribution and reproduction in any medium, provided the original work is properly cited.

Distributed under
Creative Commons CC-BY 4.0

© 2025 The Authors.
Diversity and Distributions Published by SBI

Official Journal of the
Sociedade Brasileira de Ictiologia